Transient Beam Loading Effect and Coupled Bunch Instability in High Intensity Proton Synchrotron

（大強度陽子シンクロトロンにおける過渡的ビーム負荷効果と結合バンチ不安定性）

平成11年度

大阪大学大学院 理学研究科 物理学専攻

山 本 昌 亘

Transient Beam Loading Effect
and
Coupled Bunch Instability
in High Intensity Proton Synchrotron

Research Center for Nuclear Physics,
OSAKA University

YAMAMOTO, Masanobu

January 28, 2000

Dedicated to my parents.

Abstract

In high intensity synchrotron, heavy beam loading effects and instabilities related to rf accelerating systems are very important problems, and many analysises have been done on typical cases so far.

However, there is a peculiar problem in a high energy synchrotron, that is, since bunches are filled in the ring non-symmetrically, transient condition arises and it makes the analysis of the beam loading and instability difficult.

In this thesis, the transient beam loading was investigated by analytical calculation particle tracking simulation and the experiment using high intensity beam. Then, it was found that transient beam loading became very severe under the peculiar condition for the cavity impedance and the transient beam loading could be suppressed by broad-band impedance of the cavity.

Furthermore, coupled bunch instability under the transient beam loading is also estimated by the analytical equations. In such analysis of instability, it was found that the transient beam loading affected the coupled bunch instability, and lumped constant circuit model that approximately expresses the cavity an impedance played a important role.

Contents

1 Introduction **1**

2 RF Acceleration in Synchrotron **5**
2.1 Longitudinal beam dynamics without beam-cavity interaction 5
2.2 Cavity Resonator 9

3 Evaluation of Cavity by Lumped Circuit Expression **11**
3.1 Series and Parallel Expression for Magnetic Loss 11
3.2 Lumped Circuit Expression of Cavity 15
3.2.1 Cavity in Series Expression 16
3.2.2 Cavity in Parallel Expression 17

4 Longitudinal beam dynamics with beam-cavity interaction **21**
4.1 Wake Voltage and Lumped Circuit Expression of Cavity 21
4.1.1 Wake Voltage in Parallel Expression 21
4.1.2 Wake Field in Series Expression 24
4.2 Synchrotron Oscillation Including Wake Field 25
4.2.1 Equilibrium Phase and Beam Loading 30
4.2.2 Small Amplitude Motion with respect to Equilibrium Phase . . . 31

5 Transient Beam Loading **37**
5.1 Periodic Transient Beam Loading 37
5.2 Calculation of Transient Beam Loading 39
5.3 Multi-bunch Particle Tracking 44
5.4 Experiment of Transient Beam Loading 49
5.4.1 Beam Loading Test Bench 49
5.4.2 Measurement Procedure 51
5.5 Beam Loading Compensation 61

6 Estimation of Coupled Bunch Instability under Non-Symmetric Bunch Filling **65**
6.1 Interpretation of Synchrotron Motion with Beam-Cavity Interaction . . . 65
6.2 Single Bunch 67
6.3 Symmetric Bunch Filling 68
6.4 Non-Symmetric Bunch Filling 70
6.5 Difference of Wake Voltage between Circuit Models and its Effect to Coupled Bunch Instability 76

7 Conclusion **79**

A Resonant Circuit of Transmission Line A-1

B Characteristics of Magnetic Cores B-1

C Approximation of Wake Field Calculation C-1

1 Introduction

In nuclear and particle physics, one of the most efficient approaches to investigate them is the experiment using particle accelerator, and synchrotron accelerators have been constructed to get high energy beams. Furthermore, physicists have strongly wished high intensity beams for the experiments of rare event and its precise measurement [1].

In the synchrotron, the beam is guaranteed to stay in a ring by restoration force, which is provided by radio frequency(rf) electric field for the longitudinal motion along the direction of acceleration and by magnetic field for its vertical one. The number of particles accumulated in a synchrotron ring is limited by space charge force and the interactions between the beam and surroundings such as beam pipe, rf accelerating system, some instruments and beam itself. The field induced in such interactions is called "wake field" as shown in Fig.1.1.

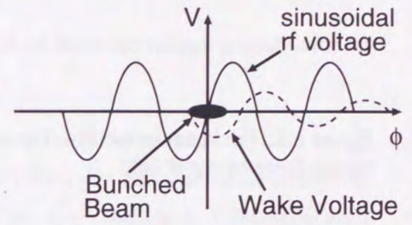

Figure 1.1: The wake voltage caused by the beam-cavity interaction.

On the rf acceleration, rf cavity gives the restoration force to the beam, but the cavity interacts with the beam simultaneously because the cavity has some impedance. Then the rf electric field for the restore force is disturbed by the wake field and this interaction may cause the beam energy loss.

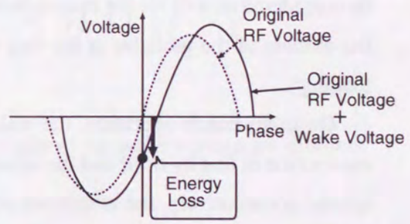

Figure 1.2: The rf acceleration under the beam loading. The beam energy is lost with respect to the original condition.

There are two issues to research the longitudinal motion of the beam under high intensity condition on the rf cavity. One is "Beam Loading" which means the continuous energy loss of the beam as shown in Fig.1.2, and it must be compensated by something to add more energy to the beam. Another is "Beam

Instability" which means the growth of the amplitude of the beam motion as shown in Fig.1.3.

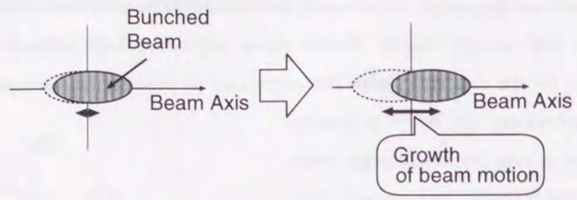

Figure 1.3: The beam instability. The amplitude of the beam motion is grown against the restore force by the rf field.

Many accelerator physicists have researched them, and many knowledges have been obtained to avoid the beam loss and to get more particles in the accelerator ring [2, 3, 4, 5, 6].

However, peculiar problem is remained to accelerate proton over a few GeV in a high intensity proton synchrotron, and they were not investigated so well in the past because the problem was considered as not so serious for the existing synchrotrons, but it should be considered as well for the future plans of very high intensity proton synchrotrons where the number of the particles in the ring will be over 10^{13} per bunch. It is "transient beam loading".

On multi-bunch operation, the wake voltage that affects on a bunch is made of the summation of that by itself and the other bunches. If the bunches are circulating in equally spaced consecutively, the amplitude of the wake voltage is the same on all bunches as shown in Fig.1.4. In this case, the effect of the beam loading is also the same on all bunches, which is called "static beam loading", so the cure for the beam loading can be applied to all bunches equally.

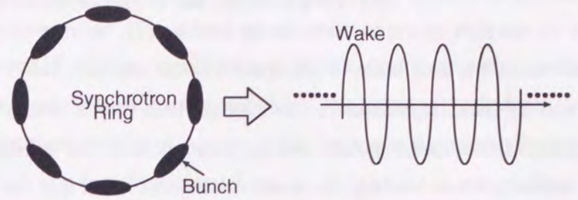

Figure 1.4: The static beam loading. The amplitude of the wake voltage are the same on the all bunches.

On the other hand, the amplitude of the wake voltage is not the same on each bunch any more as shown in Fig.1.5 if the bunches are circulating in non-symmetric configuration and intermittently. In this case, the effect of the beam loading is different on each bunch, which is called "transient beam loading", so equally cure for the beam loading is abandoned.

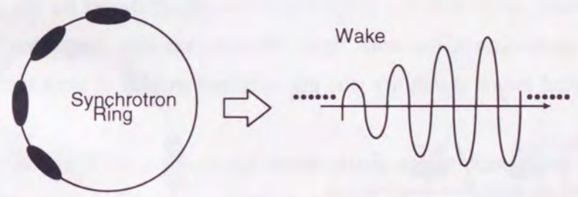

Figure 1.5: The transient beam loading. The amplitude of the wake voltage are different on each bunch.

The reason why such transient condition is made is that since the particles are bent by magnetic field, the particle energy that can be achieved on a synchrotron is limited by the field strength of the magnet, another synchrotron must be prepared to accelerate the proton over a few GeV. Generally, the number of the bunch filled in the former synchrotron is smaller than that in the latter one, the condition, where the bunches are filled non-symmetrically, may be appeared and it makes the transient condition periodically.

It was considered so far that band width of the cavity impedance should be as narrow as possible for the cure of the transient beam loading [7], because the narrow-band impedance could make the amplitude of the wake voltage smaller. However, the wake voltage on the narrow-band impedance remains longer than that on the broad-band one from the view point of transient response, and the summation of the wake voltage is important for the transient beam loading. So it can not be concluded that the narrow-band impedance always better than the broad-band impedance.

In this thesis, it will be shown that the transient beam loading becomes most severe at the peculiar band-width of the cavity, then the very broad-band impedance can also cure the transient beam loading.

Furthermore, the analytical estimation of coupled bunch instability, which is one of the beam instabilities, under the transient beam loading will be also shown in this thesis, and it has not been investigated clearly so far [8, 9, 10] because it is very complicated situation to investigate how the beam is stable. Then, it was found the transient beam loading affected the coupled bunch instability.

In such process, more realistic lumped constant circuit model for the rf cavity was applied on the evaluation of the wake field. Then, it was also found that the condition where the coupled bunch instability was not occurred existed in such lumped constant circuit model.

In order to verify such things, firstly beam dynamics of the longitudinal motion in the synchrotron and fundamentals of the rf cavity loaded with magnetic cores are introduced, then the formulas which evaluate the beam loading and the instability including the interaction between the beam and the rf cavity will be derived. According to those formulas, analytic estimations, numerical calculations and experiments using high intensity electron beam will be described on the transient beam loading. Using the results of the transient beam loading, the coupled bunch instability will be estimated by the analytical calculations.

2 RF Acceleration in Synchrotron

In a synchrotron, the beam should be stayed in a ring during the acceleration on same orbit, so the particles should be converged by the electromagnetic force. In the transverse direction, which means that it is vertical to the beam direction, the magnetic force is adopted as such one and the electric force is adopted in the longitudinal direction. The fundamentals about the longitudinal particle motion without the beam-cavity interaction and the element that realizes the acceleration will be described in this section.

2.1 Longitudinal beam dynamics without beam-cavity interaction

In a synchrotron, particles are divided into some groups called "bunch" during filling and the acceleration in the synchrotron ring as shown in Fig. 2.1 to guarantee longitudinal stability by the electric field for generating restoration force under the condition that the particles circulate on same orbit in spite of momentum changing. The sinusoidal wave voltage is basically used for generating the electric field as shown in Fig. 2.2.

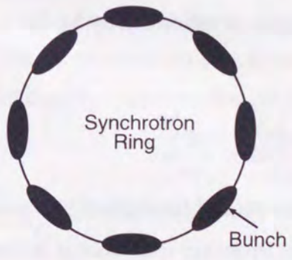

Figure 2.1: Schematic view of bunch in the ring. This case eight bunches are filled.

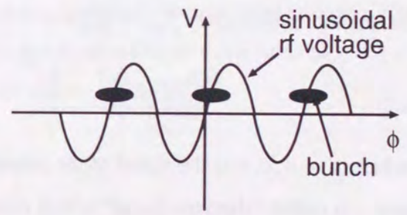

Figure 2.2: The sinusoidal rf voltage and bunches.

After this, let us regard that the bunch shape is not changed and the center of the bunch behaves as a point like charged particle. This model is called "rigid bunch model".

The longitudinal particle motion is expressed by two quantities, that is, the energy E(or the momentum p) and the phase ϕ that is respect to the sinusoidal rf voltage.

Let us consider "synchronous particle" circulating on central orbit in the ring exactly, that has the energy of E_s, and also let us consider another particle which has the energy of E circulating on different orbit from the central one.

In the ring, the particle having the momentum p circulates on the different orbit from the central one in proportion to the momentum difference $\Delta p = p - p_s$ as shown in Fig.2.3, where p_s is the momentum of the synchronous particle, because the orbit of the circulating particles is bent by Lorenz force that is proportional to the momentum. Then, it leads to the difference of the orbit length $\Delta C = C - C_s$ as

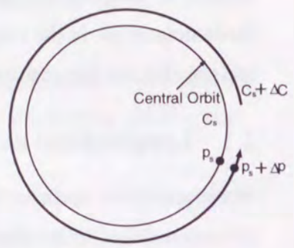

Figure 2.3: The difference of the orbit between the arbitrary particle and the synchronous one.

$$\frac{\Delta C}{C_s} = \alpha \frac{\Delta p}{p_s} \ , \tag{2.1}$$

where C_s is the circumference of the central orbit and α is called "momentum compaction factor". The difference of the orbit length leads to that of revolution frequency $f_{\rm rev} = \frac{\beta c}{2\pi C}$ as

$$\frac{\Delta f_{\rm rev}}{f_{\rm revs}} = \frac{\Delta \beta}{\beta_s} - \frac{\Delta C}{C_s} = \left(\frac{1}{\gamma_s^2} - \alpha \right) \frac{\Delta p}{p_s} = \eta \frac{\Delta p}{p_s} \ , \tag{2.2}$$

where $\beta = v/c$, v is the speed of the particle, c is the speed of the light, $\gamma = \frac{1}{\sqrt{1-\beta^2}}$, and η is called "slippage factor" which means that the frequency difference is defined by the relativity in addition to the orbit length.

On the other hand, let us express the position of the particle in the ring as the phase of the sinusoidal voltage, that is, $\phi = \omega_{\rm rf} t = 2\pi f_{\rm rf} t$, where $f_{\rm rf}$ is the frequency of it. Then, the difference of the phase per a turn $(\Delta\phi)_{\rm turn}$ between the arbitrary particle and the synchronous particle at the phase of $\phi_s = \omega_{\rm rf} t_s$ is expressed as

$$(\Delta\phi)_{\rm turn} = (\phi - \phi_s)_{\rm turn} = \omega_{\rm rf} T_{\rm rev} - \omega_{\rm rf} T_{\rm revs} = -\omega_{\rm rf} T_{\rm revs} \left(\frac{\Delta f_{\rm rev}}{f_{\rm revs}} \right) \ , \tag{2.3}$$

where the $\omega_{\rm rf} = 2\pi h f_{\rm rev}$ is angular frequency of the sinusoidal voltage, $T_{\rm rev} = 1/f_{\rm rev}$ is revolution period and h is the integer number called "harmonic number". Substituting eq.(2.2) into eq.(2.3), the relation the phase to the momentum difference can be obtained as

$$(\Delta\phi)_{\rm turn} = -2\pi h \eta \frac{\Delta p}{p} \ . \tag{2.4}$$

The other quantity, the difference of the energy per a turn $(\Delta E)_{\rm turn}$ between the a particle at the phase ϕ and the synchronous particle at the phase ϕ_s, is expressed as

$$(\Delta E)_{\rm turn} = eV \sin\phi - eV \sin\phi_s \ , \tag{2.5}$$

where V is the amplitude of the sinusoidal voltage and e is an elementary electric charge. These two difference equations of (2.4) and (2.5) are the most fundamental ones for the longitudinal motion in the synchrotron without the beam-cavity interaction.

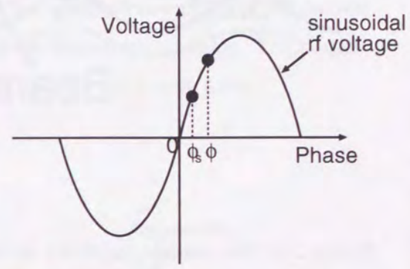

Figure 2.4: The definition of the synchronous phase ϕ_s and the phase of arbitrary particle ϕ.

For the practical analysis, these two difference equations are converted into the differential ones by supposing that $\Delta\phi$ and ΔE are not so changing in a few turns as

$$\frac{d\Delta\phi}{dt} \simeq \frac{(\Delta\phi)_{\rm turn}}{T_{\rm revs}} \ , \qquad \frac{d\Delta E}{dt} \simeq \frac{(\Delta E)_{\rm turn}}{T_{\rm revs}} \ , \tag{2.6}$$

then, two differential equations are obtained as

$$\frac{d}{dt}\left(\frac{\Delta E}{h\omega_{\rm revs}} \right) = \frac{eV}{2\pi h} (\sin\phi - \sin\phi_s) \tag{2.7}$$

$$\frac{d\Delta\phi}{dt} = -h^2 {\omega_{\rm revs}}^2 \frac{\eta}{\beta^2 E_s} \left(\frac{\Delta E}{h\omega_{\rm revs}} \right) \ . \tag{2.8}$$

These two differential equations of (2.7) and (2.8) are the most fundamental ones for the longitudinal motion in the synchrotron without the beam-cavity interaction.

The analytical solutions for eq. (2.7) and (2.8) can not be got explicitly because of the non-linearity, but it is known that the properties of the motion can be evaluated by trajectory of the motion in the phase space [11] as shown in Fig. 2.5.

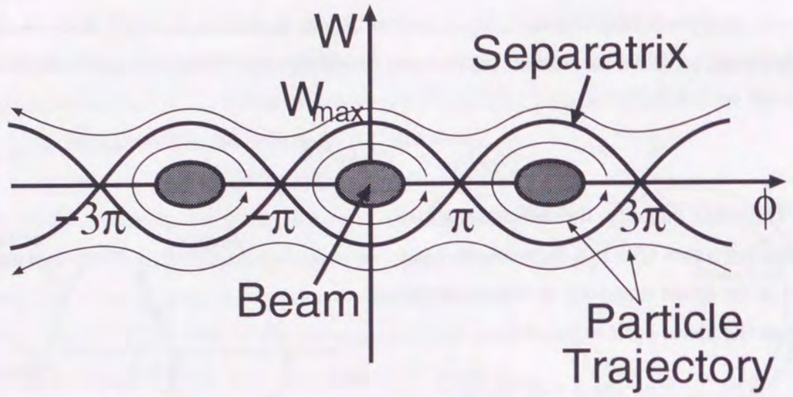

Figure 2.5: The particle trajectory in the phase space for the longitudinal motion in the synchrotron. In this case, $\phi_s = 0$ is chosen. Furthermore, $W = \frac{\Delta E}{h\omega_{\rm revs}}$.

The particle in "separatrix" can oscillate stably, whereas go away at the outside of the separatrix. This separatrix is called "rf bucket" in the longitudinal motion of the synchrotron, and this oscillation is called "synchrotron oscillation". The particles in the the rf bucket are guaranteed to stay in the ring, say the principle of "phase stability" in synchrotron which is one of the most important property in the synchrotron. The area of the rf bucket is also called "acceptance", and that of the beam is called "beam emittance". Of course, the beam emittance should be smaller than the acceptance, if it is not realized, the beam will be lost out of the ring.

Substituting eq.(2.7) into eq.(2.8), we get

$$\frac{d^2\Delta\phi}{dt^2} + \frac{eVh\eta\omega_{\rm revs}^2}{2\phi\beta^2 E_s}(\sin\phi - \sin\phi_s) = 0\ . \tag{2.9}$$

Now we have an interest in the small amplitude of the motion around the synchronous particle, then supposing that $\phi - \phi_s \ll 1$, we can obtain

$$\frac{d^2\Delta\phi}{dt^2} + {\omega_s}^2\Delta\phi = 0 \tag{2.10}$$

$$\omega_s = \sqrt{\frac{h\omega_{\rm revs}^2\eta eV cos\phi_s}{2\phi\beta^2 E_s}}\ , \tag{2.11}$$

where ω_s is called "synchrotron frequency". As clearly shown in eq.(2.10), the particle motion in small amplitude is expressed as one of the harmonic oscillator. The particle which is slipped from the central orbit is surely put back by the restore force.

2.2 Cavity Resonator

The restore force of the synchrotron oscillation is given by the sinusoidal electric voltage generated at rf accelerating cavity. The cavity is generally composed of the coaxial transmission line shorted at a terminal because it shows the resonant characteristics(see Appendix A). The schematic view of typical rf cavity is shown in Fig. 2.6. The particles feel electric field at the accelerating gap. The cavity is driven by rf amplifiers.

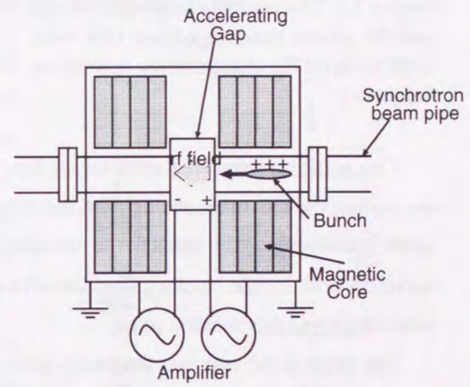

Figure 2.6: The rf cavity resonator loaded with magnetic cores.

Since the revolution frequency of the proton beam is changing greatly up to a few GeV region because of its heavy mass, magnetic cores are generally loaded in the rf cavity for the proton synchrotron to make the cavity always have some impedance over the frequency range during the acceleration. Of course, it is also the reason for loading with magnetic cores that wave length of the rf voltage should be almost same as the length of the cavity on the range of hundreds kHz$\sim$ decades MHz, which is typical frequency for the proton synchrotron.

There are two methods to keep the impedance on wide frequency range.

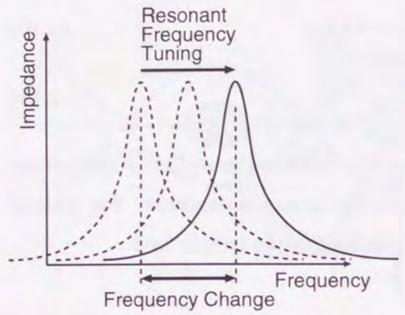

Figure 2.7: The resonant frequency tuning and the narrow band impedance type with depending on the change of the revolution frequency.

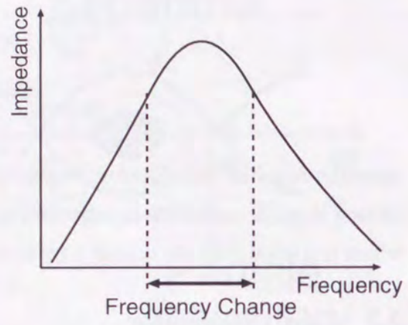

Figure 2.8: The untuned and the broad band impedance type.

One is the resonant frequency tuning type [12] as shown in Fig. 2.7, which is realized by putting the DC magnetic field on the magnetic cores, that is, the permeability of the cores is changing and it leads to the resonant frequency change. In this scheme, there are no restrictions for the band width of the cavity impedance, and many proton synchrotrons have employed this scheme so far.

The other is the resonant frequency untuning type as shown in Fig. 2.8. In this case, the impedance of the cavity must have broad-band characteristics enough to cover the frequency range [13, 14].

Since the impedance of the rf cavity for the proton synchrotron is almost defined by the characteristics of the magnetic cores, it is very important to investigate them. The core has some inductance and resistance. The resistance is caused by magnetic losses where the input rf magnetic field does not contribute to the magnetization because of some magnetic mechanisms [15, 16, 17, 18].

The analytical expressions for the magnetic cores and their effects to the beam loading and the instability will be described in section 3.1 and 6, respectively.

3 Evaluation of Cavity by Lumped Circuit Expression

It is very important for the analysis of the beam-cavity interaction to know the impedance of the cavity because the impedance of the cavity is mainly defined by the characteristics of the magnetic cores in the cavity for proton synchrotron. Although the cavity should be expressed as the distributed constant circuit precisely, it is almost equal to the lumped constant circuit near the resonant condition(see Appendix A), so let us consider how to express the characteristics of the magnetic cores as the lumped constant circuit model.

As described in section 4, the model of the cavity impedance will affect on the wake voltage because the phase of the cavity impedance plays an important role on such calculation.

3.1 Series and Parallel Expression for Magnetic Loss

Let the magnetic core magnetize by rf magnetic field $H = H_0 e^{j\omega t}$, then magnetic flux density $B = B_0 e^{j(\omega t - \delta)}$ is generated, where δ indicates the phase difference between H and B caused by the some magnetic loss mechanisms [15, 16, 17, 18]. In this case, the permeability of the core is expressed as

$$\mu = \frac{B}{H} = \frac{B_0}{H_0} e^{-j\delta} = \frac{B_0}{H_0}\cos\delta - j\frac{B_0}{H_0}\sin\delta \ , \tag{3.1}$$

and a complex permeability is defined as

$$\mu = \mu' - j\mu'' \ , \tag{3.2}$$

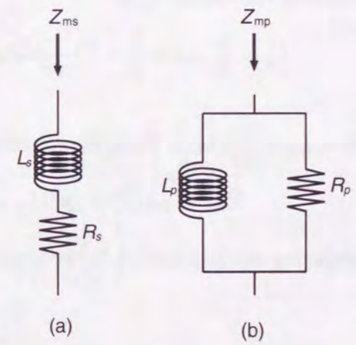

Figure 3.1: Two different expressions about rf loss at the magnetic cores.

where $\mu' = \frac{B_0}{H_0}\cos\delta$ and $\mu'' = \frac{B_0}{H_0}\sin\delta$. The μ' part indicates the contribution to the magnetization in deed, and μ'' part indicates the magnetic losses. The ratio of μ' to μ'' is defined as "quality factor" of the magnetic core

$$\frac{\mu''}{\mu'} = \tan\delta = \frac{1}{Q} \ . \tag{3.3}$$

The high Q means low magnetic losses in the core assuming μ' is constant. This quantity is very important to investigate the behavior of the rf cavity.

Then, the definition of eq.(3.2) indicates the series expression on lumped circuit as shown in Fig.3.1 (a). On this expression, the impedance of the magnetic core $Z_{\rm ms}$ becomes

$$Z_{\rm ms} = j\omega L_s + R_s \ . \tag{3.4}$$

Using a formula of an inductance L_t for the coaxial transmission line per length l,

$$L_t = \frac{\mu}{2\pi} l \ln \frac{b}{a} \tag{3.5}$$

where a and b are inner and outer radius of the core as shown in Fig.3.2, let us express the inductance and the rf magnetic loss of the magnetic core by a complex inductance L'_s as

$$L'_s = \frac{\mu}{2\pi}\mu_0 l \ln \frac{b}{a} = \frac{\mu'_s - j\mu''_s}{2\pi}\mu_0 l \ln \frac{b}{a} = (\mu'_s - j\mu''_s)L_0 \ , \tag{3.6}$$

Figure 3.2: The configuration of the toroidal core.

where $L_0 = \frac{\mu_0}{2\pi} l \ln \frac{b}{a}$. Then, the equation (3.4) becomes

$$Z_{\rm ms} = j\omega(\mu'_s - j\mu''_s)L_0 = j\omega\mu'_s L_0 + \omega\mu''_s L_0 \ . \tag{3.7}$$

Comparing eq.(3.4) with (3.7), we obtain

$$L_s = \mu'_s L_0 \tag{3.8}$$

$$R_s = \omega\mu''_s L_0 \ . \tag{3.9}$$

Thus,

$$\frac{\mu''_s}{\mu'_s} = \tan\delta = \frac{1}{Q} = \frac{R_s}{\omega L_s}$$

$$R_s = \frac{\omega L_s}{Q} = \frac{\mu'_s}{Q} f \cdot \mu_0 l \ln \frac{b}{a} \ . \tag{3.10}$$

Now, an important quantity is derived such as $\frac{\mu'_s}{Q} f$, this is proportional to the rf magnetic loss in the series expression.

By the way, since L_s and R_s are coupled strongly, all parameters are necessary in this expression when we calculate the resonant frequency of the cavity. So there is another expression using the parallel expression as shown in Fig. 3.1 (b). In this case, the circuit is simple and this expression is used usually for the cavity model. Let us consider as

$$\frac{1}{Z_{\rm mp}} = \frac{1}{j\omega L_p} + \frac{1}{R_p} \ . \tag{3.11}$$

$$Z_{\rm mp} = Z_{\rm ms} \tag{3.12}$$

Now, since we want to express the inductance and the rf magnetic loss of the magnetic core by a complex inductance L'_p as $\frac{1}{Z_{\rm mp}} = \frac{1}{j\omega L'_p}$, then

$$\frac{1}{\mu} = \frac{1}{\mu'_p} - \frac{1}{j\mu''_p} \tag{3.13}$$

becomes useful expression. The quality factor is expressed as

$$\tan\delta = \frac{1}{Q} = \frac{\mu'_p}{\mu''_p} \ . \tag{3.14}$$

Thus, the complex inductance L'_p is defined by

$$L'_p = \frac{\mu}{2\pi}\mu_0 l \ln \frac{b}{a} = \frac{1}{2\pi}\left(\frac{\mu'_p\mu''^2_p}{\mu'^2_p + \mu''^2_p} - j\frac{\mu'^2_p\mu''_p}{\mu'^2_p + \mu''^2_p}\right)\mu_0 l \ln \frac{b}{a}$$

$$= \left(\frac{\mu'_p\mu''^2_p}{\mu'^2_p + \mu''^2_p} - j\frac{\mu'^2_p\mu''_p}{\mu'^2_p + \mu''^2_p}\right) L_0 \ . \tag{3.15}$$

Multiplying $\frac{1}{j\omega L_0}$ on each side of (3.13), we obtain

$$\frac{1}{j\omega\mu L_0} = \frac{1}{j\omega L'_p} = \frac{1}{Z_p} = \frac{1}{j\omega\mu'_p L_0} - \frac{1}{j\cdot j\omega\mu''_p L_0} = \frac{1}{j\omega\mu'_p L_0} + \frac{1}{\omega\mu''_p L_0} \ . \tag{3.16}$$

Comparing eq.(3.11) with (3.16), we can get

$$L_p = \mu'_p L_0 \tag{3.17}$$

$$R_p = \omega\mu''_p L_0 \ . \tag{3.18}$$

Then,

$$\frac{\mu_p'}{\mu_p''} = \tan\delta = \frac{1}{Q} = \frac{\omega L_p}{R_p}$$
$$R_p = \omega L_p Q = \mu_p' Q f \cdot \mu_0 l \ln\frac{b}{a} . \tag{3.19}$$

Now, an important quantity is derived such as $\mu_p' Q f$, this is proportional to the rf magnetic loss in the parallel expression, and this parameter is usually used to evaluate the characteristics of the magnetic cores.

Comparing eq.(3.6) with (3.15), we can find that there are relations such as

$$\mu_s' = \frac{\mu_p' \mu_p''^2}{\mu_p'^2 + \mu_p''^2} \tag{3.20}$$

$$\mu_s'' = \frac{\mu_p'^2 \mu_p''}{\mu_p'^2 + \mu_p''^2} \tag{3.21}$$

between the series expression and the parallel expression, and they are rewritten by using Q as

$$\mu_s' = \frac{\mu_p'}{1 + \frac{1}{Q^2}} \tag{3.22}$$

$$\mu_s'' = \frac{\mu_p''}{1 + Q^2} . \tag{3.23}$$

From these equations, μ_p' is almost same as μ_s' in the high Q region.

Since the treatment of the analytical expression becomes very complicated in the series expression as shown in next section, the parallel expression has been preferred for the simplicity on analyzing the beam instabilities so far.

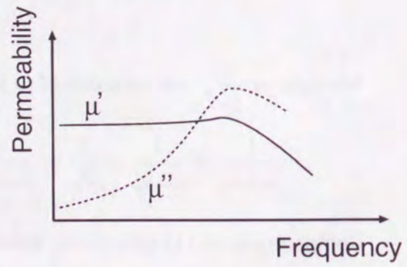

Figure 3.3: The frequency dependence of the complex permeability.

As shown in Fig. 3.3, we should note that the permeabilities, μ' and mu'' are not always constant. In case of high Q cavity, the cavity impedance is nearly zero except for the resonant frequency range. These models are consistent each other and good approximation

because we can assume the permeability is constant around the frequency where the cavity impedance is large. However, the cavity impedance is not negligible for wide range in case of a low Q cavity. We need to consider these two circuit model are not exactly same when we assume that the circuit parameters, that is, the inductance and the resistance are constant for all frequency range.

In the proton synchrotron the choice of the low Q magnetic core is probable in deed, the effects of the difference between the circuit model will affect to the beam-cavity interaction. So both cases will be shown latter sections to prove the effect of the difference.

3.2 Lumped Circuit Expression of Cavity

From the above discussion about expressing the magnetic loss, there are two models which present the rf cavity as the lumped circuit of the cavity. They are shown in Fig. 3.4.

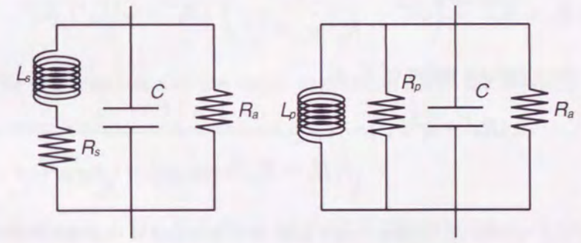

Figure 3.4: The lumped circuit model of the cavity. Parallel expression(a) and series expression(b).

Let us call the model (a) as "series expression" with respect to the magnetic loss of the core and (b) as "parallel expression". In Fig. 3.4, C is a capacitance of the cavity and R_a is an external resistance. Furthermore, the inductances of L_s and L_p are always constant over all frequency, and R_s and R_p are also regarded as the constant over all frequency for the simplicity, though the magnetic loss is changing depending on the frequency. The

value of R_s and R_p are selected at the resonant frequency as

$$R_s = \frac{\omega_{\rm rs} L_s}{Q} \tag{3.24}$$

$$R_p = \omega_{\rm rp} L_s Q \ . \tag{3.25}$$

3.2.1 Cavity in Series Expression

Next, the series expression in Fig. 3.4 (a) is adopted to the impedance of the cavity $Z_s(\omega)$ such as

$$\frac{1}{Z_s(\omega)} = \frac{1}{R_a} + \frac{1}{R_s + j\omega L_s} + j\omega C \ . \tag{3.26}$$

$$Z_s(\omega) = \frac{R_a(R_s+R_a)({R_s}^2+\omega^2{L_s}^2)}{(R_s+R_a)^2 + \left(\omega C - \dfrac{\omega L_s}{{R_s}^2+\omega^2{L_s}^2}\right)^2 ({R_s}^2+\omega^2{L_s}^2)^2{R_a}^2}$$
$$-j\frac{\left(\omega C - \dfrac{\omega L_s}{{R_s}^2+\omega^2{L_s}^2}\right)({R_s}^2+\omega^2{L_s}^2)R_a}{(R_s+R_a)^2 + \left(\omega C - \dfrac{\omega L_s}{{R_s}^2+\omega^2{L_s}^2}\right)^2 ({R_s}^2+\omega^2{L_s}^2)^2{R_a}^2} \ , \tag{3.27}$$

and we obtain the absolute value of Z_s as

$$|Z_s(\omega)| = R_a({R_s}^2+\omega^2{L_s}^2)\frac{1}{\sqrt{(R_s+R_a)^2 + \left(\omega C - \dfrac{\omega L_s}{{R_s}^2+\omega^2{L_s}^2}\right)^2}} \ . \tag{3.28}$$

The frequency $\omega_{\rm rs1}$ where $Z_s(\omega)$ becomes pure real number is derived from eq.(3.27) as

$${\omega_{\rm rs1}}^2 = \frac{1}{L_s C}\left(1 - \frac{C{R_s}^2}{L_s}\right) \ , \tag{3.29}$$

and the frequency $\omega_{\rm rs2}$ where $|Z_s(\omega)|$ becomes maximum is derived from eq.(3.28) as

$${\omega_{\rm rs2}}^2 = \frac{1}{L_s C}\left(\frac{R_s}{R_a} + 1\right) \ . \tag{3.30}$$

The feature of the series expression is that the frequency $\omega_{\rm rs1}$ is different from $\omega_{\rm rs2}$ as shown in Fig.3.5, so it makes the analysis of the cavity difficult. In the series expression, let us define the resonant frequency $\omega_{\rm rs}$ as

$${\omega_{\rm rs}}^2 = \frac{1}{L_s C}\left(\frac{R_s}{R_a} + 1\right) \ . \tag{3.31}$$

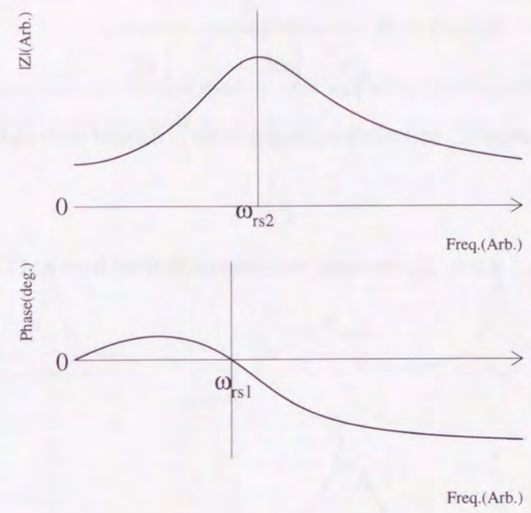

Figure 3.5: The characteristics of the series expression about the absolute value and the phase.

3.2.2 Cavity in Parallel Expression

The parallel expression in Fig. 3.4 (b) is adopted to the impedance of the cavity $Z_p(\omega)$ such as

$$\frac{1}{Z_p(\omega)} = \frac{1}{R_p} + \frac{1}{R_a} + \frac{1}{j\omega L_p} + j\omega C \tag{3.32}$$

$$= \frac{1}{R_p \frac{R_a}{R_p+R_a}} + \frac{1}{j\omega L_p} + j\omega C \ . \tag{3.33}$$

Using $R'_p = R_p \frac{R_a}{R_p+R_a}$,

$$Z_p(\omega) = \frac{R'_p}{1 + \left(\omega C - \dfrac{1}{\omega L_p}\right)^2 {R'_p}^2} - j\frac{\omega\left(\omega C - \dfrac{1}{\omega L_p}\right){R'_p}^2}{1 + \left(\omega C - \dfrac{1}{\omega L_p}\right)^2 {R'_p}^2} \ , \tag{3.34}$$

and we obtain the absolute value of Z_p as

$$|Z_p(\omega)| = R'_p \frac{1}{\sqrt{1 + \left(\omega C - \frac{1}{\omega L_p}\right) {R'_p}^2}} \ . \tag{3.35}$$

The frequency $\omega_{\rm rp1}$ where Z_p becomes pure real number is derived from eq.(3.34) as

$${\omega_{\rm rp1}}^2 = \frac{1}{L_p C} \ , \tag{3.36}$$

and the frequency $\omega_{\rm rp2}$ where $|Z_p|$ becomes maximum is derived from eq.(3.35) as

$${\omega_{\rm rp2}}^2 = \frac{1}{L_p C} \ . \tag{3.37}$$

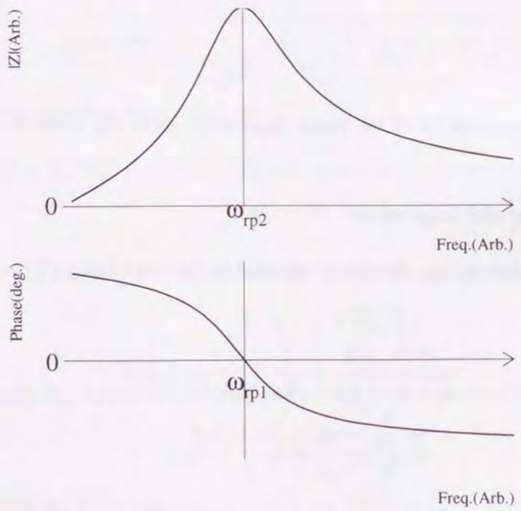

Figure 3.6: The impedance and the phase of the parallel expression.

The feature of the parallel expression is that the frequency $\omega_{\rm rp1}$ is equal to $\omega_{\rm rp2}$ as shown in Fig. 3.6, so it makes the analysis of the cavity easy. In the parallel expression,

let us define the resonant frequency $\omega_{\rm rp}$ as

$${\omega_{\rm rp}}^2 = \frac{1}{L_p C} \ . \tag{3.38}$$

Both expressions are consistent each other and good approximation for the high Q as shown in Fig.3.7 and 3.8, where the frequency $\omega_{\rm rs1}$ is close to $\omega_{\rm rs2}$.

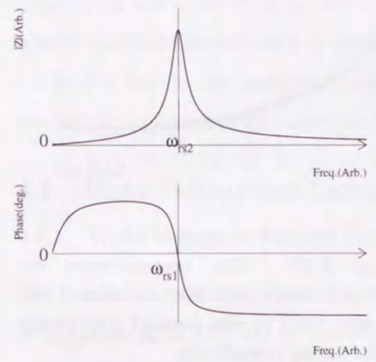

Figure 3.7: The impedance and the phase of the cavity in the series expression loaded with high Q magnetic core

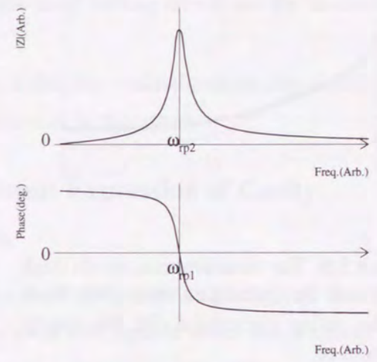

Figure 3.8: The impedance and the phase of the cavity in the parallel expression loaded with high Q magnetic core

But in very low Q region, the behavior of the series expression is different from a real cavity impedance. The Figure 3.9 shows the comparison between the measurement result of the rf cavity loaded with the magnetic alloy(see Appendix B) of $Q \sim 0.6$ and the analytical estimation using the series expression. Both absolute value of the impedance $|Z|$ and the phase of the analytical estimation are not similar to the measurement result.

On the other hand, they are similar in the parallel expression as shown in Fig. 3.10.

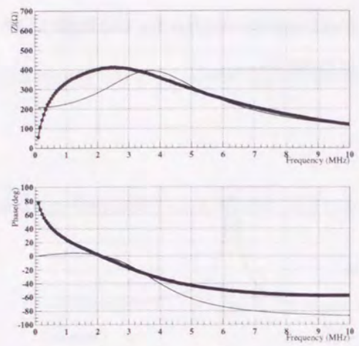

Figure 3.9: The measurement result(thick line) and the calculated result(thin line) in the series expression for the cavity impedance.

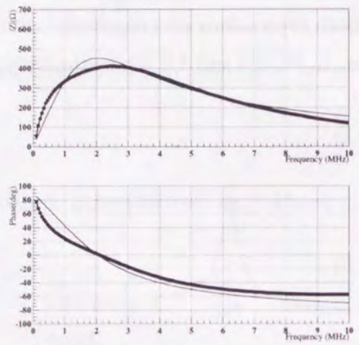

Figure 3.10: The measurement result(thick line) and the calculated result(thin line) in the parallel expression for the cavity impedance.

The reason why the estimation in series expression is different from the real cavity impedance is that we derived the lumped circuit model where the magnetic loss was always constant over the all frequency. However, we are interested in the impedance of the cavity near the resonant condition, and we want to investigate how the difference between the frequencies eq.(3.29) and (3.30) affects on the beam loading and the instability. Since the measurement result of the cavity impedance shows such frequency difference in practice, we will investigate the beam loading and the instability in both expressions.

4 Longitudinal beam dynamics with beam-cavity interaction

The rf cavity gives the energy to the particles through the electric field, but it should not be ignored that the particles also give the energy to the rf cavity through the electric field in high intensity case. The field induced by the particles is called "wake field". Especially in the high intensity proton synchrotron, the magnitude of the wake field becomes as same order as the one of the rf cavity, and it causes the beam loading effects and the instabilities which lead to the particle loss in the ring.

In this section, the analytical expression of the longitudinal motion associated with the interaction between the cavity and the beam will be described.

4.1 Wake Voltage and Lumped Circuit Expression of Cavity

4.1.1 Wake Voltage in Parallel Expression

The parallel expression as shown in Fig.3.4 (a) is adopted to the impedance of the cavity as $Z_p(\omega)$ in eq.(3.32). Let us consider that a point like particle which has a charge e is injected to the cavity. At a time $t = 0$, a point like charged particle $e\delta(t)$ passes through the cavity gap, the response of the cavity to the particle is expressed as

$$Z_p(s) = \frac{1}{C}\frac{s}{s^2 + \frac{1}{CR'_p} + \frac{1}{CL_p}}, \tag{4.1}$$

where s denotes a complex frequency. In order to know the time response of the gap voltage $V_p(t)$, the inverse Laplace transform is performed to the $Z_p(s)$ as

$$\begin{aligned} &V_p(t) \propto \mathcal{L}^{-1}[Z_p(s)] \\ &= \frac{1}{C} e^{-\frac{1}{2CR'_p}t}\left(\cos\sqrt{\frac{1}{CL_p} - \frac{1}{4C^2R'^2_p}}\cdot t - \frac{\frac{1}{2CR'_p}}{\sqrt{\frac{1}{CL_p} - \frac{1}{4C^2R'^2_p}}}\sin\sqrt{\frac{1}{CL_p} - \frac{1}{4C^2R'^2_p}}\cdot t\right). \end{aligned} \tag{4.2}$$

Now let us define the quality factor Q'_p of the cavity impedance for the parallel ex-

pression as

$$Q'_p = \frac{R'_p}{\omega_{\rm rp} L_p} \ , \tag{4.3}$$

and this Q'_p is different from Q.

Then, some important parameters in order to investigate the characteristics of $V_p(t)$ are defined as

$$\alpha_p = \frac{\omega_{\rm rp}}{2Q'_p} \tag{4.4}$$

$$\overline{\omega_p} = \omega_{\rm rp}\sqrt{1 - \frac{1}{4{Q'_p}^2}} \tag{4.5}$$

$$\tan\delta_p = -\frac{\alpha_p}{\overline{\omega_p}} \ . \tag{4.6}$$

Using equations (4.4),(4.5) and (4.6), the time response of the gap voltage $V_p(t)$ is rewritten as

$$V_p(t) \propto 2\alpha_p R'_p e^{-\alpha_p t}\left(\cos\overline{\omega_p}t - \frac{\alpha_p}{\overline{\omega_p}}\sin\overline{\omega_p}t\right) \tag{4.7}$$

$$= \frac{2\alpha R'_p}{\sqrt{1-\frac{1}{4{Q'_p}^2}}} e^{-\alpha_p t}\cos(\overline{\omega_p}t - \delta_p) \ . \tag{4.8}$$

As seen clearly, α_p is a damping constant, $\overline{\omega_p}$ is a frequency, and δ_p is an initial phase of $V_p(t)$, respectively.

The voltage $V_p(t)$, which causes "wake field" at the cavity gap, shows the characteristics of the damped oscillation as shown in Fig. 4.1, and the field at the cavity gap for the restoration force is disturbed during some periods according to the damping parameter α due to the beam-cavity interaction as shown in Fig. 4.2. As clearly seen, the amplitude of $V_p(t)$ depends on the effective resistance of the cavity R'_p and the quality factor Q', and the damping time depends on the quality factor Q'. By the way, the amplitude of $V_p(0)$ at the time $t = 0$, which is the influence of the wake field by itself, becomes $\alpha R'_p$ because

of the energy conservation low [19].

Figure 4.1: The wake voltage. A particle passes through the cavity gap at $t = 0$, then the wake field is excited and it is gradually damped. The amplitude and the damping time depends on the impedance of the cavity.

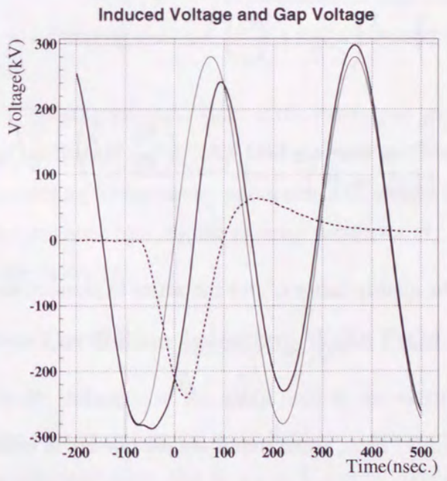

Figure 4.2: The example for the wake voltage(dotted line) and the nominal rf sinusoidal voltage(thin line). The beam is experienced the sum of both voltages(thick line).

4.1.2 Wake Field in Series Expression

Next, the series expression in Fig. 3.4 (b) is adopted to the impedance of the cavity as $Z_s(\omega)$ in eq.(3.26). Let us obtain the response of the cavity in the same way as the parallel expression. In a time at $t = 0$, a point like charged particle $e\delta(t)$ passes through the cavity gap, the response of the cavity to the particle is written as

$$Z_s(s) = \frac{1}{C} \frac{s + \dfrac{R_s}{L_s}}{s^2 + \left(\dfrac{1}{CR_a} + \dfrac{R_s}{L_s}\right) s + \dfrac{1}{CL_s}\left(\dfrac{R_s}{R_a} + 1\right)} . \tag{4.9}$$

In order to know the time response of the gap voltage $V_s(t)$, the inverse Laplace transform is performed to the $Z_s(s)$,

$$\begin{aligned} V_s(t) &\propto \mathcal{L}^{-1}[Z_s(s)] \\ &= \frac{1}{C} e^{-\frac{1}{2}\left(\frac{1}{CR_a} + \frac{R_s}{L_s}\right)t} \times \\ &\left(\cos \sqrt{\frac{1}{CL_s}\left(\frac{R_s}{R_a} + 1\right) - \frac{1}{4}\left(\frac{1}{CR_a} + \frac{R_s}{L_s}\right)^2} \cdot t \right. \\ &\left. - \frac{\frac{1}{CR_a} - \frac{R_s}{L_s}}{\sqrt{\frac{1}{CL_s}\left(\frac{R_s}{R_a} + 1\right) - \frac{1}{4}\left(\frac{1}{CR_a} + \frac{R_s}{L_s}\right)^2}} \sin \sqrt{\frac{1}{CL_s}\left(\frac{R_s}{R_a} + 1\right) - \frac{1}{4}\left(\frac{1}{CR_a} + \frac{R_s}{L_s}\right)^2} \cdot t \right) . \end{aligned} \tag{4.10}$$

Now let us define the quality factor Q'_s for the series expression as

$$Q'_s = \frac{\omega_{\mathrm{rs}} L_s}{\dfrac{L_s}{CR_a} + R_s} , \tag{4.11}$$

this Q'_s is different from Q. Then, some important parameters in order to investigate the

characteristics of the wake field are defined as

$$\alpha_s = \frac{\omega_{\mathrm{rs}}}{2Q'_s} , \tag{4.12}$$

$$\overline{\omega_s} = \omega_{\mathrm{rs}} \sqrt{1 - \frac{1}{4{Q'_s}^2}} \tag{4.13}$$

$$\tan \delta_s = -\frac{\alpha_s - \dfrac{R_s}{L_s}}{\overline{\omega_s}} \tag{4.14}$$

Using equations (4.12), (4.13) and (4.14), the time response of the gap voltage $V_s(t)$ is rewritten as

$$V_s(t) \propto \left(2\alpha_s R_a - R_a \frac{R_s}{L_s}\right) e^{-\alpha_s t} \left(\cos \overline{\omega_s} t - \frac{\alpha_s - \frac{R_s}{L_s}}{\overline{\omega_s}} \sin \overline{\omega_s} t \right) \tag{4.15}$$

$$= \left(2\alpha_s R_a - R_a \frac{R_s}{L_s}\right) \sqrt{1 + \frac{\left(\alpha_s - \dfrac{R_s}{L_s}\right)^2}{{\overline{\omega_{\mathrm{rs}}}}^2}} \times e^{-\alpha_s t} \cos(\overline{\omega_s} t - \delta_s) . \tag{4.16}$$

As seen clearly, α_s is a damping constant, $\overline{\omega_s}$ is a frequency, and δ_s is an initial phase of $V_s(t)$, respectively.

The voltage $V_s(t)$ causing the wake field at the cavity gap also shows the characteristics of the damped oscillation as Fig. 4.1, and the field at the cavity gap is disturbed during the period according to the cavity parameter. As clearly seen, the amplitude of $V_s(t)$ depends on the magnetic loss R_s, the external resistance R_a, and the damping time depends on the quality factor Q'_s.

4.2 Synchrotron Oscillation Including Wake Field

In order to consider the influence of the wake field to the synchrotron oscillation, the energy loss of the particles caused by the wake field should be included in eq.(2.5). Now, we investigate no acceleration case, that is, $\phi_s = 0$. Let us consider two bunches in the ring as shown in Fig. 4.3, the first one is set in the 1st bucket and the other is set in the k-th bucket, where the ring has h buckets. Supposing that the bunches circulate for $n+1$ turns since they were injected into the ring at the 1st turn, then the difference of the energy of

the bunch between the $n+1$-th and the n-th turns is

$$\Delta E_1 = eV\sin\phi_{1,n+1} - \sum_{m=0}^{n} eW_{1,m} - \sum_{m=0}^{n} eW_{2,m} \tag{4.17}$$

$$\Delta E_2 = eV\sin\phi_{2,n+1} - \sum_{m=0}^{n} eW_{2,m} - \sum_{m=0}^{n} eW_{1,m}\ , \tag{4.18}$$

where the suffix "1" and "2" denote the bunch number, "n" and "m" denote the turn number, and W is the wake voltage which is defined by eq.(4.8) or (4.16). The effect of the wake voltage is the summation made by each bunch in now and the past. For simplicity, let us use the standard representation for the wake voltage W as

$$W(t) = V_{\rm b0}e^{-\alpha t}\cos(\overline{\omega}t - \delta) \tag{4.19}$$

in order to apply any type of the cavity model, where $V_{\rm b0}$ is the amplitude of the wake voltage derived by substituting $t = 0$ into eq.(4.8) or (4.16).

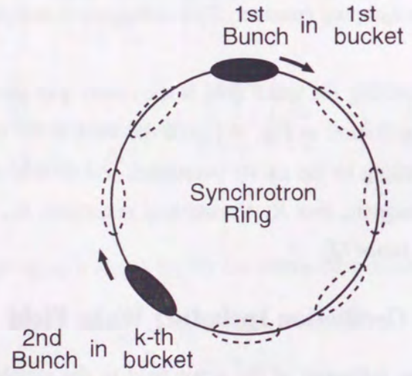

Figure 4.3: The configuration of the bunch filling.

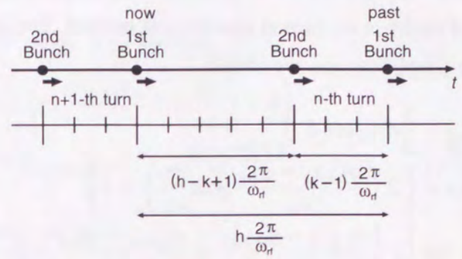

Figure 4.4: The time axis for the formalization.

Using eq.(4.19), the equation (4.17) and (4.18) are written as

$$\begin{aligned}
\Delta E_1 &= eV\sin\phi_{1,n+1} - \frac{1}{2}eV_{\rm b0}\cos\delta \\
&-eV_{\rm b0}\sum_{m=1}^{n} e^{-\alpha\left\{\frac{\phi_{1,n+1}-\phi_{1,m}}{\omega_{\rm rf}}+(n+1-m)h\frac{2\pi}{\omega_{\rm rf}}\right\}} \\
&\times\cos\left[\overline{\omega}\left\{\frac{\phi_{1,n+1}-\phi_{1,m}}{\omega_{\rm rf}}+(n+1-m)h\frac{2\pi}{\omega_{\rm rf}}\right\}-\delta\right] \\
&-eV_{\rm b0}\sum_{m=1}^{n} e^{-\alpha\left\{\frac{\phi_{1,n+1}-\phi_{2,m}}{\omega_{\rm rf}}-(k-1)\frac{2\pi}{\omega_{\rm rf}}+(n+1-m)h\frac{2\pi}{\omega_{\rm rf}}\right\}} \\
&\times\cos\left[\overline{\omega}\left\{\frac{\phi_{1,n+1}-\phi_{2,m}}{\omega_{\rm rf}}-(k-1)\frac{2\pi}{\omega_{\rm rf}}+(n+1-m)h\frac{2\pi}{\omega_{\rm rf}}\right\}-\delta\right]
\end{aligned} \tag{4.20}$$

$$\begin{aligned}
\Delta E_2 &= eV\sin\phi_{2,n+1} - \frac{1}{2}eV_{\rm b0}\cos\delta \\
&-eV_{\rm b0}\sum_{m=1}^{n} e^{-\alpha\left\{\frac{\phi_{2,n+1}-\phi_{2,m}}{\omega_{\rm rf}}+(n+1-m)h\frac{2\pi}{\omega_{\rm rf}}\right\}} \\
&\times\cos\left[\overline{\omega}\left\{\frac{\phi_{2,n+1}-\phi_{2,m}}{\omega_{\rm rf}}+(n+1-m)h\frac{2\pi}{\omega_{\rm rf}}\right\}-\delta\right] \\
&-eV_{\rm b0}\sum_{m=1}^{n} e^{-\alpha\left\{\frac{\phi_{2,n+1}-\phi_{1,m}}{\omega_{\rm rf}}-(h-k+1)\frac{2\pi}{\omega_{\rm rf}}+(n+1-m)h\frac{2\pi}{\omega_{\rm rf}}\right\}} \\
&\times\cos\left[\overline{\omega}\left\{\frac{\phi_{2,n+1}-\phi_{1,m}}{\omega_{\rm rf}}-(h-k+1)\frac{2\pi}{\omega_{\rm rf}}+(n+1-m)h\frac{2\pi}{\omega_{\rm rf}}\right\}-\delta\right]\ .
\end{aligned} \tag{4.21}$$

Since the equation (4.20) and (4.21) are so complicate, let us consider the simplification to

the summation terms by the fact that the wake field is damped quickly in a few revolution, which is true for the rf cavity in the proton synchrotron in deed. The details are described in Appendix C. After simplifications, we obtain

$$\begin{aligned}
\Delta E_1 &= eV\sin\phi_{1,n+1} - \frac{1}{2}eV_{\mathrm{b}0}\cos\delta \\
&-eV_{\mathrm{b}0}e^{-\alpha(h-k+1)\frac{2\pi}{\omega_{\mathrm{rf}}}}\cos\left\{\overline{\omega}\left(\frac{\phi_{1,n+1}-\phi_{1,n}}{\omega_{\mathrm{rf}}}+h\frac{2\pi}{\omega_{\mathrm{rf}}}\right)-\delta\right\} \\
&-eV_{\mathrm{b}0}e^{-\alpha(h-k+1)\frac{2\pi}{\omega_{\mathrm{rf}}}}\cos\left[\overline{\omega}\left\{\frac{\phi_{1,n+1}-\phi_{2,n+1}}{\omega_{\mathrm{rf}}}+\frac{\phi_{1,n+1}-\phi_{1,n}}{\omega_{\mathrm{rf}}}+(h-k+1)\frac{2\pi}{\omega_{\mathrm{rf}}}\right\}-\delta\right]
\end{aligned} \tag{4.22}$$

$$\begin{aligned}
\Delta E_2 &= eV\sin\phi_{2,n+1} - \frac{1}{2}eV_{\mathrm{b}0}\cos\delta \\
&-eV_{\mathrm{b}0}e^{-\alpha(k-1)\frac{2\pi}{\omega_{\mathrm{rf}}}}\cos\left\{\overline{\omega}\left(\frac{\phi_{2,n+1}-\phi_{2,n}}{\omega_{\mathrm{rf}}}+h\frac{2\pi}{\omega_{\mathrm{rf}}}\right)-\delta\right\} \\
&-eV_{\mathrm{b}0}e^{-\alpha(k-1)\frac{2\pi}{\omega_{\mathrm{rf}}}}\cos\left[\overline{\omega}\left\{\frac{\phi_{2,n+1}-\phi_{1,n+1}}{\omega_{\mathrm{rf}}}+\frac{\phi_{2,n+1}-\phi_{2,n}}{\omega_{\mathrm{rf}}}+(k-1)\frac{2\pi}{\omega_{\mathrm{rf}}}\right\}-\delta\right] .
\end{aligned} \tag{4.23}$$

Comparing eq.(4.22) and (4.23) with eq.(4.20) and (4.21), these simplifications mean that the wake voltage exists in the ring over two turns on each bunch, that is, the summation may be performed only on the $m = 1$ term in eq.(4.22) and (4.23). So the equation (4.22) and (4.23) are valid in such condition. After this, these equations become the basis of the analysis for the synchrotron oscillation including the wake voltage.

Since the equation (4.22) and (4.23) have a non-linear form for ϕ, let us consider to transform them into a linear one in order to investigate the motion of the bunch clearly.

Deriving following relations from eq.(2.8) such as

$$\frac{d\phi_1}{dt} = -\frac{2\pi h\eta}{\beta^2 E_s}\Delta E_1 = G\Delta E_1 , \tag{4.24}$$

$$\frac{d\phi_2}{dt} = -\frac{2\pi h\eta}{\beta^2 E_s}\Delta E_2 = G\Delta E_2 , \tag{4.25}$$

where $\phi_{1,n} = 0$ and $\phi_{2,n} = 0$ are chosen, so $\phi_{1,n+1} - \phi_{1,n} = \phi_1$ and $\phi_{2,n+1} - \phi_{2,n} = \phi_2$.

Substituting eq.(4.24) and (4.25) into eq.(4.22) and (4.23), respectively, we obtain

$$\begin{aligned}
&\frac{2\pi h}{\omega_{\mathrm{rf}}}\frac{d\Delta E_1}{dt} = eV\sin\phi_1 - \frac{1}{2}eV_{\mathrm{b}0}\cos\delta \\
&-eV_{\mathrm{b}0}e^{-\alpha h\frac{2\pi}{\omega_{\mathrm{rf}}}}\cos\left\{\overline{\omega}\left(\frac{G\Delta E_1}{\omega_{\mathrm{rf}}}+h\frac{2\pi}{\omega_{\mathrm{rf}}}\right)-\delta\right\} \\
&-eV_{\mathrm{b}0}e^{-\alpha(h-k+1)\frac{2\pi}{\omega_{\mathrm{rf}}}}\cos\left[\overline{\omega}\left\{\frac{\phi_1-\phi_2+G\Delta E_1}{\omega_{\mathrm{rf}}}+(h-k+1)\frac{2\pi}{\omega_{\mathrm{rf}}}\right\}-\delta\right] \\
&= eV\sin\phi_1 - \frac{1}{2}eV_{\mathrm{b}0}\cos\delta \\
&-eV_{\mathrm{b}0}e^{-\alpha h\frac{2\pi}{\omega_{\mathrm{rf}}}}\cos(G\Delta E_1)\cos\left\{\frac{\overline{\omega}-\omega_{\mathrm{rf}}}{\omega_{\mathrm{rf}}}(G\Delta E_1+2\pi h)-\delta\right\} \\
&+eV_{\mathrm{b}0}e^{-\alpha h\frac{2\pi}{\omega_{\mathrm{rf}}}}\sin(G\Delta E_1)\sin\left\{\frac{\overline{\omega}-\omega_{\mathrm{rf}}}{\omega_{\mathrm{rf}}}(G\Delta E_1+2\pi h)-\delta\right\} \\
&-eV_{\mathrm{b}0}e^{-\alpha(h-k+1)\frac{2\pi}{\omega_{\mathrm{rf}}}}\cos(\phi_1-\phi_2+G\Delta E_2)\cos\left[\frac{\overline{\omega}-\omega_{\mathrm{rf}}}{\omega_{\mathrm{rf}}}\{\phi_1-\phi_2+G\Delta E_2+2\pi(h-k+1)\}-\delta\right] \\
&+eV_{\mathrm{b}0}e^{-\alpha(h-k+1)\frac{2\pi}{\omega_{\mathrm{rf}}}}\sin(\phi_1-\phi_2+G\Delta E_2)\sin\left[\frac{\overline{\omega}-\omega_{\mathrm{rf}}}{\omega_{\mathrm{rf}}}\{\phi_1-\phi_2+G\Delta E_2+2\pi(h-k+1)\}-\delta\right]
\end{aligned} \tag{4.26}$$

$$\begin{aligned}
&\frac{2\pi h}{\omega_{\mathrm{rf}}}\frac{d\Delta E_2}{dt} = eV\sin\phi_2 - \frac{1}{2}eV_{\mathrm{b}0}\cos\delta \\
&-eV_{\mathrm{b}0}e^{-\alpha h\frac{2\pi}{\omega_{\mathrm{rf}}}}\cos\left\{\overline{\omega}\left(\frac{G\Delta E_2}{\omega_{\mathrm{rf}}}+h\frac{2\pi}{\omega_{\mathrm{rf}}}\right)-\delta\right\} \\
&-eV_{\mathrm{b}0}e^{-\alpha(k-1)\frac{2\pi}{\omega_{\mathrm{rf}}}}\cos\left[\overline{\omega}\left\{\frac{\phi_2-\phi_1+G\Delta E_2}{\omega_{\mathrm{rf}}}+(k-1)\frac{2\pi}{\omega_{\mathrm{rf}}}\right\}-\delta\right] \\
&= eV\sin\phi_2 - \frac{1}{2}eV_{\mathrm{b}0}\cos\delta \\
&-eV_{\mathrm{b}0}e^{-\alpha h\frac{2\pi}{\omega_{\mathrm{rf}}}}\cos(G\Delta E_2)\cos\left\{\frac{\overline{\omega}-\omega_{\mathrm{rf}}}{\omega_{\mathrm{rf}}}(G\Delta E_2+2\pi h)-\delta\right\} \\
&+eV_{\mathrm{b}0}e^{-\alpha h\frac{2\pi}{\omega_{\mathrm{rf}}}}\sin(G\Delta E_1)\sin\left\{\frac{\overline{\omega}-\omega_{\mathrm{rf}}}{\omega_{\mathrm{rf}}}(G\Delta E_2+2\pi h)-\delta\right\} \\
&-eV_{\mathrm{b}0}e^{-\alpha(k-1)\frac{2\pi}{\omega_{\mathrm{rf}}}}\cos(\phi_2-\phi_1+G\Delta E_1)\cos\left[\frac{\overline{\omega}-\omega_{\mathrm{rf}}}{\omega_{\mathrm{rf}}}\{\phi_2-\phi_1+G\Delta E_1+2\pi(k-1)\}-\delta\right] \\
&+eV_{\mathrm{b}0}e^{-\alpha(k-1)\frac{2\pi}{\omega_{\mathrm{rf}}}}\sin(\phi_2-\phi_1+G\Delta E_1)\sin\left[\frac{\overline{\omega}-\omega_{\mathrm{rf}}}{\omega_{\mathrm{rf}}}\{\phi_2-\phi_1+G\Delta E_1+2\pi(k-1)\}-\delta\right] .
\end{aligned} \tag{4.27}$$

These eq.(4.24), (4.26) and (4.25), (4.27) are simultaneous differential equations for

the synchrotron oscillation including the beam-cavity interaction.

4.2.1 Equilibrium Phase and Beam Loading

Now, let us define the "equilibrium phase", that is, the phases of ϕ_{1s} and ϕ_{2s} that satisfy $\Delta E_1 = 0$ and $\Delta E_2 = 0$, respectively. They are defined as follows;

$$\begin{aligned} eV\sin\phi_{1s} &= \frac{1}{2}eV_{b0}\cos\delta + eV_{b0}e^{-\alpha h\frac{2\pi}{\omega_{rf}}}\cos\left(\frac{\overline{\omega}-\omega_{rf}}{\omega_{rf}}2\pi h-\delta\right)\\ &+eV_{b0}e^{-\alpha(h-k+1)\frac{2\pi}{\omega_{rf}}}\cos(\phi_{1s}-\phi_{2s})\cos\left[\frac{\overline{\omega}-\omega_{rf}}{\omega_{rf}}\{\phi_{1s}-\phi_{2s}+2\pi(h-k+1)\}-\delta\right]\\ &-eV_{b0}e^{-\alpha(h-k+1)\frac{2\pi}{\omega_{rf}}}\sin(\phi_{1s}-\phi_{2s})\sin\left[\frac{\overline{\omega}-\omega_{rf}}{\omega_{rf}}\{\phi_{1s}-\phi_{2s}+2\pi(h-k+1)\}-\delta\right] \end{aligned} \tag{4.28}$$

$$\begin{aligned} eV\sin\phi_{2s} &= \frac{1}{2}eV_{b0}\cos\delta + eV_{b0}e^{-\alpha h\frac{2\pi}{\omega_{rf}}}\cos\left(\frac{\overline{\omega}-\omega_{rf}}{\omega_{rf}}2\pi h-\delta\right)\\ &+eV_{b0}e^{-\alpha(k-1)\frac{2\pi}{\omega_{rf}}}\cos(\phi_{2s}-\phi_{1s})\cos\left[\frac{\overline{\omega}-\omega_{rf}}{\omega_{rf}}\{\phi_{2s}-\phi_{1s}+2\pi(k-1)\}-\delta\right]\\ &-eV_{b0}e^{-\alpha(k-1)\frac{2\pi}{\omega_{rf}}}\sin(\phi_{2s}-\phi_{1s})\sin\left[\frac{\overline{\omega}-\omega_{rf}}{\omega_{rf}}\{\phi_{2s}-\phi_{1s}+2\pi(k-1)\}-\delta\right]. \end{aligned} \tag{4.29}$$

These equilibrium phases mean that the bunches don't lose the energy under the effect of the wake field as shown in Fig.4.5 if the bunches are just on those phases. Saying in other words, the continuous energy loss will occur on the bunches, then the particles may be lost if the bunches are on the different phases from the equilibrium ones. This effect is called "Beam Loading". In the high intensity synchrotron which has no empty bucket, the beam loading effect is compensated by changing the phase of the rf voltage, which make the condition of $\Delta E = 0$. However, it is not realized under a certain condition, and it will be described later in section 5.1 as "Periodic Transient Beam Loading".

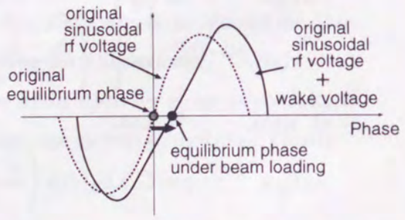

Figure 4.5: The equilibrium phase under the beam loading.

4.2.2 Small Amplitude Motion with respect to Equilibrium Phase

Next, let us consider the amplitude of the motion which is expected to oscillate around the equilibrium phase such as

$$\varphi_1 = \phi_1 - \phi_{1s}\ , \quad \varphi_2 = \phi_2 - \phi_{2s}\ , \tag{4.30}$$

where $\varphi_1 \ll 1$ and $\varphi_2 \ll 1$. Substituting eq.(4.30) into eq.(4.26) and (4.27), then also substituting eq.(4.28) and (4.29), we obtain

$$\begin{aligned} &\frac{2\pi h}{\omega_{rf}}\frac{d\Delta E_1}{dt} = eV\cos\phi_{1s}\sin\varphi_1\\ &+eV_{b0}e^{-\alpha h\frac{2\pi}{\omega_{rf}}}\sin(G\Delta E_1)\\ &\times\left\{\cos\left(\frac{\overline{\omega}-\omega_{rf}}{\omega_{rf}}2\pi h-\delta\right)\sin\left(\frac{\overline{\omega}-\omega_{rf}}{\omega_{rf}}G\Delta E_1\right)+\sin\left(\frac{\overline{\omega}-\omega_{rf}}{\omega_{rf}}2\pi h-\delta\right)\right\}\\ &-e^{-\alpha(h-k+1)\frac{2\pi}{\omega_{rf}}}\sin(G\Delta E_2+\varphi_1-\varphi_2)\\ &\times\left[-\sin(\phi_{1s}-\phi_{2s})\cos\left[\frac{\overline{\omega}-\omega_{rf}}{\omega_{rf}}\{\phi_{1s}-\phi_{2s}+2\pi(h-k+1)\}-\delta\right]\right.\\ &\left.-\cos(\phi_{1s}-\phi_{2s})\sin\left[\frac{\overline{\omega}-\omega_{rf}}{\omega_{rf}}\{\phi_{1s}-\phi_{2s}+2\pi(h-k+1)\}-\delta\right]\right]\\ &\times\sin\left\{\frac{\overline{\omega}-\omega_{rf}}{\omega_{rf}}(G\Delta E_2+\varphi_1-\varphi_2)\right\}\\ &+\sin(\phi_{1s}-\phi_{2s})\sin\left[\frac{\overline{\omega}-\omega_{rf}}{\omega_{rf}}\{\phi_{1s}-\phi_{2s}+2\pi(h-k+1)\}-\delta\right]\\ &\times\sin\left\{\frac{\overline{\omega}-\omega_{rf}}{\omega_{rf}}(G\Delta E_2+\varphi_1-\varphi_2)\right\}\Bigg] \end{aligned} \tag{4.31}$$

$$
\begin{aligned}
&\frac{2\pi h}{\omega_{\rm rf}}\frac{d\Delta E_2}{dt} = eV\cos\phi_{2\rm s}\sin\varphi_2 \\
&+eV_{\rm b0}e^{-\alpha h\frac{2\pi}{\omega_{\rm rf}}}\sin(G\Delta E_2) \\
&\times\left\{\cos\left(\frac{\overline{\omega}-\omega_{\rm rf}}{\omega_{\rm rf}}2\pi h-\delta\right)\sin\left(\frac{\overline{\omega}-\omega_{\rm rf}}{\omega_{\rm rf}}G\Delta E_2\right)+\sin\left(\frac{\overline{\omega}-\omega_{\rm rf}}{\omega_{\rm rf}}2\pi h-\delta\right)\right\} \\
&-e^{-\alpha(k-1)\frac{2\pi}{\omega_{\rm rf}}}\sin(G\Delta E_1+\varphi_2-\varphi_1) \\
&\times\left[-\sin(\phi_{2\rm s}-\phi_{1\rm s})\cos\left[\frac{\overline{\omega}-\omega_{\rm rf}}{\omega_{\rm rf}}\left\{\phi_{2\rm s}-\phi_{1\rm s}+2\pi(k-1)\right\}-\delta\right]\right. \\
&-\cos(\phi_{2\rm s}-\phi_{1\rm s})\sin\left[\frac{\overline{\omega}-\omega_{\rm rf}}{\omega_{\rm rf}}\left\{\phi_{2\rm s}-\phi_{1\rm s}+2\pi(k-1)\right\}-\delta\right] \\
&-\cos(\phi_{2\rm s}-\phi_{1\rm s})\cos\left[\frac{\overline{\omega}-\omega_{\rm rf}}{\omega_{\rm rf}}\left\{\phi_{2\rm s}-\phi_{1\rm s}+2\pi(k-1)\right\}-\delta\right] \\
&\times\sin\left\{\frac{\overline{\omega}-\omega_{\rm rf}}{\omega_{\rm rf}}(G\Delta E_1+\varphi_2-\varphi_1)\right\} \\
&+\sin(\phi_{2\rm s}-\phi_{1\rm s})\sin\left[\frac{\overline{\omega}-\omega_{\rm rf}}{\omega_{\rm rf}}\left\{\phi_{2\rm s}-\phi_{1\rm s}+2\pi(k-1)\right\}-\delta\right] \\
&\left.\times\sin\left\{\frac{\overline{\omega}-\omega_{\rm rf}}{\omega_{\rm rf}}(G\Delta E_1+\varphi_2-\varphi_1)\right\}\right] .
\end{aligned}
\tag{4.32}
$$

Differentiating eq. (4.24) and (4.25) on t, and substituting eq.(4.31) and (4.32) into them, finally we obtain two differential equations as follows;

$$
\begin{aligned}
&\frac{1}{G}\left(\frac{2\pi h}{\omega_{\rm rf}}\right)^2\frac{d^2\varphi_1}{dt^2} = [eV\cos\phi_{1\rm s} \\
&-eV_{\rm b0}e^{-\alpha(h-k+1)\frac{2\pi}{\omega_{\rm rf}}}\sin\left[\phi_{1\rm s}-\phi_{2\rm s}+\frac{\overline{\omega}-\omega_{\rm rf}}{\omega_{\rm rf}}\left\{\phi_{1\rm s}-\phi_{2\rm s}-2\pi(h-k+1)\right\}+\frac{\overline{\omega}-\omega_{\rm rf}}{\omega_{\rm rf}}2\pi h-\delta\right] \\
&-eV_{\rm b0}e^{-\alpha(h-k+1)\frac{2\pi}{\omega_{\rm rf}}}\cos\left[\phi_{1\rm s}-\phi_{2\rm s}+\frac{\overline{\omega}-\omega_{\rm rf}}{\omega_{\rm rf}}\left\{\phi_{1\rm s}-\phi_{2\rm s}-2\pi(h-k+1)\right\}+\frac{\overline{\omega}-\omega_{\rm rf}}{\omega_{\rm rf}}2\pi h-\delta\right] \\
&\times\left[\sin\frac{\overline{\omega}-\omega_{\rm rf}}{\omega_{\rm rf}}\varphi_1+\sin\frac{\overline{\omega}-\omega_{\rm rf}}{\omega_{\rm rf}}\left(\frac{2\pi h}{\omega_{\rm rf}}\frac{d\varphi_2}{dt}-\varphi_2\right)\right]\Bigg]\sin\varphi_1 \\
&+eV_{\rm b0}e^{-\alpha h\frac{2\pi}{\omega_{\rm rf}}}\left\{\sin\left(\frac{\overline{\omega}-\omega_{\rm rf}}{\omega_{\rm rf}}2\pi h-\delta\right)+\cos\left(\frac{\overline{\omega}-\omega_{\rm rf}}{\omega_{\rm rf}}2\pi h-\delta\right)\sin\left(\frac{\overline{\omega}-\omega_{\rm rf}}{\omega_{\rm rf}}\frac{2\pi h}{\omega_{\rm rf}}\frac{d\varphi_1}{dt}\right)\right\} \\
&\times\sin\left(\frac{2\pi h}{\omega_{\rm rf}}\frac{d\varphi_1}{dt}\right) \\
&+eV_{\rm b0}e^{-\alpha(h-k+1)\frac{2\pi}{\omega_{\rm rf}}}\sin\left[\phi_{1\rm s}-\phi_{2\rm s}+\frac{\overline{\omega}-\omega_{\rm rf}}{\omega_{\rm rf}}\left\{\phi_{1\rm s}-\phi_{2\rm s}-2\pi(h-k+1)\right\}+\frac{\overline{\omega}-\omega_{\rm rf}}{\omega_{\rm rf}}2\pi h-\delta\right] \\
&\times\sin\left(\frac{2\pi h}{\omega_{\rm rf}}\frac{d\varphi_2}{dt}-\varphi_2\right)
\end{aligned}
\tag{4.33}
$$

$$
\begin{aligned}
&\frac{1}{G}\left(\frac{2\pi h}{\omega_{\rm rf}}\right)^2\frac{d^2\varphi_2}{dt^2} = [eV\cos\phi_{2\rm s} \\
&-eV_{\rm b0}e^{-\alpha(k-1)\frac{2\pi}{\omega_{\rm rf}}}\sin\left[\phi_{2\rm s}-\phi_{1\rm s}+\frac{\overline{\omega}-\omega_{\rm rf}}{\omega_{\rm rf}}\left\{\phi_{2\rm s}-\phi_{1\rm s}-2\pi(k-1)\right\}+\frac{\overline{\omega}-\omega_{\rm rf}}{\omega_{\rm rf}}2\pi h-\delta\right] \\
&-eV_{\rm b0}e^{-\alpha(k-1)\frac{2\pi}{\omega_{\rm rf}}}\cos\left[\phi_{2\rm s}-\phi_{1\rm s}+\frac{\overline{\omega}-\omega_{\rm rf}}{\omega_{\rm rf}}\left\{\phi_{2\rm s}-\phi_{1\rm s}-2\pi(k-1)\right\}+\frac{\overline{\omega}-\omega_{\rm rf}}{\omega_{\rm rf}}2\pi h-\delta\right] \\
&\times\left[\sin\frac{\overline{\omega}-\omega_{\rm rf}}{\omega_{\rm rf}}\varphi_2+\sin\frac{\overline{\omega}-\omega_{\rm rf}}{\omega_{\rm rf}}\left(\frac{2\pi h}{\omega_{\rm rf}}\frac{d\varphi_2}{dt}-\varphi_1\right)\right]\Bigg]\sin\varphi_2 \\
&+eV_{\rm b0}e^{-\alpha h\frac{2\pi}{\omega_{\rm rf}}}\left\{\sin\left(\frac{\overline{\omega}-\omega_{\rm rf}}{\omega_{\rm rf}}2\pi h-\delta\right)+\cos\left(\frac{\overline{\omega}-\omega_{\rm rf}}{\omega_{\rm rf}}2\pi h-\delta\right)\sin\left(\frac{\overline{\omega}-\omega_{\rm rf}}{\omega_{\rm rf}}\frac{2\pi h}{\omega_{\rm rf}}\frac{d\varphi_1}{dt}\right)\right\} \\
&\times\sin\left(\frac{2\pi h}{\omega_{\rm rf}}\frac{d\varphi_2}{dt}\right) \\
&+eV_{\rm b0}e^{-\alpha(k-1)\frac{2\pi}{\omega_{\rm rf}}}\sin\left[\phi_{2\rm s}-\phi_{1\rm s}+\frac{\overline{\omega}-\omega_{\rm rf}}{\omega_{\rm rf}}\left\{\phi_{2\rm s}-\phi_{1\rm s}-2\pi(k-1)\right\}+\frac{\overline{\omega}-\omega_{\rm rf}}{\omega_{\rm rf}}2\pi h-\delta\right] \\
&\times\sin\left(\frac{2\pi h}{\omega_{\rm rf}}\frac{d\varphi_1}{dt}-\varphi_1\right) .
\end{aligned}
\tag{4.34}
$$

Translating eq.(4.33) and (4.34) easily to see,

$$\frac{d^2\varphi_1}{dt^2} + A_1(t)\sin\left(\frac{2\pi h}{\omega_{\rm rf}}\frac{d\varphi_1}{dt}\right) + B_1(t)\sin\left(\frac{d\varphi_2}{dt} - \varphi_2\right) + C_1(t)\sin\varphi_1 = 0 \quad (4.35)$$

$$\frac{d^2\varphi_2}{dt^2} + A_2(t)\sin\left(\frac{2\pi h}{\omega_{\rm rf}}\frac{d\varphi_1}{dt}\right) + B_2(t)\sin\left(\frac{d\varphi_1}{dt} - \varphi_1\right) + C_2(t)\sin\varphi_2 = 0 \quad (4.36)$$

As clearly seen, the equations (4.35) and (4.36) are differential ones which show the non-linear coupled oscillators with damped systems. Furthermore, since the coefficients of each variable are varying with the time, these systems include the aspect of "parametric oscillation", which is complicated to understand the motions. So we neglect the time dependent terms in $A(t)$,$B(t)$ and $C(t)$, because they have a form $\frac{d\varphi}{dt} \sim G\Delta E$, which is very small rather than $\frac{\overline{\omega}-\omega_{\rm rf}}{\omega_{\rm rf}}2\pi h - \delta$. Using such assumptions and the linear approximation for $\varphi \ll 1$, we obtain linear simultaneous equation as

$$\begin{aligned}
\frac{d^2\varphi_1}{dt^2} &= -\frac{eV\eta\omega_{\rm rf}\cos\phi_{1\rm s}}{\beta^2 E_s T_{\rm rev}}\varphi_1 \\
&-\frac{eV_{\rm b0}\eta\omega_{\rm rf}}{\beta^2 E_s}e^{-\alpha h\frac{2\pi}{\omega_{\rm rf}}}\sin\left(\frac{\overline{\omega}-\omega_{\rm rf}}{\omega_{\rm rf}}2\pi h - \delta\right)\frac{d\varphi_1}{dt} \\
&-\frac{eV_{\rm b0}\eta{\omega_{\rm rf}}^2}{2\pi h\beta^2 E_s}e^{-\alpha(h-k+1)\frac{2\pi}{\omega_{\rm rf}}} \\
&\times\sin\left[(\phi_{1\rm s}-\phi_{2\rm s}) - \frac{\overline{\omega}-\omega_{\rm rf}}{\omega_{\rm rf}}\left\{(\phi_{1\rm s}-\phi_{2\rm s}) + 2\pi(h-k+1)\right\} + \delta\right](\varphi_1-\varphi_2) \\
&+\frac{eV_{\rm b0}\eta{\omega_{\rm rf}}^2}{2\pi h\beta^2 E_s}e^{-\alpha(h-k+1)\frac{2\pi}{\omega_{\rm rf}}}\sin(\phi_{1\rm s}-\phi_{2\rm s}) \\
&\times\sin\left[\frac{\overline{\omega}-\omega_{\rm rf}}{\omega_{\rm rf}}\left\{(\phi_{1\rm s}-\phi_{2\rm s}) + 2\pi(h-k+1)\right\} - \delta\right](\varphi_1-\varphi_2) \\
&-\frac{eV_{\rm b0}\eta\omega_{\rm rf}}{\beta^2 E_s}e^{-\alpha(h-k+1)\frac{2\pi}{\omega_{\rm rf}}} \\
&\times\sin\left[(\phi_{1\rm s}-\phi_{2\rm s}) - \frac{\overline{\omega}-\omega_{\rm rf}}{\omega_{\rm rf}}\left\{(\phi_{1\rm s}-\phi_{2\rm s}) + 2\pi(h-k+1)\right\} + \delta\right]\frac{d\varphi_2}{dt} \\
&+\frac{eV_{\rm b0}\eta\omega_{\rm rf}}{\beta^2 E_s}e^{-\alpha(h-k+1)\frac{2\pi}{\omega_{\rm rf}}}\sin(\phi_{1\rm s}-\phi_{2\rm s}) \\
&\times\sin\left[\frac{\overline{\omega}-\omega_{\rm rf}}{\omega_{\rm rf}}\left\{(\phi_{1\rm s}-\phi_{2\rm s}) + 2\pi(h-k+1)\right\} - \delta\right]\frac{d\varphi_2}{dt} \qquad (4.37)
\end{aligned}$$

$$\begin{aligned}
\frac{d^2\varphi_2}{dt^2} &= -\frac{eV\eta\omega_{\rm rf}\cos\phi_{2\rm s}}{\beta^2 E_s T_{\rm rev}}\varphi_2 \\
&-\frac{eV_{\rm b0}\eta\omega_{\rm rf}}{\beta^2 E_s}e^{-\alpha h\frac{2\pi}{\omega_{\rm rf}}}\sin\left(\frac{\overline{\omega}-\omega_{\rm rf}}{\omega_{\rm rf}}2\pi h - \delta\right)\frac{d\varphi_2}{dt} \\
&-\frac{eV_{\rm b0}\eta{\omega_{\rm rf}}^2}{2\pi h\beta^2 E_s}e^{-\alpha(k-1)\frac{2\pi}{\omega_{\rm rf}}} \\
&\times\sin\left[(\phi_{2\rm s}-\phi_{1\rm s}) - \frac{\overline{\omega}-\omega_{\rm rf}}{\omega_{\rm rf}}\left\{(\phi_{2\rm s}-\phi_{1\rm s}) + 2\pi(k-1)\right\} + \delta\right](\varphi_2-\varphi_1) \\
&+\frac{eV_{\rm b0}\eta{\omega_{\rm rf}}^2}{2\pi h\beta^2 E_s}e^{-\alpha(k-1)\frac{2\pi}{\omega_{\rm rf}}}\sin(\phi_{2\rm s}-\phi_{1\rm s}) \\
&\times\sin\left[\frac{\overline{\omega}-\omega_{\rm rf}}{\omega_{\rm rf}}\left\{(\phi_{2\rm s}-\phi_{1\rm s}) + 2\pi(k-1)\right\} - \delta\right](\varphi_2-\varphi_1) \\
&-\frac{eV_{\rm b0}\eta\omega_{\rm rf}}{\beta^2 E_s}e^{-\alpha(k-1)\frac{2\pi}{\omega_{\rm rf}}} \\
&\times\sin\left[(\phi_{2\rm s}-\phi_{1\rm s}) - \frac{\overline{\omega}-\omega_{\rm rf}}{\omega_{\rm rf}}\left\{(\phi_{2\rm s}-\phi_{1\rm s}) + 2\pi(k-1)\right\} + \delta\right]\frac{d\varphi_1}{dt} \\
&+\frac{eV_{\rm b0}\eta\omega_{\rm rf}}{\beta^2 E_s}e^{-\alpha(k-1)\frac{2\pi}{\omega_{\rm rf}}}\sin(\phi_{2\rm s}-\phi_{1\rm s}) \\
&\times\sin\left[\frac{\overline{\omega}-\omega_{\rm rf}}{\omega_{\rm rf}}\left\{(\phi_{2\rm s}-\phi_{1\rm s}) + 2\pi(k-1)\right\} - \delta\right]\frac{d\varphi_1}{dt}\,. \qquad (4.38)
\end{aligned}$$

These equations are fundamental ones to investigate the synchrotron oscillation including the beam-cavity interaction. The explanations and the analyses are described in section 6.

5 Transient Beam Loading

In the previous section, the longitudinal particle motion with the beam-cavity interaction was derived approximately for proton synchrotron, and the energy loss of the particle caused by the wake field was derived as "beam loading". In this section, the behavior of the beam loading under the transient condition will be described and the experimental studied of the beam loading also will be described.

5.1 Periodic Transient Beam Loading

Usually the beam loading effects are analyzed under the "static" condition that the bunches are filled symmetrically as shown in Fig.5.1.

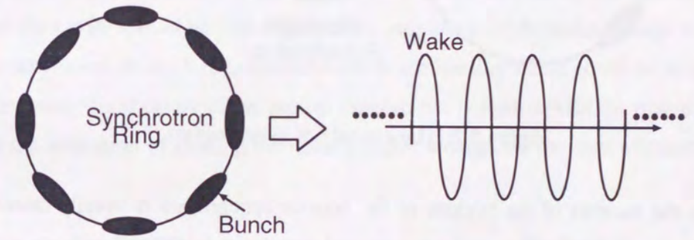

Figure 5.1: The static beam loading. The amplitude of the wake field are same on all bunches.

In this case, the amplitude of the wake voltage becomes same on all bunches, so the energy loss of the bunch becomes same on them. It is called "static beam loading", and the equilibrium phases, for example, at two bunches case as shown in eq.(4.28) and (4.29), are of course same one on all bunches. In order to compensate the energy loss, the phase of the rf field should be change as expressed in eq.(4.28)=(4.29), then all bunches are guaranteed to avoid the beam loading.

On the other hand, there is a peculiar case at the high energy proton synchrotron.

Since the particles are bend by the magnetic field, the particle energy which can be achieved on a synchrotron is limited by the field strength of the magnet. In the ordinary

process, the proton is accelerated by a linac at several decades$\sim$ hundreds MeV firstly, then injected into a synchrotron(booster synchrotron). However, since the mass of the proton is heavy and its momentum is changing greatly up to a few GeV, the proton can be accelerated up to such energy because of the limitation of the range of the magnet field. So another synchrotron(main synchrotron) must be prepared to accelerate the proton over a few GeV as shown in Fig.5.2.

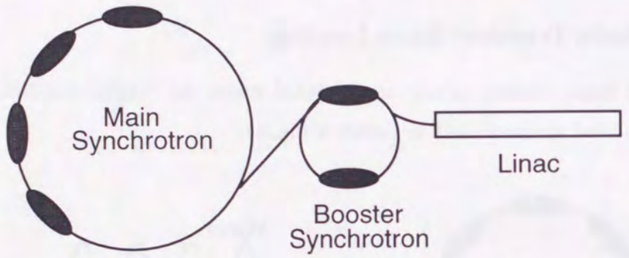

Figure 5.2: The cascade of synchrotrons.

Since the number of the buckets of the booster synchrotron is usually smaller than that of the main synchrotron, and since several decades to hundreds msec are needed to accelerate the bunch at the booster synchrotron, it is happened that the buckets of main synchrotron are not filled at all as shown in Fig. 5.3.

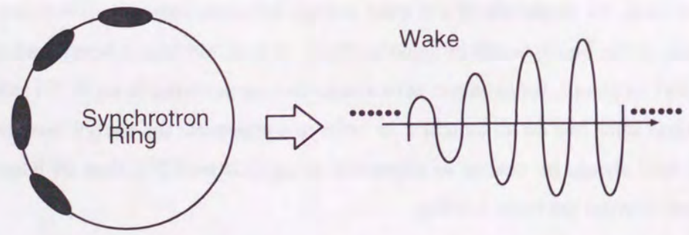

Figure 5.3: The periodic transient beam loading. The amplitude of the wake field are different on each bunch.

In this case, the amplitude of the wake field will not becomes same on all bunches, so the energy loss of the bunch will be different on each bunch. It is called "transient beam loading". Furthermore, the transient condition is periodically continued until the buckets are filled symmetrically in the main synchrotron, it is called "periodic transient beam loading" especially.

Since the amplitude of the wake field on each bunch is not same any more, the equilibrium phases, for example, at two bunches case as shown in eq.(4.28) and (4.29), become different on them. So uniform change of the phase of the rf voltage can not guarantee the stable acceleration under the periodic transient beam loading.

5.2 Calculation of Transient Beam Loading

In the past, it was considered to suppress the transient beam loading that that the quality factor of the cavity should be high [7], then the amplitude of the wake voltage was made small as expressed in eq.(4.19), naturally any beam loading effect could be suppressed. However, since the rf cavity of the proton synchrotron is loaded with the magnetic core, there is the limitation of making the quality factor so high by the characteristics of the core.

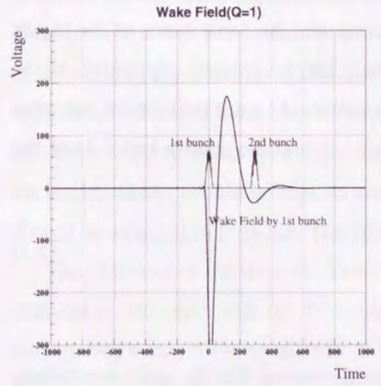

Figure 5.4: The wake field caused by $Q = 1$ cavity.

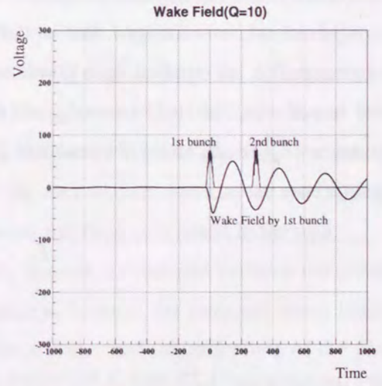

Figure 5.5: The wake field caused by $Q = 10$ cavity.

On the other hand, another method to suppress the transient effect is found. Since the transient effect is caused by overlapping the wake voltage of each bunch, if the wake field is damped quickly enough that the wake field of a bunch will not remain on the next bunch, then no transient effect will be vanished. It is the case that the quality factor of the cavity is very small as shown in Fig.5.4.

In order to investigate such a thing, the equilibrium phases expressed in eq.(4.28) and (4.29) were calculated for the case listed in Table 5.1.

harmonic number	4
number of bunch	2
number of particles per bunch	1.0×10^{13}
revolution freq.	858.9 kHz
gap voltage	420 kV
peak impedance of cavity	10 kΩ
resonant freq. of cavity	3.436 MHz

Table 5.1: The condition of the calculation for the equilibrium phase.

In these calculations, the impedance of the cavity was supposed that the peak value of the impedance and the resonant frequency were made constant, then the quality factor of the magnetic core was changed, that is, the inductance and the capacitance of the cavity were changed to be satisfied such conditions. Then, for the parallel expression of the cavity impedance, the inductance L_p and the capacitance C were derived by the peak impedance $|Z_p| = R_p$ using the resonant frequency $\omega_{\rm rp}$ and the quality factor Q of the magnetic core as

$$L_p = \frac{R_p}{\omega_{\rm rp} Q} \tag{5.1}$$

$$C = \frac{1}{{\omega_{\rm rp}}^2 L_p}\ , \tag{5.2}$$

where the equation (3.25) and (3.38) were used in the derivation. For the series expression, the inductance L_s, the capacitance C and the magnetic loss R_s were derived by the peak impedance $|Z_s|$ using the resonant frequency $\omega_{\rm rs}$ and the quality factor Q of the magnetic

core as

$$R_s = \frac{|Z_s|}{Q\sqrt{1+Q^2}} \tag{5.3}$$

$$L_s = \frac{R_s Q}{\omega_{\rm rs}} \tag{5.4}$$

$$C = \frac{1}{{\omega_{\rm rs}}^2 L_s}\ , \tag{5.5}$$

where the equation (3.24) and (3.31) were used in the derivation. These equations were derived without the external resistance R_a in Fig. 3.4.

The Figure 5.7 and 5.8 show the calculation results of the equilibrium phase of two bunches for the case the bunches are filled in non-symmetric configuration in the ring. The parallel expression of the cavity impedance was used in the calculation for Fig. 5.7 and the series one was used in the calculation for Fig. 5.8.

The horizontal axis is the quality factor of the magnetic core and the vertical axis is the equilibrium phase(upper graph) and the difference of the equilibrium phase(lower graph) expressed as the time $\phi_{\rm s}/\omega_{\rm rf}$.

As can be clearly seen, the equilibrium phase of each bunch became small at high Q region because since the amplitude of the wake voltage itself was made small and it also leads that the summation of the wake voltage by many bunches is made small. Furthermore, it was found that the transient effect, which was measured by the difference of the equilibrium phase, was also small in the low Q region. Then the difference of the equilibrium phase of each bunch became maximum around $Q \sim h/2$. So it was found that there were two choices about suppressing the transient beam loading, one was that the quality factor should be high as known so far, and another was that the quality factor should be as small as possible. The latter case has not been concerned in the past.

The behavior of the transient beam loading was not so changed between the parallel expression and series one on the cavity impedance because the transient beam loading almost depended on the amplitude of the wake voltage, and the difference of the phase was not so contributed to it.

Of course, since the amplitude of the wake voltage is so high at the low Q region as shown in Fig.5.4, and since the bunch is spread to some extent which is not expressed

at the rigid bunch model, the particles in a bunch apart from the center are affected by such high wake voltage. In order to avoid such disturbance at the low Q region, the beam loading compensation scheme as shown in section 5.5 is valid because of the quick response of the cavity.

Figure 5.6: The non-symmetric configuration of the bunch filling.

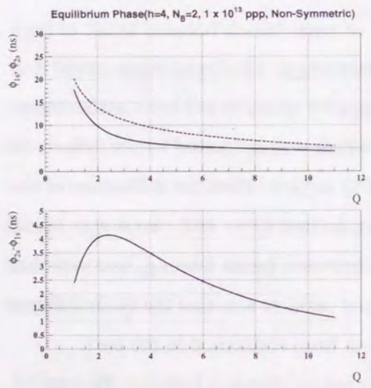

Figure 5.7: The calculation result of the transient beam loading in non-symmetric bunch filling using the parallel expression.

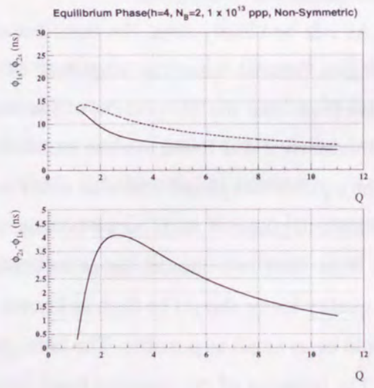

Figure 5.8: The calculation result of the transient beam loading in non-symmetric bunch filling using the series expression.

Furthermore, there is better scheme to avoid periodic transient beam loading. It is the case that the bunches are filled in symmetric configuration in the ring as shown in Fig. 5.9.

The calculation results for such case are also shown in Fig. 5.10 for the parallel expression and in Fig. 5.11 for the series expression of the cavity impedance, respectively, and the difference of the equilibrium phase on each bunch became always zero on all quality factors of the magnetic core, so the transient effects could not be occurred.

Figure 5.9: The symmetric configuration of the bunch filling.

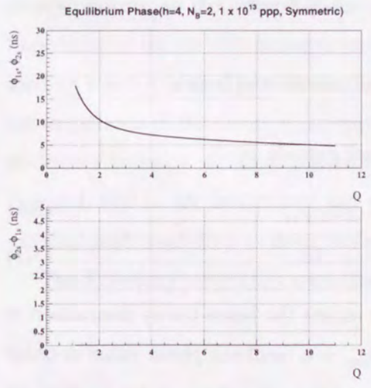

Figure 5.10: The calculation result of the transient beam loading in symmetric bunch filling using the parallel expression.

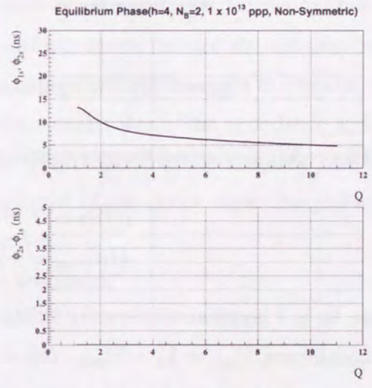

Figure 5.11: The calculation result of the transient beam loading in symmetric bunch filling using the series expression.

5.3 Multi-bunch Particle Tracking

Since the bunch is spread to some extent, the particles which are apart from the center of the bunch are affected by the different wake voltage from that at the center as shown in Fig.5.12. In order to investigate the transient beam loading in such a practical condition, we have also developed a multi-particle/multi-bunch simulation code in the longitudinal motion.

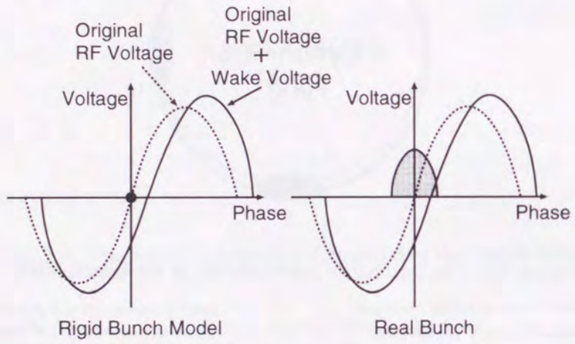

Figure 5.12: The rigid bunch model and the real bunch.

This code calculates difference equations for each particle as

$$(\delta E)_{\text{turn}} = eV_{\text{gap}}(\phi) - eV_0(\phi_{\text{s}}) \tag{5.6}$$

$$(\delta\phi)_{\text{turn}} = -2\pi h\eta\frac{\Delta p}{p} + \Delta\phi, \tag{5.7}$$

where V_0 is a nominal accelerating voltage which means the beam-cavity interaction is not considered, $V_{\text{gap}} = V_0 - V_{\text{wake}}$, $\Delta\phi = \phi_{\text{b}} - \phi_{\text{gap}}$ is a feedback phase value in order to suppress the beam loading by adjusting the phase of the gap voltage to the equilibrium phase, where ϕ_{b} and ϕ_{gap} are the phase of the bunch center and that of the gap voltage, respectively.

The wake voltage V_{wake} is obtained with a frequency domain as

$$V_{\text{wake}}(\omega) = Z_{\text{cav}}(\omega) \times I_{\text{b}}(\omega), \tag{5.8}$$

where $V_{\text{wake}}(\omega)$ is the wake voltage on the frequency ω component, I_{b} is the beam current on the frequency ω component, and $Z_{\text{cav}}(\omega)$ is an impedance of the rf cavity. In eq.(5.8), $I_{\text{b}}(\omega)$ is obtained by a Fourier transformation based on a revolution frequency for the particle distribution in time $I_{\text{b}}(t)$ as

$$I_{\text{b}}(N\omega_{\text{rev}}) = \frac{2\pi}{\omega_{\text{rev}}}\int_{-\frac{\pi}{\omega_{\text{rev}}}}^{\frac{\pi}{\omega_{\text{rev}}}} I_{\text{b}}(t)e^{-j(N\omega_{\text{rev}})t}dt\ . \tag{5.9}$$

The wake voltage $V_{\text{wake}}(\omega)$ in eq. (5.8) is transformed to the time domain voltage $V_{\text{wake}}(t)$ through an inverse Fourier transformation,

$$V_{\text{wake}}(t) = \sum_N V_{\text{wake}}(N\omega_{\text{rev}})e^{-iN\omega_{\text{rev}}t} \tag{5.10}$$
$$(N = 1, 2, 3, \cdots)\ .$$

This wake voltage is consistent with (4.2) and (4.10) because the Laplace transformation becomes the Fourier transformation in the periodic condition.

In this simulation, eight bunches were filled in 17 buckets, and therefore there were empty buckets, so the beam had many harmonics of the revolution frequency, and the impedance of the cavity was employed the parallel expression because the transient beam loading was not so change between the parallel expression and the series expression, and the impedance of the cavity was supposed that the peak value of the impedance and the resonant frequency are made constant, then the quality factor of the magnetic core was changed, that is, the inductance and the capacitance of the cavity were changed to be satisfied such conditions as described in section 5.2.

The following parameters were used in this simulation.

Ring Circumference	1445 m
Nominal Accelerating Voltage V_0	280 kV
Harmonic Number	17
Initial Revolution Frequency	201.5 kHz
Initial Energy	3 GeV
Initial $\Delta p/p$	$\pm$ 0.4 %
Initial Bunch Length	120 nsec.
Bunch Shape	Parabola
Synchronous Phase ϕ_s	0 Deg.
Momentum Compaction Factor $\alpha_{\rm p}$	-0.001
Number of Particle per Bunch	1.25×10^{13}

Table 5.2: Simulation parameters.

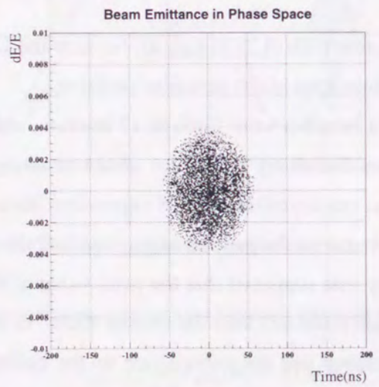

Figure 5.13: Initial beam emittance used in the simulation.

The Figure 5.13 shows an initial beam emittance in the longitudinal phase space, and 5000 macro particles, where each particle had 2.5×10^9 coulomb charge, were used in this simulation.

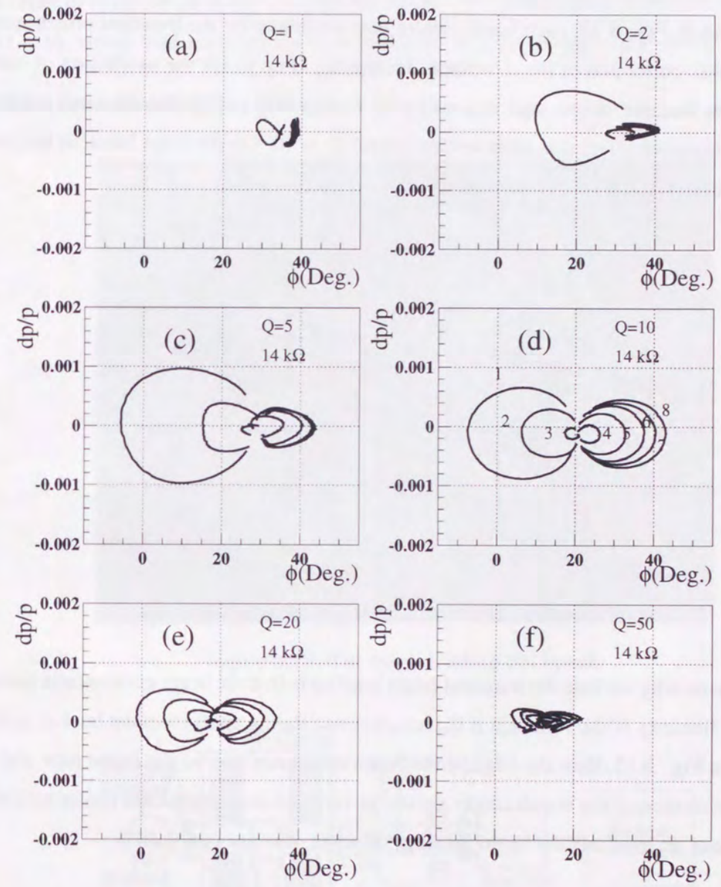

Figure 5.14: Trajectory of the bunch center in the longitudinal phase space.

The Figure 5.14 shows the Q-dependence of the transient effects. Beam intensity was same in all Q value, 1.25×10^{13} particles per bunch, and shunt impedance was 14 kΩ.

In Fig. 5.14, each line shows a trajectory of a bunch center in the longitudinal phase

space. Vertical axis and horizontal axis are momentum difference and the phase measured from the nominal synchronous particle, respectively, which is free from any beam loading.

As shown in Fig. 5.14, each bunch center was oscillated by the transient effect apart from the phase correction of the rf voltage. Increasing Q up to 10, the oscillation of each bunch center became larger, and increasing Q further, the oscillation became smaller again. The transient effect was most severe around $Q = 10$. On the other hand, in the low Q case the transient effect was very small.

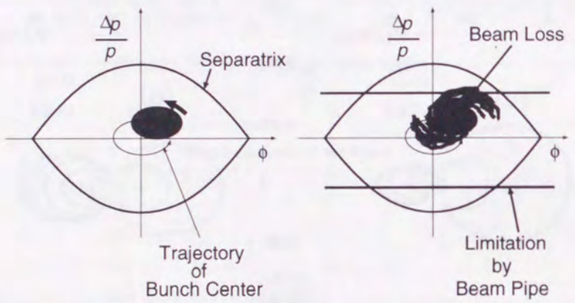

Figure 5.15: The beam emittance growth and beam loss.

The reason why we hate the transient beam loading is that the beam emittance is grown by the non-linearity of the rf bucket if the bunch is oscillating apart from the bucket center as shown in Fig. 5.15, then the edge of the beam emittance hits on the beam pipe and is lost. So the motion of the bunch center should be retained near the bucket center to avoid the beam loss. In the transient beam loading, however, it is not guaranteed.

5.4 Experiment of Transient Beam Loading

In order to examine the beam loading effects, we have developed a test bench as shown in Fig.5.16, where high intensity electron beam can be injected into the rf cavity in deed.

5.4.1 Beam Loading Test Bench

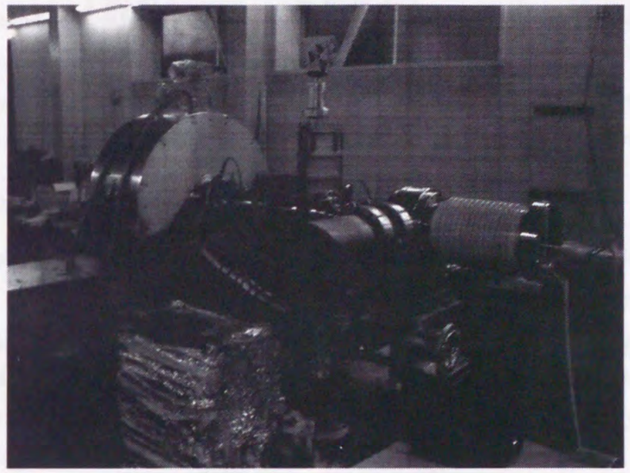

Figure 5.16: The beam loading test bench.

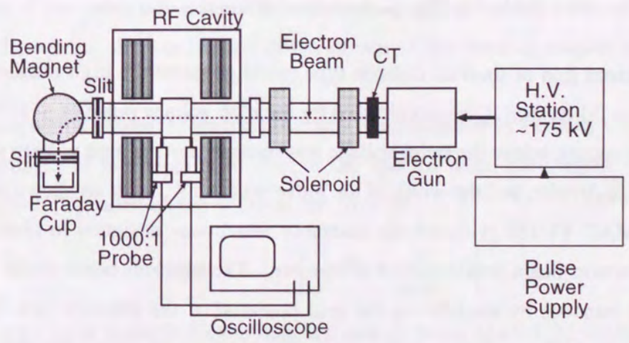

Figure 5.17: The Schematic view of the beam loading test bench.

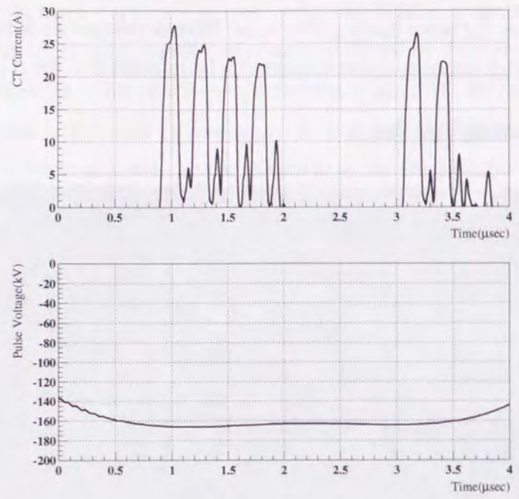

Figure 5.18: An example of the bunch shape and the high voltage pulse.

Beam Energy	$\sim$ 175 kV
Beam Intensity	$\sim$ 30 A
Bunch Width	100 ns $\sim$
Bunch Separation	200 ns $\sim$

Table 5.3: The performance of the electron gun.

The electron gun of thermal cathode type could generate the high intensity electron beam up to $\sim$ 30 A, then it was accelerated by the high voltage pulse of $\sim$ 175 kV by the pulse power supply, where the pulse voltage was measured in the high voltage transformer by the voltage divider, and the width of the pulse was about 3 μsec as shown in Fig. 5.18

The EIMAC YU156 grid-cathode assembly which was designed to obtain the high intensity electron beam was installed in the gun. The electron beam could be divided into several bunches by modulating the grid potential of the electron tube by the high voltage FET(Field Effect Transistor) switch. The Figure 5.18 shows the generated electron bunches measured by the Fast Current Transformer(FCT), which is very wide-band

type(1 MHz$\sim$1GHz), located between the electron gun and the cavity. Some parameters about the beam are listed in Table 5.3.

The bunched electron beam was focused by solenoids not to spread by the self space charge, then injected into the cavity. The wake voltage at the cavity gap could be measured by the 1000:1 high voltage probe directly, as shown in Fig.5.17.

Furthermore, the energy of the beam could be measured at the downstream of the cavity by simple spectrometer which consisted of a bending magnet and two slits located at upper-stream and downstream of the bending magnet, also as shown in Fig.5.17. Since the cavity gap could be shorted electrically, the energy loss of the beam at the cavity gap could be measured by comparing between "gap short"case and "gap open" one.

5.4.2 Measurement Procedure

We have measured the transient beam loading on the rf cavity. To begin with, the impedance of the cavity was measured and its quality factor was defined beforehand. The parallel expression of the cavity impedance was used to define the quality factor and the peak impedance of the cavity. The quality factor could be controlled keeping the resonant frequency constant by changing the radial gap of the cut core and the added capacitance at the cavity gap as shown in Appendix B.

Then, the high intensity electron beam was injected into the cavity. In order to evaluate the effect of the cavity impedance, there was a gap shot relay in the cavity. On the downstream of the cavity, there was the first beam slit which has the width of 1mm. Furthermore, the second slit was located down-stream of the bending magnet as shown in Fig. 5.17.

The beam which passed through the two slits was measured by Faraday Cup Changing the field strength of the bending magnet at the spectrometer, the current $I_{\rm fc}$ was also changing which depended on the width of the slit a as

$$I_{\rm fc}(B) = 1 - \left| \frac{p}{ae{B_0}^3} B^2 - \frac{p}{ae{B_0}^2} B \right| , \tag{5.11}$$

where B_0 is the field strength for the matched energy beam against the double slit passing. The example of the measured Faraday Cup signal is shown in Fig.5.19. Each peak

indicates the current by each bunch. Then, the current peak is regarded as the energy beam.

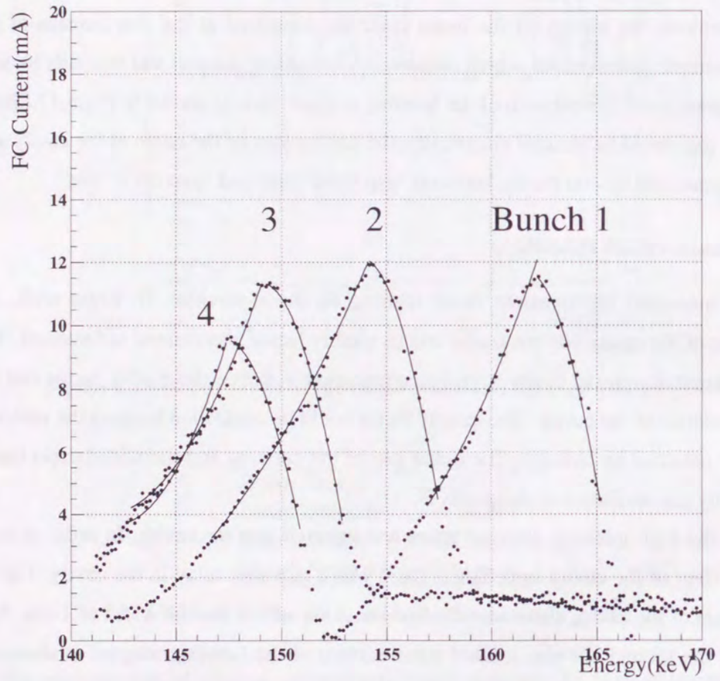

Figure 5.19: The measured signal at the Faraday Cup for four bunches.

In order to investigate the quality factor dependence of the transient beam loading, the measurements were performed by keeping the beam intensity, the bunch shape and the resonant frequency of the cavity constant. The rf cavity used in this measurements was loaded with six Magnetic Alloy cores which could change the quality factor as shown in

Appendix B. Since we were adjusting the resonant frequency constant, capacitances were added at the cavity gap, then the peak value of the impedance of the cavity was changed to some extent.

We have measured about the following cases listed in Table 5.4.

Q	Impedance (Ω)
30	711
6.7	825
4.0	755
2.4	720
1.1	322

Table 5.4: The measured parameters.

The beam intensity and the bunch shape used at these measurements are shown in Fig. 5.20.

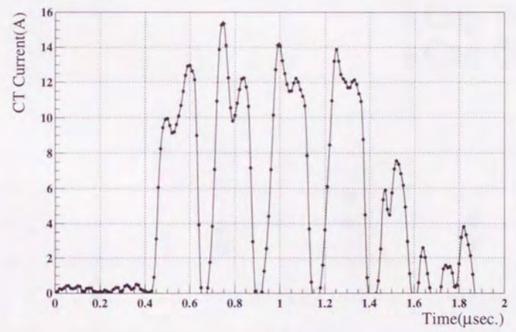

Figure 5.20: The beam intensity and the bunch shape used at the measurements of the transient beam loading.

The experimental results for each case are shown in Fig. 5.21, 5.22, 5.23, 5.24, 5.25 for $Q = 30$, 6.7, 4.0, 2.4, 1.1, respectively. On each case, the wake voltage measured at cavity gap(upper graph) and the energy the each bunch reconstructed by the Faraday

Cup signal(lower graph) are shown. In these experiments, the transient beam loading in case that the harmonic number is 8 and 4 bunches were filled non-symmetrically was examined in deed, and we could investigate the energy loss of each bunch by comparing the cases between the gap-short, which means no impedance is seen by the bunch, and the gap open, which means the impedance of the cavity affects on the bunch.

The Figure 5.26 shows the energy loss which was measured by subtracting the bunch energy at the gap open from that at the gap short. As can be clearly seen, the difference of the energy loss on each bunches was larger at the case of $Q = 6.7$ and 4.0 than that of the other Q value. This tendency, which was the transient beam loading became severe around $Q \sim h/2$, was consistent with the analytical result and the particle tracking simulation.

Thus, it was proved actually that not only very high Q value but also very low Q value was valid to suppress the difference of the energy loss on each bunch, that is, to suppress the transient beam loading.

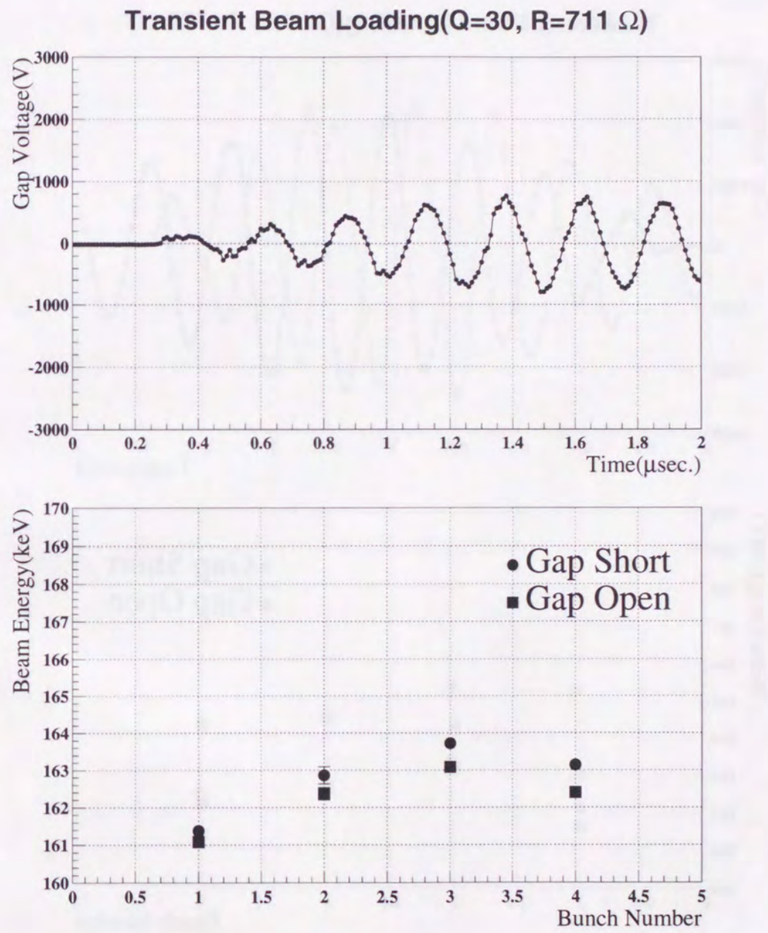

Figure 5.21: Measurement results of the transient beam loading at $Q = 30$.

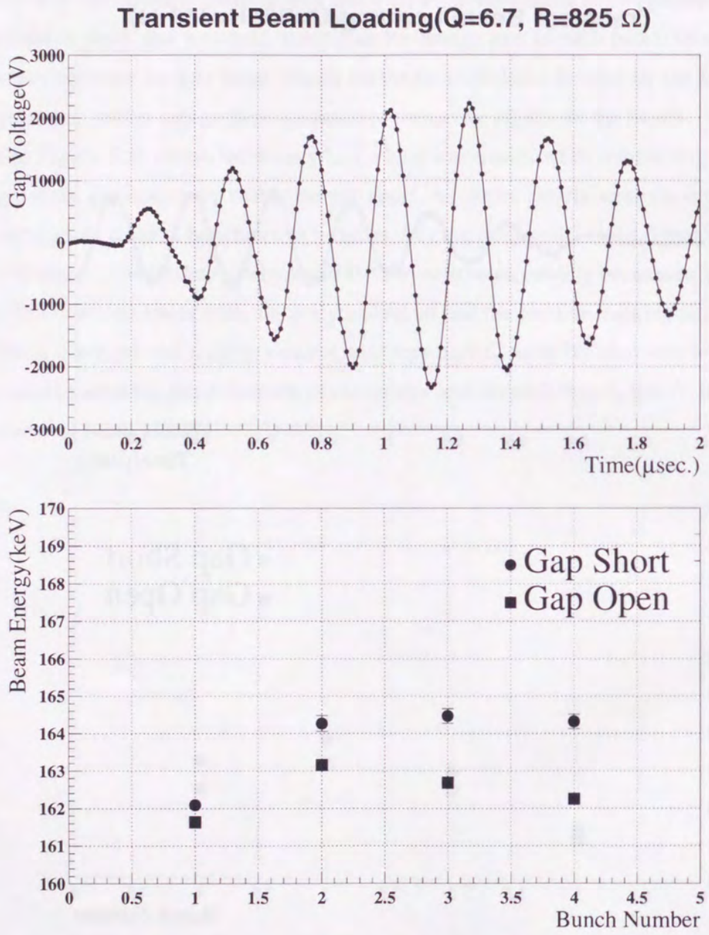

Figure 5.22: Measurement results of the transient beam loading at $Q = 6.7$.

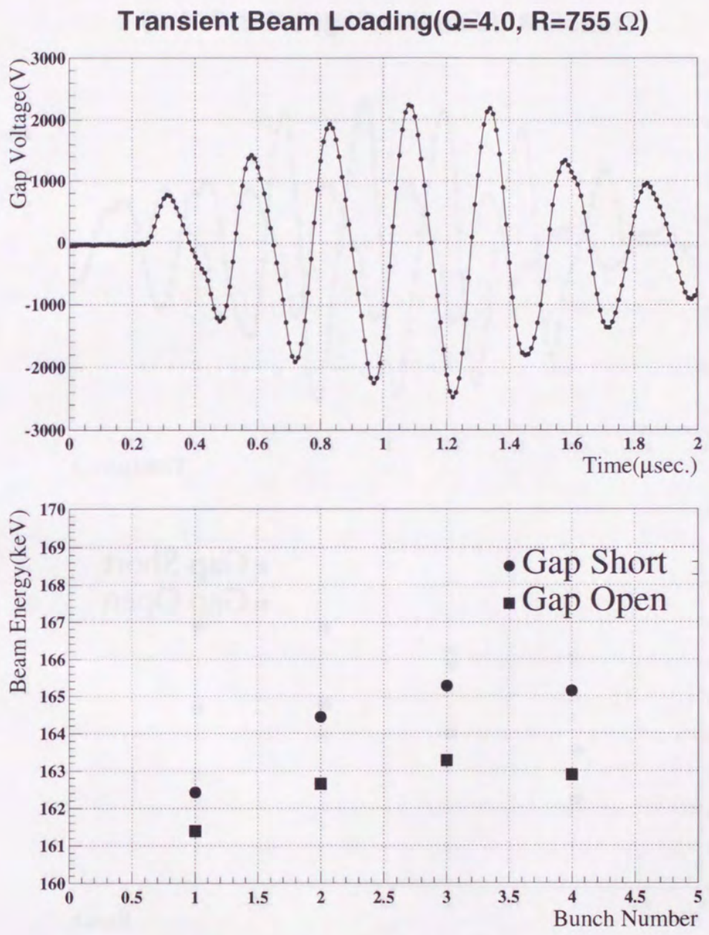

Figure 5.23: Measurement results of the transient beam loading at $Q = 4$.

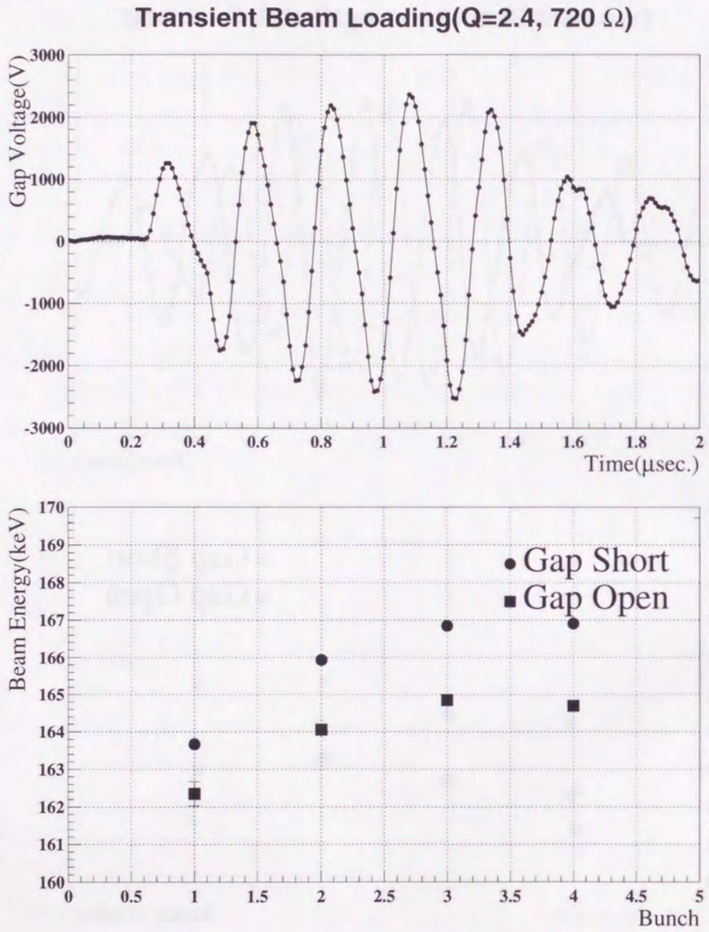

Figure 5.24: Measurement results of the transient beam loading at $Q = 2.4$.

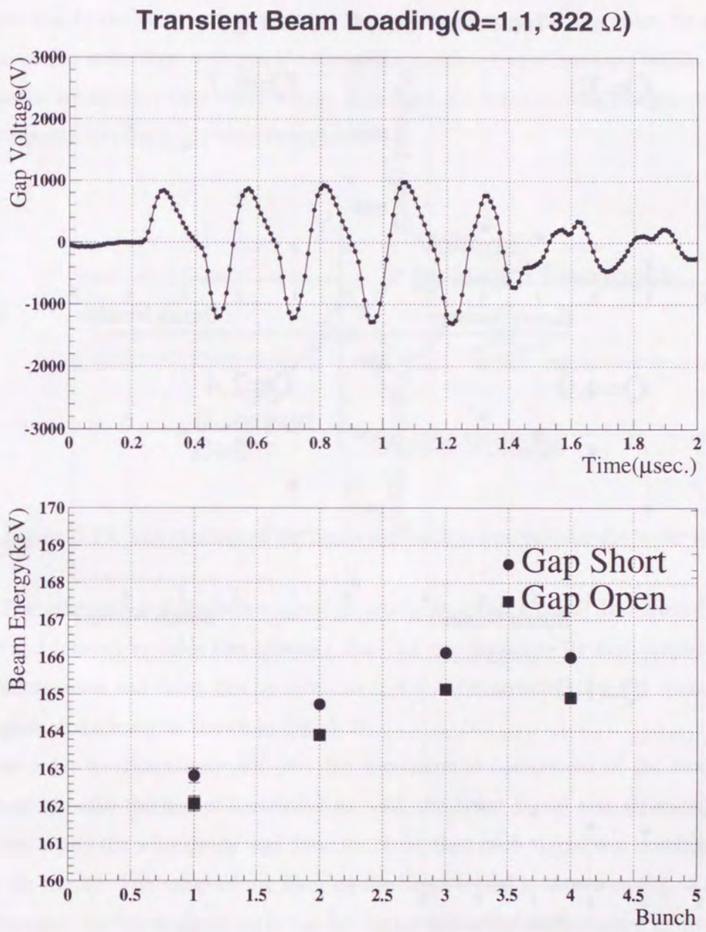

Figure 5.25: Measurement results of the transient beam loading at $Q = 1.1$.

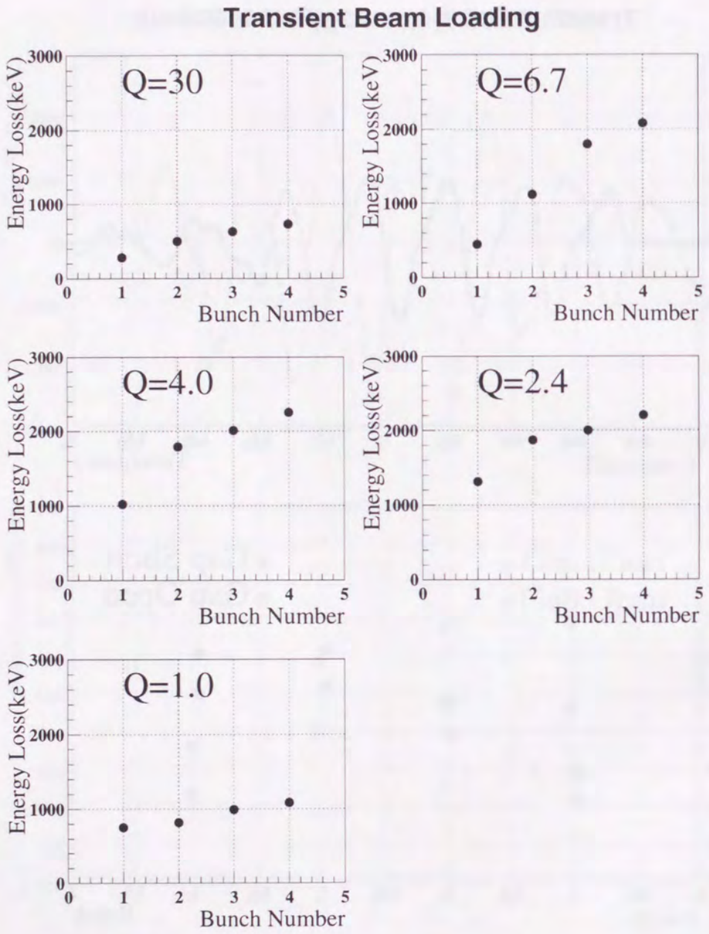

Figure 5.26: The measured energy loss of each bunch for each Q value.

5.5 Beam Loading Compensation

In the low-Q cavity, it was found that the transient beam loading could be suppressed because the wake field was quickly damped enough not to affect next bunch. However, since the amplitude of the wake voltage is so high, the beam loading compensation by the beam signal feedback has been considered.

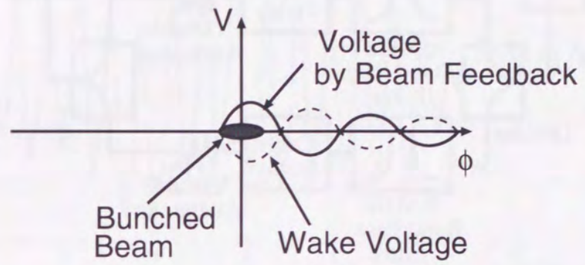

Figure 5.27: The concept of the beam feedback to compensate the wake voltage.

The scheme is that the beam signal picked up by a Fast Current Transformer is attenuated and delayed by cable line arbitrary, then fed into the cavity through amplifiers. When the attenuation and delay can be optimized, it will be expected that the wake voltage is compensated clearly as shown in Fig. 5.27.

In order to compensate not only the fundamental component of the beam induced voltage but also the higher harmonics as well, the beam signal was separated into each harmonic and the adjustment was done for them, then each signal was combined and fed into the cavity. The setup of the filtering the beam signal is shown in Fig. 5.28. In this experiment, the beam signal up to the 3rd higher harmonic was returned to the cavity.

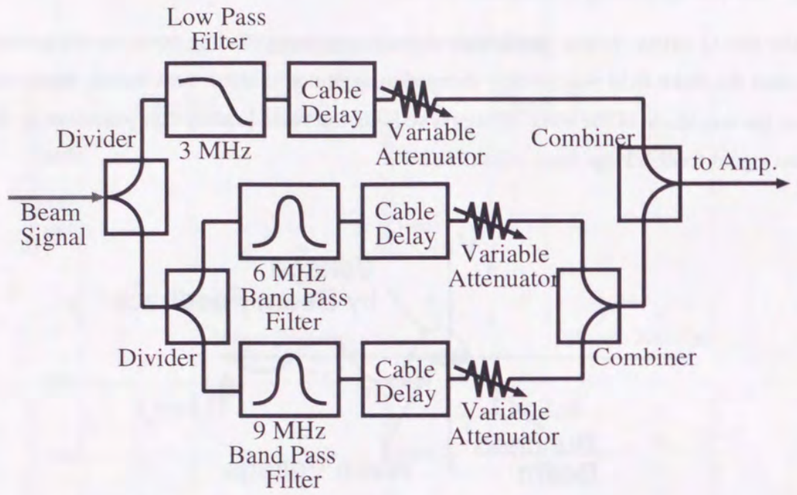

Figure 5.28: The setup of filtering the beam signal.

The measured voltage of the cavity gap without compensation and with compensation are shown in Fig. 5.29-(a) and -(b), respectively, and frequency spectrum is shown in Fig. 5.30, white bar is the spectrum without compensation, and black one is the spectrum with compensation. In this Fourier analysis, ten bunches were counted by a period. As clearly seen in Fig. 5.30, the fundamental component of the gap voltage became about one hundredth. The second and the third higher harmonic also became one tenth and one fourth, respectively.

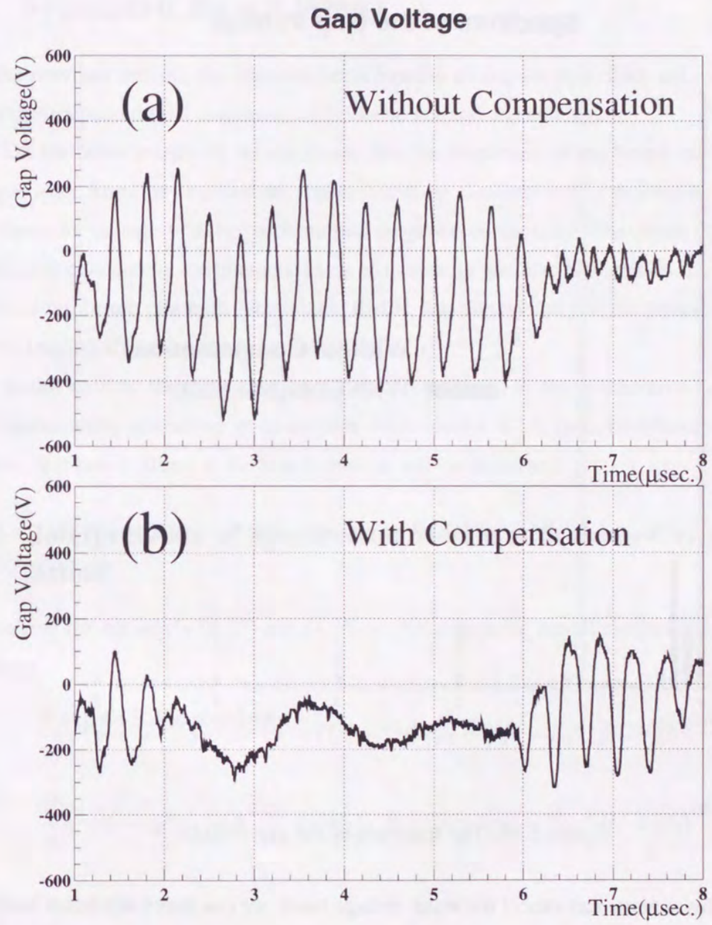

Figure 5.29: The measured gap voltage with compensation and without compensation.

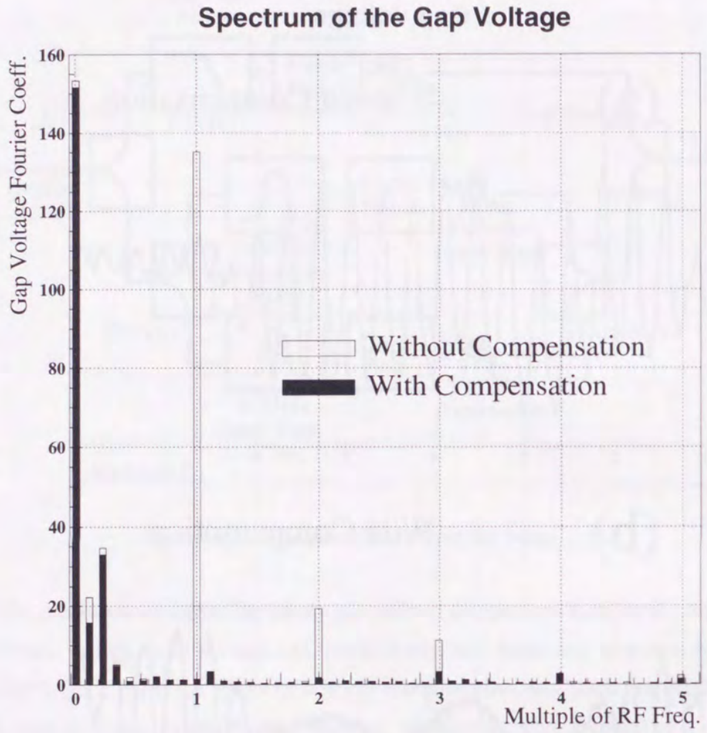

Figure 5.30: The spectrum of the gap voltage.

Since this scheme can cancel the wake voltage itself, we can make any beam loading and instability suppress. However, this scheme is not applicable to the high Q cavity because the feedback response of the cavity is not quick on such a cavity.

6 Estimation of Coupled Bunch Instability under Non-Symmetric Bunch Filling

In the previous section, the transient beam loading effects are described and it was found that they depend on the amplitude of the wake voltage on each bunch.

On the beam instability which means that the amplitude of the bunch motion grows larger apart from the equilibrium phase, it will be shown that it is defined by the phase of the wake voltage whether such motion is grown or damped. The phase of the wake voltage is changed by the characteristics of the cavity and also changed by the difference of the equilibrium phase on each bunch, that is, it is considered that the periodic transient beam loading affects on the beam instability.

In this section, the motion of the bunches is analyzed by the synchrotron motion with the beam-cavity interaction in succession from Section 4.2.2, then the effects of the non-symmetric bunch filling to the bunch motion will be described.

6.1 Interpretation of Synchrotron Motion with Beam-Cavity Interaction

Recalling the equations (4.37) and (4.38) to investigate the bunch motion with the wake voltage

$$\frac{d^2\varphi_1}{dt^2} = -{\omega_{s1}}^2\varphi_1 - A\frac{d\varphi_1}{dt} - (B_1 - D_1)(\varphi_1 - \varphi_2) - T_{\text{rev}}(B_1 - D_1)\frac{d\varphi_2}{dt} \tag{6.1}$$

$$\frac{d^2\varphi_2}{dt^2} = -{\omega_{s2}}^2\varphi_2 - A\frac{d\varphi_2}{dt} - (B_2 - D_2)(\varphi_2 - \varphi_1) - T_{\text{rev}}(B_2 - D_2)\frac{d\varphi_1}{dt}\ , \tag{6.2}$$

where

$$\omega_{s1}{}^2 = \frac{eV\eta\omega_{rf}\cos\phi_{1s}}{\beta^2 E_s T_{rev}} \tag{6.3}$$

$$\omega_{s2}{}^2 = \frac{eV\eta\omega_{rf}\cos\phi_{2s}}{\beta^2 E_s T_{rev}} \tag{6.4}$$

$$A = \frac{eV_{b0}\eta\omega_{rf}}{\beta^2 E_s} e^{-\alpha h \frac{2\pi}{\omega_{rf}}} \sin\left(\frac{\overline{\omega}-\omega_{rf}}{\omega_{rf}} 2\pi h - \delta\right) \tag{6.5}$$

$$B_1 = \frac{eV_{b0}\eta\omega_{rf}{}^2}{2\pi h\beta^2 E_s} e^{-\alpha(h-k+1)\frac{2\pi}{\omega_{rf}}}$$
$$\times \sin\left[(\phi_{1s}-\phi_{2s}) - \frac{\overline{\omega}-\omega_{rf}}{\omega_{rf}}\{(\phi_{1s}-\phi_{2s})+2\pi(h-k+1)\}+\delta\right] \tag{6.6}$$

$$B_2 = \frac{eV_{b0}\eta\omega_{rf}{}^2}{2\pi h\beta^2 E_s} e^{-\alpha(k-1)\frac{2\pi}{\omega_{rf}}}$$
$$\times \sin\left[(\phi_{2s}-\phi_{1s}) - \frac{\overline{\omega}-\omega_{rf}}{\omega_{rf}}\{(\phi_{2s}-\phi_{1s})+2\pi(k-1)\}+\delta\right] \tag{6.7}$$

$$D_1 = \frac{eV_{b0}\eta\omega_{rf}{}^2}{2\pi h\beta^2 E_s} e^{-\alpha(h-k+1)\frac{2\pi}{\omega_{rf}}} \sin(\phi_{1s}-\phi_{2s})$$
$$\times \sin\left[\frac{\overline{\omega}-\omega_{rf}}{\omega_{rf}}\{(\phi_{1s}-\phi_{2s})+2\pi(h-k+1)\}-\delta\right] \tag{6.8}$$

$$D_2 = \frac{eV_{b0}\eta\omega_{rf}{}^2}{2\pi h\beta^2 E_s} e^{-\alpha(k-1)\frac{2\pi}{\omega_{rf}}} \sin(\phi_{2s}-\phi_{1s})$$
$$\times \sin\left[\frac{\overline{\omega}-\omega_{rf}}{\omega_{rf}}\{(\phi_{2s}-\phi_{1s})+2\pi(k-1)\}-\delta\right] \tag{6.9}$$

These equations show the coupled oscillator with the damping system as shown in Fig. 6.1. Comparing eq.(6.1) and (6.2) with eq.(2.10), ω_{s1} and ω_{s2} are considered as the renormalized synchrotron frequency under the beam loading, in other words, it is shown that the restoration force at the harmonic oscillation is changed by the beam loading.

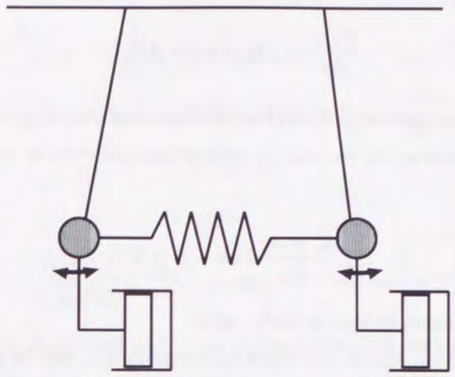

Figure 6.1: The coupled oscillator with the damped system.

Furthermore, the coupled force which executes through the term $\varphi_1 - \varphi_2$ or $\varphi_2 - \varphi_1$ is included in this system. In the coupled system, the well-known "mode analysis" will be valid, a certain "mode" characterized by the difference of the phase on each oscillator will be excited with a "characteristic frequency".

Then, it is derived by the damping term whether the amplitude of such mode motion will be growth or damped. It can be distinguished by the sign attached with the damping term, the negative sign shows that the amplitude of the motion will be decreased, and the positive sign shows that since the negative resistant force will be executed on the system. Then the amplitude of the motion will be increased, which means the motion of the bunch will grow, it leads the particle loss in the ring.

6.2 Single Bunch

When only one bunch is circulating in the ring, the equation of the longitudinal bunch motion can be expressed simply. In this case, the coupled term and the damping term in eq.(6.1) are vanishing, i.e., B and D are equal to zero, then one equation of motion is

derived as

$$\frac{d^2\varphi_1}{dt^2} = -{\omega_{s1}}^2\varphi_1 - A\frac{d\varphi_1}{dt} \tag{6.10}$$

The solution of this case is known well as the harmonic oscillator with damped system. If the sign of A is positive, the motion φ_1 will be damped even at any initial conditions, that is, if

$$\frac{\overline{\omega} - \omega_{\rm rf}}{\omega_{\rm rf}} 2\pi h - \delta > 0 \tag{6.11}$$

is satisfied, then the bunch motion is made stable.

On the contrary, if the sign of A is negative, the motion φ_1 will be growing indefinitely. This growth of the motion is called "Robinson instability [2]", so the high intensity synchrotrons should be designed that the growth is not occurring or if it is occurring, the growth rate should be smaller than the period of the injection and the extraction.

6.3 Symmetric Bunch Filling

In order to investigate coupled bunch instability, we try the mode analysis, where the normal coordinate system exists which can uncouple the simultaneous equation consists of (6.1) and (6.2) into two independent equations by a linear transformation.

Since the equilibrium phase ϕ_{1s} is consistent with ϕ_{2s} in the symmetric bunch filling as seen in Fig.5.10, the coefficients of eq.(6.3)-(6.9) become same under the replacement of the suffix between 1 and 2. In the coefficients of eq.(6.3)-(6.9), $\omega_{s1} = \omega_{s2} = \omega_s$, $B_1 = B_2 = B$, $D_1 = D_2 = D$ with $\phi_{1s} - \phi_{2s} = 0$ and $k = \frac{h}{2} + 1$ are substituted, and the normal coordinate system is defined as

$$\psi_1 = \varphi_1 + \varphi_2 \tag{6.12}$$

$$\psi_2 = \varphi_1 - \varphi_2 \ , \tag{6.13}$$

then the two uncoupled equations for each normal coordinate system are obtained as

follows:

$$\frac{d^2\psi_1}{dt^2} = -{\omega_s}^2\psi_1 - \left(A + BT_{\rm rev}\right)\frac{d\psi_1}{dt} \tag{6.14}$$

$$\frac{d^2\psi_2}{dt^2} = -\left({\omega_s}^2 + 2B\right)\psi_2 - \left(A - BT_{\rm rev}\right)\frac{d\psi_2}{dt} \ , \tag{6.15}$$

where

$$B = \frac{eV_{\rm b0}\eta{\omega_{\rm rf}}^2}{2\pi h\beta^2 E_s} e^{-\alpha\frac{h}{2}\frac{2\pi}{\omega_{\rm rf}}} \times \sin\left[-\frac{\overline{\omega} - \omega_{\rm rf}}{\omega_{\rm rf}} 2\pi\frac{h}{2} + \delta\right] \ . \tag{6.16}$$

Since the equation (6.14) and (6.15) are independent with each other, the distinction of the growth of the bunch motion were performed on each mode in the same way at the case of the single bunch.

ψ_1 mode

The condition where the motion ψ_1 will be damped is

$$\begin{aligned} &A + BT_{\rm rev} > 0 \\ \therefore\quad &e^{-\alpha h\frac{2\pi}{\omega_{\rm rf}}} \sin\left(\frac{\overline{\omega} - \omega_{\rm rf}}{\omega_{\rm rf}} 2\pi h - \delta\right) - e^{-\alpha h\frac{\pi}{\omega_{\rm rf}}} \sin\left(\frac{\overline{\omega} - \omega_{\rm rf}}{\omega_{\rm rf}}\pi h - \delta\right) > 0 \ . \end{aligned} \tag{6.17}$$

In this mode, each bunch moves keeping same phase difference as shown in Fig.6.2.

ψ_2 mode

The condition where the motion ψ_2 will be damped is

$$\begin{aligned} &A - BT_{\rm rev} > 0 \\ \therefore\quad &e^{-\alpha h\frac{2\pi}{\omega_{\rm rf}}} \sin\left(\frac{\overline{\omega} - \omega_{\rm rf}}{\omega_{\rm rf}} 2\pi h - \delta\right) + e^{-\alpha h\frac{\pi}{\omega_{\rm rf}}} \sin\left(\frac{\overline{\omega} - \omega_{\rm rf}}{\omega_{\rm rf}}\pi h - \delta\right) > 0 \ . \end{aligned} \tag{6.18}$$

In this mode, each bunch moves keeping inverse phase difference as shown in Fig.6.3.

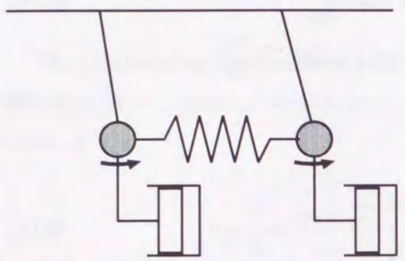

Figure 6.2: The motion of bunch in ψ_1 mode.

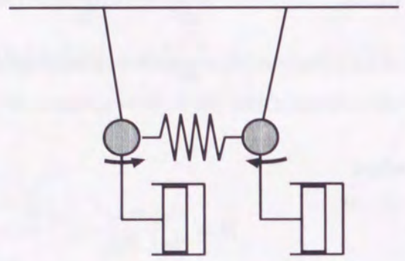

Figure 6.3: The motion of bunch in ψ_2 mode.

In the synchrotron ring, each mode is expressed as shown in Fig. 6.4 and 6.5.

Figure 6.4: The motion of bunch in ψ_1 mode in the ring.

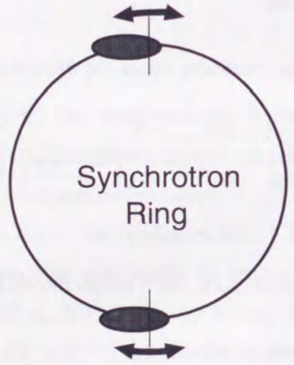

Figure 6.5: The motion of bunch in ψ_2 mode in the ring.

6.4 Non-Symmetric Bunch Filling

In this case, the classical mode analysis is abandoned because we can not discover the normal coordinate system which can uncouple the simultaneous equation consists of (6.1)

and (6.2) into two independent equations by a "linear" transformation. So let us try to solve the simultaneous equation by Laplace transformation.

Rewriting eq.(6.1) and eq.(6.2) as a matrix form

$$\begin{bmatrix}1 & 0\\ 0 & 1\end{bmatrix}\begin{pmatrix}\frac{d^2\varphi_1}{dt^2}\\ \frac{d^2\varphi_2}{dt^2}\end{pmatrix}+\begin{bmatrix}A & T_{\rm rev}(B_1-D_1)\\ T_{\rm rev}(B_2-D_2) & A\end{bmatrix}\begin{pmatrix}\frac{d\varphi_1}{dt}\\ \frac{d\varphi_2}{dt}\end{pmatrix}$$
$$+\begin{bmatrix}{\omega_{s1}}^2+(B_1-D_1) & -(B_1-D_1)\\ -(B_2-D_2) & {\omega_{s2}}^2+(B_2-D_2)\end{bmatrix}\begin{pmatrix}\varphi_1\\ \varphi_2\end{pmatrix}=0\ . \tag{6.19}$$

The equation (6.19) is written as the vector form,

$$[1](\ddot{x}(t))+[c](\dot{x}(t))+[k](x(t))=0\ , \tag{6.20}$$

where

$$x(t)=\begin{pmatrix}\varphi_1\\ \varphi_2\end{pmatrix} \tag{6.21}$$
$$[1]=\begin{bmatrix}1 & 0\\ 0 & 1\end{bmatrix}$$
$$[c]=\begin{bmatrix}A & T_{\rm rev}(B_1-D_1)\\ T_{\rm rev}(B_2-D_2) & A\end{bmatrix}$$
$$[k]=\begin{bmatrix}{\omega_{s1}}^2+(B_1-D_1) & -(B_1-D_1)\\ -(B_2-D_2) & {\omega_{s2}}^2+(B_2-D_2)\end{bmatrix}$$

Performing Laplace transformation for each side of eq.(6.20),

$$[1]\left\{s^2\overline{x}(s)-sx(0)-\dot{x}(0)\right\}+[c]\left\{s\overline{x}(s)-x(0)\right\}+[k]\overline{x}(s)=0\ , \tag{6.22}$$

where $\overline{x}(s)=\pounds[x(t)]$. Then,

$$\overline{x}(s)=\frac{\{s[1]+[c]\}\,x(0)+[m]\dot{x}(0)}{s^2[1]+s[c]+[k]}=[Z(s)]^{-1}\left\{\overline{R}(s)\right\}\ , \tag{6.23}$$

where

$$Z(s)=s^2[1]+s[c]+[k] \tag{6.24}$$

is called "Mechanical Impedance" of the damped system and

$$\left\{\overline{R}(s)\right\}=[s[1]+[c]]\left\{x(0)\right\}+[1]\left\{\dot{x}(0)\right\} \tag{6.25}$$

is a Laplace transformed input at the initial condition. Let us define a matrix of transfer function $G(s)$ given by

$$[G(s)] = [Z(s)]^{-1} = \frac{[A(s)]}{|Z(s)|} , \tag{6.26}$$

where $[A(s)]$ is the adjoint and $|Z(s)|$ is the determinant of the impedance matrix $[Z(s)]$. Introducing eq.(6.26) in (6.23), we can write the transformed response as

$$\{\overline{x}(s)\} = [G(s)]\{\overline{R}(s)\} , \tag{6.27}$$

and the response if obtained by writing the inverse Laplace transformation,

$$\{x(t)\} = \pounds^{-1}[\overline{x}(s)] = \pounds^{-1}[G(s)]\{\overline{R}(s)\} . \tag{6.28}$$

In order to perform the inverse Laplace transformation, we must know the poles for the matrix of the transfer function by

$$\begin{aligned} |Z(s)| = \Bigg| & s^2 \begin{bmatrix} 1 & 0 \\ 0 & 1 \end{bmatrix} + s \begin{bmatrix} A & T_{\mathrm{rev}}(B_1 - D_1) \\ T_{\mathrm{rev}}(B_2 - D_2) & A \end{bmatrix} \\ & + \begin{bmatrix} {\omega_{s1}}^2 + (B_1 - D_1) & -(B_1 - D_1) \\ -(B_2 - D_2) & {\omega_{s2}}^2 + (B_2 - D_2) \end{bmatrix} \Bigg| = 0 , \end{aligned} \tag{6.29}$$

then

$$\begin{aligned} & s^4 + As^3 + \left[A^2 + \left\{{\omega_{s1}}^2 + (B_1 - D_1)\right\} + \left\{{\omega_{s2}}^2 + (B_2 - D_2)\right\} - {T_{\mathrm{rev}}}^2(B_1 - D_1)(B_2 - D_2)\right] s^2 \\ & + \left[A\left\{{\omega_{s1}}^2 + (B_1 - D_1)\right\} + A\left\{{\omega_{s2}}^2 + (B_2 - D_2)\right\} + 2T_{\mathrm{rev}}(B_1 - D_1)(B_2 - D_2)\right] s \\ & + \left\{{\omega_{s1}}^2 + (B_1 - D_1)\right\}\left\{{\omega_{s2}}^2 + (B_2 - D_2)\right\} - (B_1 - D_1)(B_2 - D_2) = 0 . \end{aligned} \tag{6.30}$$

Supposing that four poles s_1, s_2, s_3, s_4 are obtained from the characteristic equation (6.30),

$$[G(s)] = \frac{\begin{bmatrix} s^2 + As + {\omega_{s2}}^2 + (B_2 - D_2) & (B_1 - D_1) - T_{\mathrm{rev}}(B_1 - D_1)s \\ (B_2 - D_2) - T_{\mathrm{rev}}(B_2 - D_2)s & s^2 + As + {\omega_{s1}}^2 + (B_1 - D_1) \end{bmatrix}}{(s - s_1)(s - s_2)(s - s_3)(s - s_4)} . \tag{6.31}$$

Substituting eq.(6.31) into (6.27),

$$\begin{aligned} \overline{x} = & \frac{1}{(s - s_1)(s - s_2)(s - s_3)(s - s_4)} \\ & \times \begin{bmatrix} s^2 + As + {\omega_{s2}}^2 + (B_2 - D_2) & (B_1 - D_1) - T_{\mathrm{rev}}(B_1 - D_1)s \\ (B_2 - D_2) - T_{\mathrm{rev}}(B_2 - D_2)s & s^2 + As + {\omega_{s1}}^2 + (B_1 - D_1) \end{bmatrix} (s[1] + [c])x(0) \end{aligned}$$

$$\begin{aligned} \begin{pmatrix} \overline{\varphi_1}(s) \\ \overline{\varphi_2}(s) \end{pmatrix} = & \frac{1}{(s - s_1)(s - s_2)(s - s_3)(s - s_4)} \\ & \times \begin{bmatrix} s^2 + As + {\omega_{s2}}^2 + (B_2 - D_2) & (B_1 - D_1) - T_{\mathrm{rev}}(B_1 - D_1)s \\ (B_2 - D_2) - T_{\mathrm{rev}}(B_2 - D_2)s & s^2 + As + {\omega_{s1}}^2 + (B_1 - D_1) \end{bmatrix} \\ & \cdot \begin{bmatrix} A & T_{\mathrm{rev}}(B_1 - D_1) \\ T_{\mathrm{rev}}(B_2 - D_2) & A \end{bmatrix} \begin{pmatrix} \varphi_1(0) \\ \varphi_2(0) \end{pmatrix} \\ = & \frac{1}{(s - s_1)(s - s_2)(s - s_3)(s - s_4)} \begin{bmatrix} G_{11}(s) & G_{12}(s) \\ G_{21}(s) & G_{22}(s) \end{bmatrix} \begin{pmatrix} \varphi_1(0) \\ \varphi_2(0) \end{pmatrix} \end{aligned} \tag{6.32}$$

where

$$G_{11}(s) = A\left\{s^2 + As + {\omega_{s2}}^2 + (B_2 - D_2)\right\} + T_{\mathrm{rev}}(B_2 - D_2) \tag{6.33}$$

$$G_{12}(s) = T_{\mathrm{rev}}(B_1 - D_1)\left\{s^2 + As + {\omega_{s2}}^2 + (B_2 - D_2)\right\} + A\left\{(B_1 - D_1) - T_{\mathrm{rev}}(B_1 - D_1)\right\} \tag{6.34}$$

$$G_{21}(s) = T_{\mathrm{rev}}(B_2 - D_2)\left\{s^2 + As + {\omega_{s1}}^2 + (B_1 - D_1)\right\} + A\left\{(B_2 - D_2) - T_{\mathrm{rev}}(B_2 - D_2)\right\} \tag{6.35}$$

$$G_{22}(s) = A\left\{s^2 + As + {\omega_{s1}}^2 + (B_1 - D_1)\right\} + T_{\mathrm{rev}}(B_1 - D_1) \tag{6.36}$$

From the equation (6.32),

$$\begin{aligned} \overline{\varphi_1}(s) &= \frac{1}{(s - s_1)(s - s_2)(s - s_3)(s - s_4)}(G_{11}(s)\varphi_1(0) + G_{12}(s)\varphi_2(0)) \\ \overline{\varphi_2}(s) &= \frac{1}{(s - s_1)(s - s_2)(s - s_3)(s - s_4)}(G_{21}(s)\varphi_1(0) + G_{22}(s)\varphi_2(0)) . \end{aligned}$$

Finally, the bunch motion of $\varphi_1(t)$ and $\varphi_2(t)$ are obtained as

$$\varphi_1(t) = \mathcal{L}^{-1}[\overline{\varphi_1}(s)] = A_{1G_{11}}e^{s_1 t} + A_{2G_{11}}e^{s_2 t} + A_{3G_{11}}e^{s_3 t} + A_{4G_{11}}e^{s_4 t} + A_{1G_{12}}e^{s_1 t} + A_{2G_{12}}e^{s_2 t} + A_{3G_{12}}e^{s_3 t} + A_{4G_{12}}e^{s_4 t} \tag{6.37}$$

$$\varphi_2(t) = \mathcal{L}^{-1}[\overline{\varphi_2}(s)] = A_{1G_{21}}e^{s_1 t} + A_{2G_{21}}e^{s_2 t} + A_{3G_{21}}e^{s_3 t} + A_{4G_{21}}e^{s_4 t} + A_{1G_{22}}e^{s_1 t} + A_{2G_{22}}e^{s_2 t} + A_{3G_{22}}e^{s_3 t} + A_{4G_{22}}e^{s_4 t} , \tag{6.38}$$

where

$$\frac{A_{1G_{11}}}{s-s_1} + \frac{A_{2G_{11}}}{s-s_2} + \frac{A_{3G_{11}}}{s-s_3} + \frac{A_{4G_{11}}}{s-s_4} = \frac{G_{11}(s)}{(s-s_1)(s-s_2)(s-s_3)(s-s_4)} \tag{6.39}$$

$$\frac{A_{1G_{12}}}{s-s_1} + \frac{A_{2G_{12}}}{s-s_2} + \frac{A_{3G_{12}}}{s-s_3} + \frac{A_{4G_{12}}}{s-s_4} = \frac{G_{12}(s)}{(s-s_1)(s-s_2)(s-s_3)(s-s_4)} \tag{6.40}$$

$$\frac{A_{1G_{21}}}{s-s_1} + \frac{A_{2G_{21}}}{s-s_2} + \frac{A_{3G_{21}}}{s-s_3} + \frac{A_{4G_{21}}}{s-s_4} = \frac{G_{21}(s)}{(s-s_1)(s-s_2)(s-s_3)(s-s_4)} \tag{6.41}$$

$$\frac{A_{1G_{22}}}{s-s_1} + \frac{A_{2G_{22}}}{s-s_2} + \frac{A_{3G_{22}}}{s-s_3} + \frac{A_{4G_{22}}}{s-s_4} = \frac{G_{22}(s)}{(s-s_1)(s-s_2)(s-s_3)(s-s_4)} . \tag{6.42}$$

Now, since we are interested whether the motion of the bunch is grown or not, that is, interested in the sign of the real part at s_1, s_2, s_3, s_4. In order to know the sign of them, we must obtain the roots of the characteristic equation (6.30), but there is no analytical method to get the roots of such quartic equation, so it is solved numerically.

However, we can guess the characteristics of the solutions. If the solutions are consist of the complex number as $s_1 = a_1 + j\Omega_1$, $s_2 = a_2 + j\Omega_2$, $s_3 = a_3 + j\Omega_3$, and $s_4 = a4 + j\Omega_4$, then the following relation should be satisfied because the coefficients in eq.(6.30) should be the pure real number: $a_2 = a_1$ with $\Omega_2 = -\Omega_1$ and $a_4 = a_3$ with $\Omega_4 = -\Omega_3$. They shows that the roots of eq.(6.30) are consists of complex conjugate pairs as

$$\begin{aligned} s_1 &= a_1 + j\Omega_1 \\ s_2 &= a_1 - j\Omega_1 \\ s_3 &= a_2 + j\Omega_2 \\ s_4 &= a_2 - j\Omega_2 . \end{aligned} \tag{6.43}$$

So the motion of the bunch in the non-symmetric filling is made of two modes though the characteristic equation is quartic one. In the equation (6.43) a_1 and a_2 indicate the damping(or growth) constant and Ω_1 and Ω_2 indicate the mode frequency on each mode.

Though the explicit expression for the decision whether the coupled bunch instability is grown or damped can not be derived analytically, the transient beam loading may affect the coupled bunch instability because the difference of the equilibrium phase are included in the coefficients of eqs.(6.3)-(6.7).

By the way, the transient beam loading also make the bunch motion grow from the beginning, whereas the bunch motion grown by the coupled bunch instability gradually as shown in Fig. 6.6.

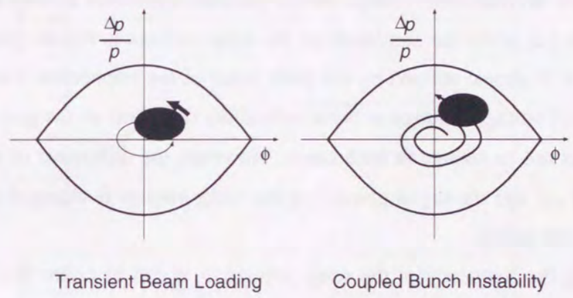

Figure 6.6: The difference of the growth of the bunch motion caused by the transient beam loading and coupled bunch instability.

So if the effect of the transient beam loading is small enough to avoid the beam loss, we must care the coupled bunch instability, but if the effect of the transient beam loading is so large, the beam loss is occurred before the bunch motion is grown by the coupled bunch instability.

6.5 Difference of Wake Voltage between Circuit Models and its Effect to Coupled Bunch Instability

Watching the coefficients of eqs.(6.3)-(6.7), the sign of them is defined by the following conditions:

1. The periodic transient beam loading: ϕ_{1s}, ϕ_{2s}
2. The difference of the frequency between the wake voltage and the rf voltage: $\frac{\overline{\omega} - \omega_{rf}}{\omega_{rf}}$
3. Initial phase of the wake voltage: δ.

Recalling the derived wake voltage for the parallel expression and the series expression in Section 3.2, since the amplitude of the wake voltage is not so changed in both cases because it is almost defined by the peak value of the impedance which is needed to generate the rf voltage required at the acceleration, the effect of the periodic transient beam loading is not so change in both cases. However, the difference of the frequency between $\overline{\omega}$ and ω_{rf} and the initial phase δ of the wake voltage is changed depending on the lumped circuit model.

Considering the frequency of the wake voltage $\overline{\omega}$, it can be controlled by changing the cavity resonant frequency ω_{rp} in eq.(3.38) or ω_{rs} in eq.(3.31) on each circuit model, respectively, the sign of $\frac{\overline{\omega} - \omega_{rf}}{\omega_{rf}}$ can be changed arbitrary in both cases.

On the other hand, the behavior of δ_s is quite different between in the parallel expression and in the series one. The Figure 6.7 shows the calculation result of δ on each case under the condition that L and C are constant and only the quality factor Q of the magnetic core is changing. As can be seen, δ_p is monotonously increasing, then is close to 0 on the high Q region, and δ_s is also monotonously increasing, but it is crossing 0 and the sign is different from δ_p on the high Q region.

These facts shows that the sign of δ can not be changed in the parallel expression, but it can be realized in the series one, and also can be made zero. The condition where

$\delta_s = 0$ is derived from eq.(4.14) as

$$\alpha_s - \frac{R_s}{L_s} = 0 \ ,$$
$$\text{then} \quad \frac{R_s}{L_s} = \frac{1}{CR_a} \ , \tag{6.44}$$

where the resonant frequency ω_{rs} becomes

$$\omega_{rs}{}^2 = \frac{1}{L_s C} \ . \tag{6.45}$$

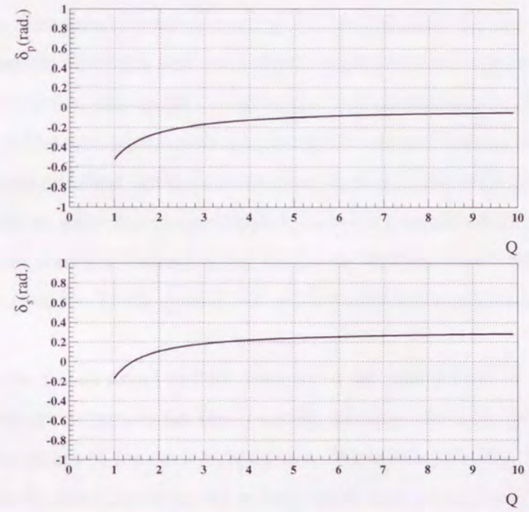

Figure 6.7: The difference between δ_p and δ_s.

Thus, $\overline{\omega_s} - \omega_{rf} = 0$ and $\delta_s = 0$ can be realized in the series expression, which means that the damping terms of eq.(6.1) and (6.2) are clearly vanished, when the bunches are filled in the ring symmetrically.

The real cavity impedance shows that the frequency where the absolute value of the impedance is maximum is not exactly equal to the frequency where the impedance become pure real number as shown in Fig. 3.9 and 3.10. This suggests the possibility that the phase parameter δ of the wake voltage may be vanish if we could choose the optimum external resistor at the condition in eq.(6.44). However, we should note that the series expression for the cavity impedance can not express the real cavity impedance completely, so we only pointed out the feasibility to vanish the phase parameter, which can not be realize in the parallel expression of the cavity.

7 Conclusion

The beam loading and the coupled bunch instability were investigated under not only in symmetric bunch filling but also in non-symmetric bunch filling in the synchrotron.

On the transient beam loading, so far the cavity which had a high quality factor to reduce the amplitude of the wake voltage was preferred. However it was found that the low quality factor was also valid to suppress the transient beam loading by the analytical calculation and the particle tracking simulation. Furthermore, it is also found that the transient beam loading becomes most sever around the condition that the quality factor of the cavity becomes the half of the harmonic number when the bunches are filled non-symmetrically. Obviously, the transient condition can be canceled in the symmetric bunch filling. The transient beam loading was investigated experimentally in the beam loading test bench, where the high intensity electron beam was injected into the prototype rf cavity, then same results as the calculation and the simulation were obtained.

The coupled bunch instability under the transient beam loading was estimated to have a smaller growth rate than that under symmetric bunch filling in the past. We could get the analytical form to solve the coupled bunch instability of the proton synchrotron. Then, it was found the transient beam loading affects the coupled bunch instability because the characteristic equation for the growth rate of the bunch motion includes the transient beam loading.

Furthermore, it was found that the analysis of the coupled bunch instability depended on the lumped circuit model for the rf cavity, because the coupled bunch instability is sensitive to the phase of the cavity impedance. We investigated the coupled bunch instability using the lumped circuit model in both series and parallel expressions with respect to the loss of the magnetic core, then, it was found that the condition where the growth or damping of the bunch motion would not occur could be made in peculiar impedance of the cavity.

Acknowledgments

When I intended to major accelerator physics in 1995, I did not know so well that "What is curious and important in the accelerator physics ?", but I felt somehow interesting without foundation. Now, I have not known all of the accelerator physics completely, but I will explain "What is curious and important ?" for me to any people. I would like to appreciate many people who motioned me to change myself.

I want to thank my academic advisor at RCNP, Osaka University, Professor Kenji Sato, for his constant encouragement and concern about the progress since I entered graduate school.

I want to thank my thesis advisor at KEK, Professor Yoshiharu Mori, for his instructive discussions and suggesting the experimental subject.

On the calculations and experimental works at KEK, I received a great deal of help from Dr. Chihiro Ohmori and Mr. Yoshinori Hashimoto, I thank them for their kind help.

My works have been done with many people, discussing and working together. I also thank Dr. Masahito Yoshii, Dr. Akira Takagi, Professor Shinji Machida, Mr. Yasuo Sato, Dr. Kiyomi Koba, Ms. Miho Fujieda, Mr. Tom Uesugi and Mr. Ryosaku Muramatsu.

Finally, I would like to thank my parents for their persistent support in my education.

A Resonant Circuit of Transmission Line

The frequency of the rf field becomes usually from hundreds kHz to decades MHz, so the wave length of it becomes from a few m to a few cm in consideration of the permeability of the magnetic cores. Since it is almost consistent with the length of the cavity, it is necessary that the impedance of the cavity is obtained by the analysis of the distributed constant circuit model precisely. In this case, the voltage and the current in the cavity depend on not only the time but also the position.

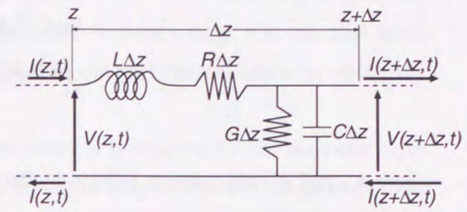

Figure A.1: The distributed constant circuit.

Let us consider a transmission line of the length Δz as shown in Fig. A.1, where L, C, R, G means an inductance, a capacitance, a resistance and a conductance of the unit length, respectively. Now we have the relation of the voltage v to the current i at the position z and $z+\Delta z$, then we execute the limitation $\Delta z \to 0$, we can obtain the equation of the transmission line as

$$\frac{\partial^2 v}{\partial z^2} = RGv + (RC + LG)\frac{\partial v}{\partial t} + LC\frac{\partial^2 v}{\partial t^2} \tag{A.1}$$

$$\frac{\partial^2 i}{\partial z^2} = RGi + (RC + LG)\frac{\partial i}{\partial t} + LC\frac{\partial^2 i}{\partial t^2} \tag{A.2}$$

The complex expression to the voltage and the current is employed as $v(z,t) = V(z)e^{j\omega t}, i(z,t) = I(z)e^{j\omega t}$, then eq.(A.1) and (A.2) become

$$\frac{d^2 V(z)}{dz^2} = \gamma^2 V(z) \tag{A.3}$$

$$\frac{d^2 I(z)}{dz^2} = \gamma^2 I(z) \tag{A.4}$$

$$\gamma = \alpha + j\beta = \sqrt{(R + j\omega L)(G + j\omega C)}\,, \tag{A.5}$$

where γ is called "phase parameter". Then the solution of eq. (A.3) and (A.4) is expressed as

$$V(z) = K_1 e^{-\gamma z} + K_2 e^{\gamma z} \tag{A.6}$$

$$I(z) = \frac{1}{Z_0}(K_1 e^{-\gamma z} - K_2 e^{\gamma z}) \ , \tag{A.7}$$

$$\tag{A.8}$$

where K_1 and K_2 are constant defined by the boundary condition and Z_0 is called "characteristic impedance

$$Z_0 = \sqrt{\frac{R + j\omega L}{G + j\omega C}} \ . \tag{A.9}$$

Furthermore, the equation (A.6) and (A.7) becomes as follows when the voltage and the current at $z = 0$, which $V(0) = V_1$ and $I(0) = I_1$, are already known,

$$V(z) = V_1 \cosh \gamma z - Z_0 I_1 \sinh \gamma z \tag{A.10}$$

$$I(z) = -\frac{V_1}{Z_0} \sinh \gamma z + I_1 \cosh \gamma z \ . \tag{A.11}$$

Since $G = 0$ in the rf cavity, the phase parameter and the characteristic impedance becomes $\gamma = \sqrt{(R + j\omega L) j\omega C}$ and $Z_0 = \sqrt{\frac{R + j\omega L}{j\omega C}}$, respectively. If the line is shorted at the position $z = l$, that is $V(l) = 0$, then the impedance measured at $z = 0$ becomes

$$Z_{\text{in}} = \frac{V_1}{I_1} = Z_0 \tanh \gamma l. \tag{A.12}$$

Let us use this transmission line as $\gamma l \ll 1$, then

$$Z_{\text{in}} \cong R + j\omega L \ . \tag{A.13}$$

Usually, the cavity has a capacitance C_g at the cavity gap as shown in Fig. A.2, then the resonant condition is appeared at $\omega_r = \frac{1}{\sqrt{LC_g}}$.

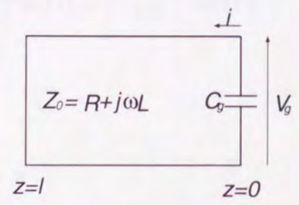

Figure A.2: The coaxial line and the cavity gap capacitance.

B Characteristics of Magnetic Cores

In the past, rf cavities almost loaded with ferrite cores due to the suitable characteristics such as low rf losses on a few MHz $\sim$ decades MHz frequency range. On the other hand, some kind of core made of magnetic alloy(MA) have very different characteristics from the ferrite one.

In order to generate high voltage at the rf cavity, it is required for the magnetic cores that the impedance of them should be stable under the magnetic field of large amplitude. The Figure B.1 shows that the measurement results of the $\mu Q f$ product for some magnetic cores. As shown clearly, the $\mu Q f$ product falls down drastically with some ferrite cores such as SY-2 and 4M3 under the magnetic field of large amplitude, whereas it is still constant with some MA such as FT3M and Metglas. These results show that MA has a possibility to generate very higher voltage than ferrite.

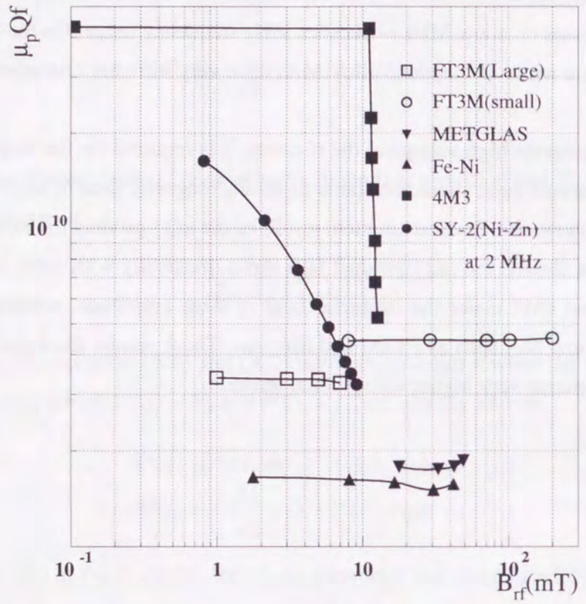

Figure B.1: The measurement of various magnetic cores under the rf magnetic field of large amplitude.

From the view point of the beam instabilities, Q of the cores is important. In the past, it is limited around ten or higher with ferrite cores. On the other hand, MA has a very low Q around one, and can control it by using "Cut Core" as shown in Fig. B.2. The results of the measurement for the cut core of MA are shown in Fig. B.3, where Q was con-

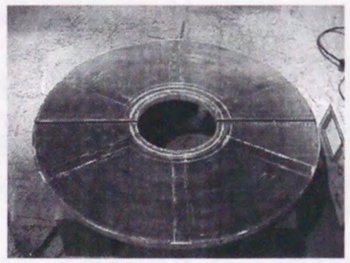

Figure B.2: The cut core of MA.

trolled by changing the gap between each half of the core.

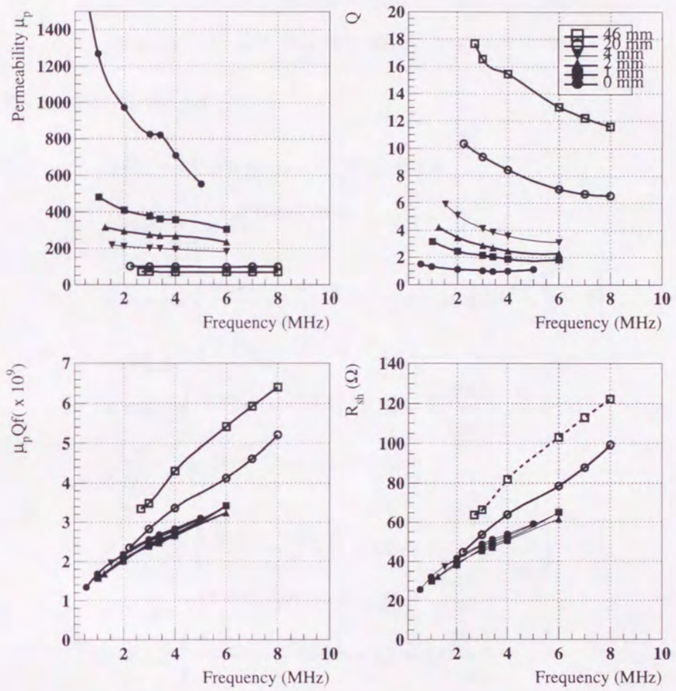

Figure B.3: The measurement for Cut Core of MA at measurement bench.

C Approximation of Wake Field Calculation

Substituting following relations

$$\phi_{1,n+1} - \phi_{2,m} = \phi_{1,n+1} - \phi_{2,n+1} + \phi_{2,n+1} - \phi_{2,m} \tag{C.1}$$

$$\phi_{2,n+1} - \phi_{1,m} = \phi_{2,n+1} - \phi_{1,n+1} + \phi_{1,n+1} - \phi_{1,m} \tag{C.2}$$

into (4.20) and (4.18), we get

$$\begin{aligned}
\Delta E_1 &= eV \sin\phi_{1,n+1} - \frac{1}{2}eV_{\mathrm{b0}}\cos\delta \\
&-eV_{\mathrm{b0}}\sum_{m=1}^{n} e^{-\alpha\left\{\frac{\phi_{1,n+1}-\phi_{1,m}}{\omega_{\mathrm{rf}}}+(n+1-m)h\frac{2\pi}{\omega_{\mathrm{rf}}}\right\}} \\
&\times\cos\left[\overline{\omega}\left\{\frac{\phi_{1,n+1}-\phi_{1,m}}{\omega_{\mathrm{rf}}}+(n+1-m)h\frac{2\pi}{\omega_{\mathrm{rf}}}\right\}-\delta\right] \\
&-eV_{\mathrm{b0}}e^{-\alpha\left\{\frac{\phi_{1,n+1}-\phi_{2,n+1}}{\omega_{\mathrm{rf}}}-(k-1)\frac{2\pi}{\omega_{\mathrm{rf}}}\right\}} \\
&\times\cos\overline{\omega}\left\{\frac{\phi_{1,n+1}-\phi_{2,n+1}}{\omega_{\mathrm{rf}}}-(k-1)\frac{2\pi}{\omega_{\mathrm{rf}}}\right\} \\
&\times\sum_{m=1}^{n} e^{-\alpha\left\{\frac{\phi_{2,n+1}-\phi_{2,m}}{\omega_{\mathrm{rf}}}+(n+1-m)h\frac{2\pi}{\omega_{\mathrm{rf}}}\right\}} \\
&\times\cos\left[\overline{\omega}\left\{\frac{\phi_{2,n+1}-\phi_{2,m}}{\omega_{\mathrm{rf}}}+(n+1-m)h\frac{2\pi}{\omega_{\mathrm{rf}}}\right\}-\delta\right] \\
&+eV_{\mathrm{b0}}e^{-\alpha\left\{\frac{\phi_{1,n+1}-\phi_{2,n+1}}{\omega_{\mathrm{rf}}}-(k-1)\frac{2\pi}{\omega_{\mathrm{rf}}}\right\}} \\
&\times\sin\overline{\omega}\left\{\frac{\phi_{1,n+1}-\phi_{2,n+1}}{\omega_{\mathrm{rf}}}-(k-1)\frac{2\pi}{\omega_{\mathrm{rf}}}\right\} \\
&\times\sum_{m=1}^{n} e^{-\alpha\left\{\frac{\phi_{2,n+1}-\phi_{2,m}}{\omega_{\mathrm{rf}}}+(n+1-m)h\frac{2\pi}{\omega_{\mathrm{rf}}}\right\}} \\
&\times\sin\left[\overline{\omega}\left\{\frac{\phi_{2,n+1}-\phi_{2,m}}{\omega_{\mathrm{rf}}}+(n+1-m)h\frac{2\pi}{\omega_{\mathrm{rf}}}\right\}-\delta\right]
\end{aligned} \tag{C.3}$$

$$
\begin{aligned}
\Delta E_2 &= eV\sin\phi_{2,n+1} - \frac{1}{2}eV_{\rm b0}\cos\delta \\
&-eV_{\rm b0}\sum_{m=1}^{n} e^{-\alpha\left\{\frac{\phi_{2,n+1}-\phi_{2,m}}{\omega_{\rm rf}}+(n+1-m)h\frac{2\pi}{\omega_{\rm rf}}\right\}} \\
&\times\cos\left[\overline{\omega}\left\{\frac{\phi_{2,n+1}-\phi_{2,m}}{\omega_{\rm rf}}+(n+1-m)h\frac{2\pi}{\omega_{\rm rf}}\right\}-\delta\right] \\
&-eV_{\rm b0}e^{-\alpha\left\{\frac{\phi_{2,n+1}-\phi_{1,n+1}}{\omega_{\rm rf}}-(h-k+1)\frac{2\pi}{\omega_{\rm rf}}\right\}} \\
&\times\cos\overline{\omega}\left\{\frac{\phi_{2,n+1}-\phi_{1,n+1}}{\omega_{\rm rf}}-(h-k+1)\frac{2\pi}{\omega_{\rm rf}}\right\} \\
&\times\sum_{m=1}^{n} e^{-\alpha\left\{\frac{\phi_{1,n+1}-\phi_{1,m}}{\omega_{\rm rf}}+(n+1-m)h\frac{2\pi}{\omega_{\rm rf}}\right\}} \\
&\times\cos\left[\overline{\omega}\left\{\frac{\phi_{1,n+1}-\phi_{1,m}}{\omega_{\rm rf}}+(n+1-m)h\frac{2\pi}{\omega_{\rm rf}}\right\}-\delta\right] \\
&+eV_{\rm b0}e^{-\alpha\left\{\frac{\phi_{2,n+1}-\phi_{1,n+1}}{\omega_{\rm rf}}-(h-k+1)\frac{2\pi}{\omega_{\rm rf}}\right\}} \\
&\times\sin\overline{\omega}\left\{\frac{\phi_{2,n+1}-\phi_{1,n+1}}{\omega_{\rm rf}}-(h-k+1)\frac{2\pi}{\omega_{\rm rf}}\right\} \\
&\times\sum_{m=1}^{n} e^{-\alpha\left\{\frac{\phi_{1,n+1}-\phi_{1,m}}{\omega_{\rm rf}}+(n+1-m)h\frac{2\pi}{\omega_{\rm rf}}\right\}} \\
&\times\sin\left[\overline{\omega}\left\{\frac{\phi_{1,n+1}-\phi_{1,m}}{\omega_{\rm rf}}+(n+1-m)h\frac{2\pi}{\omega_{\rm rf}}\right\}-\delta\right] . \qquad \text{(C.4)}
\end{aligned}
$$

Since the configuration at the summation terms in eq.(C.3) and (C.4) is same ones except the suffix, we consider it without the suffix. Supposing that the range of the summation is restricted from $n-N$ to n because the wake field does not affects over so many

turns, then we obtain

$$
\begin{aligned}
&\sum_{m=1}^{n} e^{-\alpha\left\{\frac{\phi_{n+1}-\phi_m}{\omega_{\rm rf}}+(n+1-m)h\frac{2\pi}{\omega_{\rm rf}}\right\}} \\
&\times\begin{cases}\cos\left[\overline{\omega}\left\{\frac{\phi_{n+1}-\phi_m}{\omega_{\rm rf}}+(n+1-m)h\frac{2\pi}{\omega_{\rm rf}}\right\}-\delta\right] \\ \quad\text{or} \\ \sin\left[\overline{\omega}\left\{\frac{\phi_{n+1}-\phi_m}{\omega_{\rm rf}}+(n+1-m)h\frac{2\pi}{\omega_{\rm rf}}\right\}-\delta\right]\end{cases} \\
&\cong\sum_{m=n-N}^{n} e^{-\alpha\left\{\frac{\phi_{n+1}-\phi_m}{\omega_{\rm rf}}+(n+1-m)h\frac{2\pi}{\omega_{\rm rf}}\right\}} \\
&\times\begin{cases}\cos\left[\overline{\omega}\left\{\frac{\phi_{n+1}-\phi_m}{\omega_{\rm rf}}+(n+1-m)h\frac{2\pi}{\omega_{\rm rf}}\right\}-\delta\right] \\ \quad\text{or} \\ \sin\left[\overline{\omega}\left\{\frac{\phi_{n+1}-\phi_m}{\omega_{\rm rf}}+(n+1-m)h\frac{2\pi}{\omega_{\rm rf}}\right\}-\delta\right]\end{cases} \\
&=\sum_{m'=0}^{N} e^{-\alpha\left\{\frac{\phi_{n+1}-\phi_{m'+n-N}}{\omega_{\rm rf}}-(m'-N-1)h\frac{2\pi}{\omega_{\rm rf}}\right\}} \\
&\times\begin{cases}\cos\left[\overline{\omega}\left\{\frac{\phi_{n+1}-\phi_{m'+n-N}}{\omega_{\rm rf}}-(m'-N-1)h\frac{2\pi}{\omega_{\rm rf}}\right\}-\delta\right] \\ \quad\text{or} \\ \sin\left[\overline{\omega}\left\{\frac{\phi_{n+1}-\phi_{m'+n-N}}{\omega_{\rm rf}}-(m'-N-1)h\frac{2\pi}{\omega_{\rm rf}}\right\}-\delta\right]\end{cases} . \qquad \text{(C.5)}
\end{aligned}
$$

Furthermore, using $m'-N \ll n$, which means that N has a slightly smaller value than n, the relation between $\phi_{n+1}-\phi_n$ and $\phi_{n+1}-\phi_{m'+n-N}$ becomes

$$
\begin{aligned}
\phi_{n+1}-\phi_{m'+n-N} &= (\phi_{n+1}-\phi_n)+(\phi_n-\phi_{n-1})+\cdots+(\phi_{m'+n-N+1}-\phi_{m'+n-N}) \\
&= (\phi_{n+1}-\phi_n)\left[1+\frac{\phi_n-\phi_{m'+n-N}}{\phi_{n+1}-\phi_n}\right] \\
&\cong -(m'-N-1)(\phi_{n+1}-\phi_n) . \qquad \text{(C.6)}
\end{aligned}
$$

Substituting eq.(C.6) into (C.5), we get

$$
\begin{aligned}
S &= e^{-\alpha(N+1)\left(\frac{\phi_{n+1}-\phi_{m'+n-N}}{\omega_{\rm rf}}+h\frac{2\pi}{\omega_{\rm rf}}\right)} \\
&\times\sum_{m'=0}^{N} e^{\alpha m'\left(\frac{\phi_{n+1}-\phi_n}{\omega_{\rm rf}}+h\frac{2\pi}{\omega_{\rm rf}}\right)} \\
&\times\begin{cases}\cos\left[-\overline{\omega}m'\left(\frac{\phi_{n+1}-\phi_n}{\omega_{\rm rf}}+h\frac{2\pi}{\omega_{\rm rf}}\right)+\overline{\omega}(N+1)\left(\frac{\phi_{n+1}-\phi_n}{\omega_{\rm rf}}+h\frac{2\pi}{\omega_{\rm rf}}\right)-\delta\right] \\ \quad\text{or} \\ \sin\left[-\overline{\omega}m'\left(\frac{\phi_{n+1}-\phi_n}{\omega_{\rm rf}}+h\frac{2\pi}{\omega_{\rm rf}}\right\}+\overline{\omega}(N+1)\left(\frac{\phi_{n+1}-\phi_n}{\omega_{\rm rf}}+h\frac{2\pi}{\omega_{\rm rf}}\right)-\delta\right]\end{cases} \qquad \text{(C.7)}
\end{aligned}
$$

Supposing $|\frac{\phi_{n+1}-\phi_n}{\omega_{\rm rf}}| \ll h\frac{2\pi}{\omega_{\rm rf}}$ on the exponential term in the eq.(C.7), we get in the end

$$S = e^{-\alpha(N+1)h\frac{2\pi}{\omega_{\rm rf}}} \times \sum_{m'=0}^{N} e^{\alpha m' h\frac{2\pi}{\omega_{\rm rf}}}$$

$$\times \begin{cases} \cos\left[-\overline{\omega}m'\left(\frac{\phi_{n+1}-\phi_n}{\omega_{\rm rf}}+h\frac{2\pi}{\omega_{\rm rf}}\right)+\overline{\omega}(N+1)\left(\frac{\phi_{n+1}-\phi_n}{\omega_{\rm rf}}+h\frac{2\pi}{\omega_{\rm rf}}\right)-\delta\right] & \text{(C.8)} \\ \text{or} \\ \sin\left[-\overline{\omega}m'\left(\frac{\phi_{n+1}-\phi_n}{\omega_{\rm rf}}+h\frac{2\pi}{\omega_{\rm rf}}\right)+\overline{\omega}(N+1)\left(\frac{\phi_{n+1}-\phi_n}{\omega_{\rm rf}}+h\frac{2\pi}{\omega_{\rm rf}}\right)-\delta\right] . & \text{(C.9)} \end{cases}$$

Using the formula for the summations as

$$\sum_{m=0}^{n} a^m \cos mx = \frac{1-a\cos x - a^{n+1}\cos(n+1)x + a^{n+2}\cos nx}{1-2a\cos x+a^2} \quad \text{(C.10)}$$

$$\sum_{m=0}^{n} a^m \sin mx = \frac{a\sin x - a^{n+1}\sin(n+1)x + a^{n+2}\sin nx}{1-2a\cos x+a^2} \quad \text{(C.11)}$$

the equation (C.8) can be rewritten as

$$\begin{aligned}
&\frac{e^{-\alpha(N+1)h\frac{2\pi}{\omega_{\rm rf}}}\cos\left\{\overline{\omega}(N+1)\left(\frac{\phi_{n+1}-\phi_n}{\omega_{\rm rf}}+h\frac{2\pi}{\omega_{\rm rf}}\right)-\delta\right\}}{1-2e^{\alpha h\frac{2\pi}{\omega_{\rm rf}}}\cos\left\{-\overline{\omega}\left(\frac{\phi_{n+1}-\phi_n}{\omega_{\rm rf}}+h\frac{2\pi}{\omega_{\rm rf}}\right)\right\}+e^{2\alpha h\frac{2\pi}{\omega_{\rm rf}}}} \\
&\times\left[1-e^{\alpha h\frac{2\pi}{\omega_{\rm rf}}}\cos\left\{-\overline{\omega}\left(\frac{\phi_{n+1}-\phi_n}{\omega_{\rm rf}}+h\frac{2\pi}{\omega_{\rm rf}}\right)\right\}\right. \\
&-e^{\alpha(N+1)h\frac{2\pi}{\omega_{\rm rf}}}\cos(N+1)\left\{-\overline{\omega}\left(\frac{\phi_{n+1}-\phi_n}{\omega_{\rm rf}}+h\frac{2\pi}{\omega_{\rm rf}}\right)\right\} \\
&\left.-e^{\alpha(N+2)h\frac{2\pi}{\omega_{\rm rf}}}\cos N\left\{-\overline{\omega}\left(\frac{\phi_{n+1}-\phi_n}{\omega_{\rm rf}}+h\frac{2\pi}{\omega_{\rm rf}}\right)\right\}\right] \\
&-\frac{e^{-\alpha(N+1)h\frac{2\pi}{\omega_{\rm rf}}}\sin\left\{\overline{\omega}(N+1)\left(\frac{\phi_{n+1}-\phi_n}{\omega_{\rm rf}}+h\frac{2\pi}{\omega_{\rm rf}}\right)-\delta\right\}}{1-2e^{\alpha h\frac{2\pi}{\omega_{\rm rf}}}\cos\left\{-\overline{\omega}\left(\frac{\phi_{n+1}-\phi_n}{\omega_{\rm rf}}+h\frac{2\pi}{\omega_{\rm rf}}\right)\right\}+e^{2\alpha h\frac{2\pi}{\omega_{\rm rf}}}} \\
&\times\left[e^{\alpha h\frac{2\pi}{\omega_{\rm rf}}}\sin\left\{-\overline{\omega}\left(\frac{\phi_{n+1}-\phi_n}{\omega_{\rm rf}}+h\frac{2\pi}{\omega_{\rm rf}}\right)\right\}\right. \\
&-e^{\alpha(N+1)h\frac{2\pi}{\omega_{\rm rf}}}\sin(N+1)\left\{-\overline{\omega}\left(\frac{\phi_{n+1}-\phi_n}{\omega_{\rm rf}}+h\frac{2\pi}{\omega_{\rm rf}}\right)\right\} \\
&\left.-e^{\alpha(N+2)h\frac{2\pi}{\omega_{\rm rf}}}\sin N\left\{-\overline{\omega}\left(\frac{\phi_{n+1}-\phi_n}{\omega_{\rm rf}}+h\frac{2\pi}{\omega_{\rm rf}}\right)\right\}\right] \\
&= S_{\cos}\ , \qquad \text{(C.12)}
\end{aligned}$$

and the equation (C.9) can be rewritten as

$$
\begin{aligned}
&\frac{e^{-\alpha(N+1)h\frac{2\pi}{\omega_{\rm rf}}}\cos\left\{\overline{\omega}(N+1)\left(\frac{\phi_{n+1}-\phi_n}{\omega_{\rm rf}}+h\frac{2\pi}{\omega_{\rm rf}}\right)-\delta\right\}}{1-2e^{\alpha h\frac{2\pi}{\omega_{\rm rf}}}\cos\left\{-\overline{\omega}\left(\frac{\phi_{n+1}-\phi_n}{\omega_{\rm rf}}+h\frac{2\pi}{\omega_{\rm rf}}\right)\right\}+e^{2\alpha h\frac{2\pi}{\omega_{\rm rf}}}}\\
&\times\left[e^{\alpha h\frac{2\pi}{\omega_{\rm rf}}}\sin\left\{-\overline{\omega}\left(\frac{\phi_{n+1}-\phi_n}{\omega_{\rm rf}}+h\frac{2\pi}{\omega_{\rm rf}}\right)\right\}\right.\\
&-e^{\alpha(N+1)h\frac{2\pi}{\omega_{\rm rf}}}\sin(N+1)\left\{-\overline{\omega}\left(\frac{\phi_{n+1}-\phi_n}{\omega_{\rm rf}}+h\frac{2\pi}{\omega_{\rm rf}}\right)\right\}\\
&\left.-e^{\alpha(N+2)h\frac{2\pi}{\omega_{\rm rf}}}\sin N\left\{-\overline{\omega}\left(\frac{\phi_{n+1}-\phi_n}{\omega_{\rm rf}}+h\frac{2\pi}{\omega_{\rm rf}}\right)\right\}\right]\\
&+\frac{e^{-\alpha(N+1)h\frac{2\pi}{\omega_{\rm rf}}}\sin\left\{\overline{\omega}(N+1)\left(\frac{\phi_{n+1}-\phi_n}{\omega_{\rm rf}}+h\frac{2\pi}{\omega_{\rm rf}}\right)-\delta\right\}}{1-2e^{\alpha h\frac{2\pi}{\omega_{\rm rf}}}\cos\left\{-\overline{\omega}\left(\frac{\phi_{n+1}-\phi_n}{\omega_{\rm rf}}+h\frac{2\pi}{\omega_{\rm rf}}\right)\right\}+e^{2\alpha h\frac{2\pi}{\omega_{\rm rf}}}}\\
&\times\left[1-e^{\alpha h\frac{2\pi}{\omega_{\rm rf}}}\cos\left\{-\overline{\omega}\left(\frac{\phi_{n+1}-\phi_n}{\omega_{\rm rf}}+h\frac{2\pi}{\omega_{\rm rf}}\right)\right\}\right.\\
&-e^{\alpha(N+1)h\frac{2\pi}{\omega_{\rm rf}}}\cos(N+1)\left\{-\overline{\omega}\left(\frac{\phi_{n+1}-\phi_n}{\omega_{\rm rf}}+h\frac{2\pi}{\omega_{\rm rf}}\right)\right\}\\
&\left.-e^{\alpha(N+2)h\frac{2\pi}{\omega_{\rm rf}}}\cos N\left\{-\overline{\omega}\left(\frac{\phi_{n+1}-\phi_n}{\omega_{\rm rf}}+h\frac{2\pi}{\omega_{\rm rf}}\right)\right\}\right]\\
&S_{\rm sin}\ . \qquad\qquad (C.13)
\end{aligned}
$$

After above mentioned approximation for the summation, eq. (C.3) and (C.4) are simplified as follows

$$
\begin{aligned}
&\Delta E_1 = eV\sin\phi_{1,n+1}-\frac{1}{2}eV_{\rm b0}\cos\delta-eV_{\rm b0}S_{1,\cos}\\
&-eV_{\rm b0}e^{\alpha(k-1)\frac{2\pi}{\omega_{\rm rf}}}\cos\overline{\omega}\left(\frac{\phi_{1,n+1}-\phi_{2,n+1}}{\omega_{\rm rf}}-(k-1)\frac{2\pi}{\omega_{\rm rf}}\right)\cdot S_{2,\cos}\\
&+eV_{\rm b0}e^{\alpha(k-1)\frac{2\pi}{\omega_{\rm rf}}}\sin\overline{\omega}\left(\frac{\phi_{1,n+1}-\phi_{2,n+1}}{\omega_{\rm rf}}-(k-1)\frac{2\pi}{\omega_{\rm rf}}\right)\cdot S_{2,\sin} \qquad (C.14)
\end{aligned}
$$

$$
\begin{aligned}
&\Delta E_2 = eV\sin\phi_{2,n+1}-\frac{1}{2}eV_{\rm b0}\cos\delta-eV_{\rm b0}S_{2,\cos}\\
&-eV_{\rm b0}e^{\alpha(h-k+1)\frac{2\pi}{\omega_{\rm rf}}}\cos\overline{\omega}\left(\frac{\phi_{2,n+1}-\phi_{1,n+1}}{\omega_{\rm rf}}-(h-k+1)\frac{2\pi}{\omega_{\rm rf}}\right)\cdot S_{1,\cos}\\
&+eV_{\rm b0}e^{\alpha(h-k+1)\frac{2\pi}{\omega_{\rm rf}}}\sin\overline{\omega}\left(\frac{\phi_{2,n+1}-\phi_{1,n+1}}{\omega_{\rm rf}}-(h-k+1)\frac{2\pi}{\omega_{\rm rf}}\right)\cdot S_{1,\sin}\ , \qquad (C.15)
\end{aligned}
$$

where $S_{1,\cos}$ and $S_{2,\cos}$ express the case that the suffix 1 and 2 are attached on ϕ terms in eq.(C.12),respectively, and $S_{1,\sin}$ and $S_{2,\sin}$ express the case that the suffix 1 and 2 are attached on ϕ terms in eq.(C.13),respectively.

Let us consider more simplification for eq.(C.12) and (C.13). Supposing $e^{\alpha h\frac{2\pi}{\omega_{\rm rf}}}\gg 1$, $S_{1,\sin}$, $S_{2,\sin}$, $S_{1,\cos}$ and $S_{2,\cos}$ are simplified, then we obtain

$$
\begin{aligned}
&\Delta E_1 = eV\sin\phi_{1,n+1}-eV_{\rm b0}\cos\delta\\
&-eV_{\rm b0}e^{-\alpha(h-k+1)\frac{2\pi}{\omega_{\rm rf}}}\cos\left\{\overline{\omega}\left(\frac{\phi_{1,n+1}-\phi_{1,n}}{\omega_{\rm rf}}+h\frac{2\pi}{\omega_{\rm rf}}\right)-\delta\right\}\\
&-eV_{\rm b0}e^{-\alpha(h-k+1)\frac{2\pi}{\omega_{\rm rf}}}\cos\left[\overline{\omega}\left\{\frac{\phi_{1,n+1}-\phi_{2,n+1}}{\omega_{\rm rf}}+\frac{\phi_{1,n+1}-\phi_{1,n}}{\omega_{\rm rf}}+(h-k+1)\frac{2\pi}{\omega_{\rm rf}}\right\}-\delta\right] \qquad (C.16)
\end{aligned}
$$

$$
\begin{aligned}
&\Delta E_2 = eV\sin\phi_{2,n+1}-eV_{\rm b0}\cos\delta\\
&-eV_{\rm b0}e^{-\alpha(k-1)\frac{2\pi}{\omega_{\rm rf}}}\cos\left\{\overline{\omega}\left(\frac{\phi_{2,n+1}-\phi_{2,n}}{\omega_{\rm rf}}+h\frac{2\pi}{\omega_{\rm rf}}\right)-\delta\right\}\\
&-eV_{\rm b0}e^{-\alpha(k-1)\frac{2\pi}{\omega_{\rm rf}}}\cos\left[\overline{\omega}\left\{\frac{\phi_{2,n+1}-\phi_{1,n+1}}{\omega_{\rm rf}}+\frac{\phi_{2,n+1}-\phi_{2,n}}{\omega_{\rm rf}}+(k-1)\frac{2\pi}{\omega_{\rm rf}}\right\}-\delta\right]\ . \qquad (C.17)
\end{aligned}
$$

References

[1] For example, The joint Project team of JAERI and KEK, Proposal for Japan Hadron Facility, KEK Report 99-4, 1999

[2] K.W. Robinson, Stability of Beam in Radiofrequency System, CEAL-1010, 1964

[3] F. Pedersen, BEAM LOADING EFFECTS IN THE CERN PS BOOSTER, IEEE Trans. Nucl. Sci., Vol. NS-22, No.3, 1975

[4] A.W. Chao, PHYSICS OF COLLECTIVE BEAM INSTABILITIES IN HIGH ENERGY ACCELERATORS, John Wiley & sons, Inc., New York, 1993

[5] S. Koscielniak, ANALYTIC CRITERIA FOR STABILITY OF BEAM-LOADED RADIO-FREQUENCY SYSTEMS, Particle Accelerators Vol. 48, pp.135-168, 1994

[6] S. Myers, INSTABILITIES AND BEAM INTENSITY LIMITATIONS IN CIRCULAR ACCELERATORS, CERN-SL-97-48 DI 1997

[7] J.M.Brennan, THE UPGREADED RF SYSTEM FOR THE AGS AND HIGH INTENSITY PROTON BEAMS, Proc. of Part. Acc. Conf. 95, 1995, pp.1489-1493

[8] R.D. Kohaupt, ON MULTI-BUNCH INSTABILITIES FOR FRACTIONALLY FILLED RINGS, DESY 85-139, 1985

[9] S.A. Bogacz and J.E. Griffin, Effect of Empty Buckets on Coupled Bunch Instability in RHIC Booster $\sim$ Longitudinal Phase-Space Simulation, FN-486, 1988

[10] S. Koscielniak, Calculation of seed values for longitudinal coupled bunch dipole instability due to uneven bucket population, TRI-PP-91-21, 1991

[11] For example, M. Conte and W.W. Mackay, AN INTRODUCTION TO THE PHYSICS OF PARTICLE ACCELERATORS, World Scientific

[12] I.S.K. Gardner, FERRITE DOMINATED CAVITIES, CERN ACCELERATOR SCHOOL RF ENGINEERING FOR PARTICLE ACCELERATORS, CERN 92-03, Vol. II(1992), p.349

[13] C. Ohmori *et al.*, High Field-Gradient Cavities Loaded with Magnetic Alloys for Synchrotrons, Proc. of Part. Acc. Conf. 99, to be published.

[14] J.I.Hirota et al, An Untuned Type RF Cavity using Multiple Power Feeding, Proc. of 10th Symp. on Acc. Sci. Tech., 1995

[15] R.M. Bozorth, FERROMAGNETISM, D.VAN NOSTRAND COMPANY, INC, 1951

[16] J.E.Griffin et al., A Review of Some Dynamic Loss Properties of Ni-Zn Accelerator RF System, IEEE Trans. Nucl. Sci. NS-26(1979), p.3965

[17] S.Watabe et al., A Study on Ferrites for Particle Accelerators, FERRITES: Proc. of Inter. Conf.(1980)

[18] H.Shul, The non-linear behavior of ferrites at high signal levels, Proc. IRE, 44(1956), p.1256

[19] P.B. Wilson, High Energy Electron Linacs, SLAC-PUB-2884, 1982

[20] S.Y. Zhang and W.T. Weng, Static and Transient Beam Loading of a Synchrotron, BNL-47773(AGS/AD/92-1), 1992

[21] S.Y. Zhang and W.T. Weng, Analysis of Periodic Transient Beam Loading of the AGS, BNL-47771(AGS/AD/92-2), 1992

[22] T. Uesugi et al., Summary of the Measurement of magnetic Materials for JHP RF Cavity(1)(in Japanese), JHP-31

[23] H. Nakayama et al., Summary of the Measurement of the Magnetic Materials for JHF RF Cavity(2)(in Japanese), KEK Report 98-13, 1999

Curriculum Vitae

1995 March, Bachelor at Department of Physics, Okayama University
1997 March, Master Degree at Department of Physics, Osaka University

Publications

1. M. Yamamoto *et al.*, BEAM LOADING EFFECTS ON HIGH GRADIENT MA-LOADED CAVITY, Proc. PAC99, 1999, to be published
2. M. Yamamoto *et al.*, MULTI-HARMONIC ACCELERATION WITH HIGH GRADIENT MA CAVITY AT HIMAC, Proc. PAC99, 1999, to be published
3. Y. Hashimoto *et at.*, BEAM LOADING EXPERIMENT WITH SHORT BUNCHED ELECTRON BEAMS FOR NEW TYPE OF ACCELERATING RF SYSTEM OF HIGH INTENSITY PROTON SYNCHROTRON, Proc. EPAC98, 1998
4. M. Yamamoto *et al.*, BEAM LOADING EFFECTS IN JHF SYNCHROTRON, Proc. APAC98, 1998
5. M. Yamamoto *et al.*, Beam Loading in JHF 50 GeV Proton Synchrotron, Proc. Symp. on Acc. Sci. Tech.(SAST97), 1997

Presentations

1. BEAM LOADING EFFECTS ON HIGH-GRADIENT MAGNETIC ALLOY-LOADED CAVITY, 1999 Annual Meeting of the Atomic Energy Society of Japan